Article

Not peer-reviewed version

Chronon Field Theory I: Covariant Mass, Solitonic Matter, and Emergent U(1) A Background-Independent Foundation for QED-like Dynamics, the Coulomb Law, and Fermionic Matter with Emergent ($\hbar$, G, e, c)

Bin Li *

Posted Date: 19 September 2025

doi: 10.20944/preprints202509.1667.v1

Keywords: Chronon Field Theory; emergent gauge fields; covariant mass density; topological solitons; spin–statistics; Berry phase; background independence

Article

Chronon Field Theory I: Covariant Mass, Solitonic Matter, and Emergent U(1): A Background-Independent Foundation for QED-Like Dynamics, the Coulomb Law, and Fermionic Matter with Emergent $(\hbar, G, e, c)$

Bin Li

Research Department, Silicon Minds Inc., Clarksville, USA; libin63@yahoo.com

Abstract

We present a self-contained formulation of Chronon Field Theory (CFT) in which (i) a smooth, unit-norm, future-directed timelike field Φ^μ induces foliation, causal structure, and an emergent Lorentzian metric; (ii) a covariant *local mass/energy density* is defined as $\rho(x) = T_{\mu\nu}\,\Phi^\mu\Phi_\mu$, furnishing a unified and positive notion of inertial/gravitational mass; (iii) matter arises as topologically stable solitons with $w = 1$, carrying spin-$\frac{1}{2}$ and Fermi–Dirac statistics via a Finkelstein–Rubinstein/Berry holonomy mechanism; and (iv) a *U(1)* gauge sector *emerges* from chronon holonomy, yielding Maxwell dynamics on the emergent metric and a massless "photon" as a Goldstone-like excitation. We prove positivity and conservation properties for ρ, establish existence of finite-energy soliton minimizers under mild assumptions, and state a holonomy-matching theorem that ties the FR $\mathbb{Z}_2$ class to the emergent spacetime *U(1)* connection. A key outcome is that the familiar constants of Nature are not postulated but emerge: the effective action unit $\hbar_{\text{eff}} \sim E_c\tau_c$, Newton's constant $G \sim (c(\alpha_i, \gamma)\Lambda^2)^{-1}$, the elementary charge $e = q_0/\sqrt{\kappa_A}$, and the universal light speed $c = \ell_\Phi/\tau_c$. In the gravitational sector we recover Einstein–Maxwell on stabilized domains at two-derivative order, while allowing controlled, power-counted deviations (æther-like and higher-derivative terms) that are constrained phenomenologically. We further derive the Coulomb law on stabilized leaves, $V(r) = e_1e_2/(4\pi r)$, whose normalization fixes the holonomy stiffness via the observed Coulomb constant (equivalently α_{em}), yielding $\kappa_A = q_0^2/(4\pi\alpha_{\text{em}})$. We outline collective-coordinate quantization where splittings scale with $\hbar_{\text{eff}}$, and identify falsifiable signatures (achromatic birefringence; exchange-phase interferometry). This paper (I) lays the foundation for non-Abelian extensions (II) and QCD-like dynamics (III).

Keywords: Chronon Field Theory; emergent gauge fields; covariant mass density; topological solitons; spin–statistics; Berry phase; background independence

---

1. Introduction and Main Contributions

Chronon Field Theory (CFT) postulates a single smooth, unit–norm, future–directed timelike field Φ^μ whose integral curves define a preferred time–flow and induce a foliation $\{\Sigma_\tau\}$ together with an emergent Lorentzian metric $g_{\mu\nu}[\Phi]$ [9,116]. On stabilized domains (defined below), this structure supplies (i) causal cones and an ADM–like split, (ii) a relational Hilbert space $\mathcal{H}[\Sigma_\tau]$ with Schrödinger evolution in intrinsic time τ [37,40], and (iii) a covariant stress tensor $T_{\mu\nu}$ obtained from the CFT action [92]. Our aim in Paper I is to show that, within this background–independent setting, one can formulate a rigorous and self–contained account of *mass*, *matter*, an emergent Abelian *gauge sector*, and—crucially—the familiar constants of Nature, which appear as derived quantities rather than inputs [10,117].

Preprints.org (www.preprints.org) | NOT PEER-REVIEWED | Posted: 19 September 2025 doi:10.20944/preprints202509.1667.v1

Standing Conventions

We work in 3+1 dimensions with signature $(-,+,+,+)$, set units so that the emergent light speed is $c=1$, and keep the emergent action unit $\hbar_{\rm eff}$ explicit. Greek indices run over spacetime components; spatial operations are performed with the projector $h_{\mu\nu} := g_{\mu\nu} + \Phi_\mu\Phi_\nu$; D_μ denotes the induced spatial covariant derivative on a leaf. Unless stated otherwise, fields are smooth and decay so that boundary terms vanish on Σ_τ.

Stabilized Domains

A spacetime region is *stabilized* if Φ^μ is smooth, strictly timelike with $\Phi^\mu\Phi_\mu = -1$, and its gradients are bounded so that (a) the foliation $\{\Sigma_\tau\}$ is well defined, (b) the field equations are hyperbolic with respect to the induced time, and (c) the Peierls bracket reduces to canonical commutators on $\mathcal{H}[\Sigma_\tau]$ up to controllable $O(|\nabla\Phi|)$ corrections [37,96]. All results below are stated and proved on stabilized domains.

On local Lorentz Symmetry

The chronon field selects a unit timelike direction and thus a preferred foliation in vacuum. As a result, *local Lorentz symmetry is spontaneously broken* even though the action is written in a Lorentz–covariant and diffeomorphism–invariant form. We therefore regard the framework as an æther–like effective field theory on stabilized domains and explicitly track the induced preferred–frame operators and propagation effects [72,73]. For clarity, we use "chronon" to denote the unit–norm timelike sector introduced here, while emphasizing that its structure is closely analogous to Einstein–æther models. In the infrared, these deformations are parametrically suppressed and compatible with existing constraints (PPN preferred–frame bounds [121,122], gravitational–wave equal–speed tests [1,2], and birefringence limits [30,79,85]), so that the dynamics reduce to Einstein–Maxwell up to small, controlled corrections. Radiative corrections cannot destabilize this suppression, since the stabilized domain symmetry prevents the regeneration of unsuppressed Lorentz–violating operators at low energies. We map the leading operators to standard test frameworks (SME/PPN) [78,79] and state parameter priors accordingly; any phenomenology beyond these bounds is confined to strongly curved or topological regions where the foliation is highly distorted. For completeness, we also outline in Appendix N a broader interpretation—the *Co-Moving Concealment Mechanism*—in which all matter and observers emerge from the chronon foliation itself, so that local Lorentz violation is fundamentally present but operationally concealed. In the present work, however, we adopt the more conservative EFT perspective, ensuring consistency with established experimental tests while leaving the deeper emergent interpretation for future development.

On Emergent Metrics and Causal Structure

The chronon sector deforms propagation operators in a manner that can be usefully recast in terms of an induced or "emergent" effective metric. In this sense the chronon may be viewed as generating a secondary causal structure, an idea we regard as a promising avenue for future work. In the present paper, however, we restrict to the more conservative interpretation: an æther-like effective field theory defined on the background spacetime metric $g_{\mu\nu}$, with chronon-induced operators systematically mapped to SME/PPN test frameworks. This ensures that the claims made in this paper remain within the well-established EFT regime, while a rigorous treatment of chronon-induced emergent geometry is deferred to subsequent studies.

1.1. Main Results

- (C1) **Covariant local mass/energy density.** Definition and positivity of ρ connects to the dominant energy condition [63,116].
- (C2) **GR as an IR fixed point with controlled deviations.** Effective field theory reasoning follows [73,117], with constraints informed by PPN tests [122].

Preprints.org (www.preprints.org) | NOT PEER-REVIEWED | Posted: 19 September 2025 doi:10.20944/preprints202509.1667.v1

(C3) **Existence of finite–energy w=1 solitons.** Existence and stability of topological solitons connect to Skyrme-type and Derrick arguments [38,86,106].

(C4) **Spin–statistics for solitons via FR/Berry holonomy.** The Finkelstein–Rubinstein mechanism and Berry phase arguments [20,47] underpin the soliton spin–statistics connection.

(C5) **Emergent Abelian gauge sector from chronon holonomy.** Parallel transport and holonomy yielding emergent gauge fields relates to work on gauge connections and Berry bundles [89,125].

(C6) **Emergent fundamental constants and parameter constraints.** The idea that $G, \hbar, e, c$ may emerge rather than be postulated resonates with Sakharov's induced gravity [102] and effective action derivations in quantum field theory [127].

1.2. *Intuition and Roadmap: From Chronon Flow to Emergent* $\mathrm{U}(1)$

Starting picture.

Envision the chronon field Φ^μ as a locally defined "clock vector" that threads spacetime, picking out at each point a preferred timelike direction. Imposing the unit–norm constraint

$$\Phi^\mu \Phi_\mu = -1$$

does two things at once: it fixes the pace of this clock (no arbitrary rescalings) and makes the orthogonal complement $\Phi^\perp$ well defined. Geometrically, this splits the tangent space into a time direction spanned by Φ and a three–dimensional space orthogonal to it. Integrating the distribution $\Phi^\perp$ produces a foliation of spacetime into spatial leaves $\{\Sigma_\tau\}$, with τ the time measured along the chronon flow. Observers comoving with Φ measure the local energy density

$$\rho \ = \ T_{\mu\nu} \, \Phi^\mu \Phi^\nu,$$

and we call a region *stabilized* when $\rho > 0$ and fluctuations of Φ remain bounded. Intuitively: a stabilized domain is a medium with a coherent local clock and well–behaved spatial slices.

Why Compact Gauge Structure Is Natural

Within a stabilized domain, parallel transport along a closed curve $C \subset \Sigma_\tau$ returns any spatial vector back to itself up to a *rotation* inside the plane orthogonal to Φ. Because Φ is unit timelike, the induced metric on $\Phi^\perp$ is positive–definite, so these transports form a compact rotation group. The smallest nontrivial such subgroup is the circle $\mathrm{U}(1)$: transporting an internal "pointer" $\xi \in \Phi^\perp$ around C rotates its angle by some phase $\theta(C)$. This is the intuitive origin of the emergent Abelian gauge symmetry: the *phase* picked up by leafwise parallel transport is the holonomy of a circle bundle.

From Phases to a Gauge Field

To bookkeeping these phases, we assign to each path a phase factor and demand consistency when paths concatenate. Locally, this is encoded by a one–form A (the *connection*) whose integral around C gives the phase, $\exp\left(i \oint_C A\right)$. The *curvature* $F = \mathrm{d}A$ measures how phases accumulate across small tiles of a surface; in a coarse fluid picture it plays the role of a vorticity two–form living on the leaves. The usual Maxwell–like equations then arise as the continuum limit of these holonomy constraints on the emergent metric $g[\Phi]$ defined by the chronon sector. For non–specialists: A is the device that tells you how much the internal pointer twists as you move; F tells you how much twist per unit area the medium stores.

Why the Unit Norm Really Matters

Keeping $\Phi^\mu \Phi_\mu = -1$ is not a cosmetic choice. It (i) makes the projector $\Pi^\mu{}_\nu = \delta^\mu{}_\nu + \Phi^\mu \Phi_\nu$ a *true* projector onto $\Phi^\perp$ (so the foliation is clean and the leaf metric is Riemannian), (ii) keeps holonomy compact (rotations, not boosts or scalings), ensuring that the internal fiber is a circle, and (iii) cleanly

Preprints.org (www.preprints.org) | NOT PEER-REVIEWED | Posted: 19 September 2025 doi:10.20944/preprints202509.1667.v1

separates *phase* (angle on the circle) from *amplitude* (norm fluctuations). This separation underlies flux quantization and the stability criteria we use later.

Solitons and Quantized Flux, in Pictures

Because the fiber is a circle, winding the phase by $2\pi n$ around a loop cannot be undone continuously: it labels a topological sector ($\pi_1(S^1) = \mathbb{Z}$). Spatial textures of Φ that carry this winding behave as *solitons*. Their flux is quantized, $\int_\Sigma F = 2\pi n$, and they act as localized, robust excitations of the chronon medium. Upon quantization, these solitons furnish particle states; the simple mental model is that defects in the "phase field" of the medium behave as charges and, when moved around, imprint their statistics through the accumulated holonomy (the detailed spin/statistics analysis is carried out in the main text).

How the Derivations Follow This Story

The technical development mirrors the intuition:

1. **Kinematics from the clock:** impose $\Phi^2 = -1$, build the projector and induced metric on leaves, and define stabilized domains via ρ.
2. **Holonomy data:** track phase changes under parallel transport on leaves, show they patch consistently over a good cover, and assemble the circle bundle.
3. **Fields from holonomy:** identify the local connection A and curvature F as the infinitesimal description of these phases; derive Maxwell–type dynamics on $g[\Phi]$.
4. **Topology and matter:** classify defects by winding, show flux quantization, and couple solitonic excitations minimally to A.

Technical Notes

The foliation gives a natural $\mathrm{U}(1)$ reduction of the frame bundle on $\Phi^\perp$; the connection one–form arises as the leafwise Berry connection for the chronon fiber; compactness and the unit normalization guarantee that the Čech cocycles land in $\mathrm{U}(1)$ and that the resulting Abelian sector is globally well defined.

Analogy

Think of the chronon medium as a fluid with an internal compass. The unit norm fixes the clock; the compass's angle is the gauge phase. Carrying the compass around a loop twists it by an amount that depends only on what the fluid is doing inside the loop. That twist is the Wilson phase, its density is F, and its topological windings are the solitons. The rest of the paper turns this picture into geometry and equations.

2. Background and Setup

2.1. Chronon Field, Foliation, and Emergent Geometry

We postulate a smooth, unit timelike vector field Φ^μ on a four-dimensional spacetime manifold $(\mathcal{M}, g_{\mu\nu})$, satisfying

$$\Phi^\mu \Phi_\mu = -1, \qquad \Phi^0 > 0. \tag{1}$$

The integral curves of Φ define a preferred time function τ (unique up to affine reparameterization) and a foliation by Cauchy hypersurfaces $\{\Sigma_\tau\}$ [32,53,116]. The orthogonal projector onto the tangent bundle of each leaf is

$$h_{\mu\nu} := g_{\mu\nu} + \Phi_\mu \Phi^\mu, \tag{2}$$

which is a positive-definite metric on $T\Sigma_\tau$ [57,116]. The Levi–Civita connection ∇ of g induces a *leafwise* covariant derivative on tensor fields X by

$$D_\mu X := h_\mu{}^\alpha \nabla_\alpha X, \qquad h_\mu{}^\alpha := g_\mu{}^\alpha + \Phi_\mu \Phi^\alpha. \tag{3}$$

Kinematic invariants of the congruence Φ are defined as

$$a_\mu := \Phi^\alpha \nabla_\alpha \Phi_\mu, \quad \theta := D_\mu \Phi^\mu, \quad \sigma_{\mu\nu} := D_{(\mu}\Phi_{\nu)} - \tfrac{1}{3}\theta\, h_{\mu\nu}, \quad \omega_{\mu\nu} := D_{[\mu}\Phi_{\nu]}, \tag{4}$$

and obey the standard Raychaudhuri/Ehlers relations for timelike congruences [43,101,116]. The extrinsic curvature of the leaves is $K_{\mu\nu} := D_\mu \Phi_\nu$, with the decomposition $K_{\mu\nu} = \sigma_{\mu\nu} + \frac{1}{3}\theta\, h_{\mu\nu} + \omega_{\mu\nu}$ [57]. Throughout we work on *stabilized domains*: regions where Φ is smooth, strictly timelike, and $\|\nabla\Phi\|$ is uniformly bounded so that (i) the foliation exists, (ii) the Cauchy problem for the field equations is well posed in the intrinsic time τ, and (iii) equal-time operator algebras on $\mathcal{H}[\Sigma_\tau]$ are well defined up to controllable $O(\|\nabla\Phi\|)$ corrections [32,37,96].

Role of the Unit–Norm Constraint in the Abelian Sector

Throughout Paper I we impose $\Phi^\mu \Phi_\mu = -1$ on stabilized domains. This normalization has three indispensable consequences for the emergence of the $\mathrm{U}(1)$ sector. First, it fixes the chronon flow as a unit timelike congruence, so the orthogonal projector $\Pi^\mu{}_\nu = \delta^\mu{}_\nu + \Phi^\mu \Phi_\nu$ is a true projector and the induced leaf metric $h_{\mu\nu} = g_{\mu\nu}[\Phi] + \Phi_\mu \Phi_\nu$ is Riemannian [57,116]. In particular, $\rho = T_{\mu\nu}\Phi^\mu\Phi^\nu$ is then the physical energy density in the comoving frame, providing a clean, scale–independent criterion for stabilized domains. Second, restricting parallel transport to $\Phi^\perp$ preserves h and yields a compact residual isotropy $\mathrm{SO}(2) \simeq \mathrm{U}(1)$ on the internal fiber, so that holonomy produces a genuine circle bundle rather than a noncompact $\mathbb{R}$ symmetry; this compactness underlies flux quantization and the integer winding of solitonic defects ($\pi_1(S^1) = \mathbb{Z}$) [89,125]. Third, the unit baseline separates angular (phase) and radial (amplitude) degrees of freedom: the former define the emergent $\mathrm{U}(1)$ connection and Berry–like holonomy on leaves, while the latter encode norm–restoring fluctuations of Φ without contaminating gauge phases [20]. If the norm were allowed to drift, the projector would cease to be idempotent without ad hoc rescaling, ρ would pick up spurious conformal factors, and leafwise holonomy would no longer be guaranteed to land in a compact Abelian group, obstructing the $\mathrm{U}(1)$ construction. Related unit-timelike constructions appear in Einstein–æther–type effective theories [72,73].

2.2. Dynamics and Stress Tensor

We take a local, diffeomorphism-invariant CFT action for Φ on $(\mathcal{M}, g)$ truncated at mass-dimension ≤ 4 (parity-even sector):

$$\begin{aligned} S_\Phi[g,\Phi] &= \int \mathrm{d}^4x\, \sqrt{-g}\, \mathcal{L}_\Phi, \\ \mathcal{L}_\Phi &= \alpha_1 (\nabla_\mu \Phi_\nu)(\nabla^\mu \Phi^\nu) + \alpha_2 (\nabla_\mu \Phi_\nu)(\nabla^\nu \Phi^\mu) + \alpha_3 (\nabla_\mu \Phi^\mu)^2 + \gamma\, R_{\mu\nu}\Phi^\mu\Phi^\nu + \lambda\,(\Phi^\mu\Phi_\mu + 1). \end{aligned} \tag{5}$$

Here $R_{\mu\nu}$ is the Ricci tensor, and λ enforces the unit-norm constraint (one may alternatively use a steep potential). The structure mirrors familiar unit-timelike vector EFTs (e.g., Einstein–æther) while remaining background independent in our setting [72,73]. Variation with respect to Φ yields the Euler–Lagrange equations

$$\alpha_1 \nabla_\mu \nabla^\mu \Phi^\nu + \alpha_2 \nabla_\mu \nabla^\nu \Phi^\mu + \alpha_3 \nabla^\nu (\nabla \cdot \Phi) + \gamma R^\nu{}_\mu \Phi^\mu + \lambda \Phi^\nu \; = \; 0, \tag{6}$$

with λ fixed by contracting (6) with Φ_ν and using $\Phi^2 = -1$. The symmetric (Hilbert) stress tensor is defined by

$$T_{\mu\nu} \; := \; -\frac{2}{\sqrt{-g}} \frac{\delta S_\Phi}{\delta g^{\mu\nu}} \; = \; 2\frac{\partial \mathcal{L}_\Phi}{\partial g^{\mu\nu}} - g_{\mu\nu}\,\mathcal{L}_\Phi \; + \; (\text{metric-variation terms from covariant derivatives}), \tag{7}$$

Preprints.org (www.preprints.org) | NOT PEER-REVIEWED | Posted: 19 September 2025 doi:10.20944/preprints202509.1667.v1

which is conserved on shell, $\nabla_\mu T_{\mu\nu} = 0$, by diffeomorphism invariance [116]. The *covariant local mass/energy density* measured by comoving observers is

$$\rho(x) = T_{\mu\nu}(\Phi, \nabla\Phi, g)\, \Phi^\mu \Phi_\mu, \tag{8}$$

and the leafwise total (rest) mass is $\mathsf{M}[\Sigma_\tau] := \int_{\Sigma_\tau} \rho\, d^3x$, where the volume element is induced by $h_{\mu\nu}$ [116]. Positivity and conservation properties of ρ are established in §4.

2.3. Emergent Action Unit $\hbar_{\text{eff}}$ and Operator Algebra

CFT posits that quantum weighting arises from coarse-graining chronon microdynamics over mesoscale domains. Let S denote the classical action for admissible histories and $\mathcal{E}_\xi$ an ensemble of coarse-grained configurations at scale ξ with N_ξ effectively independent subdomains. Define the *emergent action unit* as the asymptotic action-variance density

$$\hbar_{\text{eff}} := \lim_{\xi\to\infty} \frac{\text{Var}_{\mathcal{E}_\xi}[S]}{N_\xi}, \tag{9}$$

and the coarse-grained path measure

$$\mathcal{Z} = \int \mathcal{D}(\text{fields})\ \exp\Big\{ - \frac{S_\Phi[g,\Phi] + S_{\text{matter}} + S_{\text{gauge}}}{\hbar_{\text{eff}}} \Big\}, \tag{10}$$

with boundary/regularity conditions inherited from the stabilized domain [98,102]. Kinematically, Poisson brackets of gauge-invariant functionals F, G are defined leafwise via the Peierls prescription. In stabilized domains, equal-time commutators on $\mathcal{H}[\Sigma_\tau]$ obey

$$[\widehat{F}, \widehat{G}] = i\hbar_{\text{eff}}\{F, G\}_{\text{P}} + O(\|\nabla\Phi\|), \tag{11}$$

so the canonical algebra is recovered in the strong-stabilization limit ($\nabla\Phi \to 0$ at the scales of interest) [37,96]. Together with (19), this underpins the uncertainty relations and the quantum corrections summarized in §7.

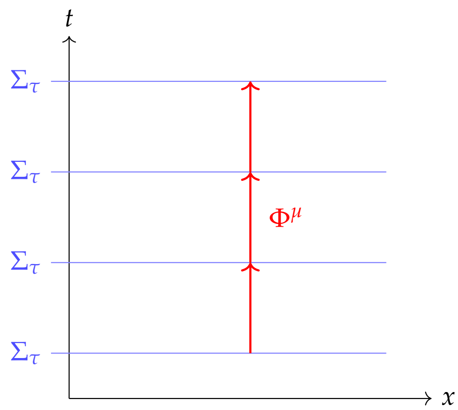

Figure 1. Chronon field Φ^μ defining stabilized leaves Σ_τ as spatial slices orthogonal to the flow.

2.4. EFT and Power Counting

Beyond the two-derivative truncation, the low-energy action on stabilized domains reads

$$S_{\text{eff}} = \int \sqrt{-g}\Big[\frac{M_{\text{P}}^2}{2}R - \frac{1}{4}\kappa_A F^2 + \mathcal{L}_\Phi^{(2)}[g,\Phi] + \sum_i \alpha_i\, \mathcal{O}_i^{(2)}[g,\Phi] + \frac{1}{\Lambda^2}\sum_j d_j\, \mathcal{O}_j^{(4)}[g,\Phi,A] + \cdots\Big],$$

where $\mathcal{O}_i^{(2)}$ are æther-like two-derivative invariants built from Φ (shear, expansion, acceleration) and $\mathcal{O}_j^{(4)}$ are higher-derivative operators. On stabilized leaves with small $|\nabla\Phi|$, $\mathcal{O}_i^{(2)}$ are naturally

Preprints.org (www.preprints.org) | NOT PEER-REVIEWED | Posted: 19 September 2025 doi:10.20944/preprints202509.1667.v1

suppressed, while $\mathcal{O}_j^{(4)}$ scale as $(E/\Lambda)^2$. This organizes deviations from GR in a controlled expansion [28,42,73,117].

3. Emergent $\mathrm{U}(1)$ from Chronon Holonomy

3.1. Holonomy Phase and Connection

We work on a stabilized domain (cf. §2.1). Parallel transport of the unit timelike field Φ along smooth curves $\gamma \subset \Sigma_\tau$ (with Levi–Civita connection of g) induces a rotation in the two–plane orthogonal to Φ. This defines a principal $\mathrm{SO}(2) \simeq \mathrm{U}(1)$ bundle over each leaf [50,77,88]. Locally on a chart $U \subset \Sigma_\tau$, choose a smooth section and let $\theta : U \to \mathbb{R}/2\pi\mathbb{Z}$ be the associated *holonomy phase*. We then define a spacetime one–form whose leafwise pullback equals the leaf connection:

$$A_\mu \, \mathrm{d}x^\mu \big|_U := \mathrm{d}\theta \big|_U, \qquad \text{i.e.} \qquad A_\mu := \partial_\mu \theta \quad \text{(locally)}. \tag{12}$$

A change of section shifts $\theta \mapsto \theta + \alpha$ for some smooth α, hence

$$A_\mu \;\mapsto\; A_\mu + \partial_\mu \alpha, \tag{13}$$

and the curvature two–form is the exterior derivative

$$F_{\mu\nu} \;:=\; \partial_\mu A_\nu - \partial_\nu A_\mu \;=\; (\mathrm{d}A)_{\mu\nu}, \tag{14}$$

which coincides with the holonomy two–form of the induced $\mathrm{U}(1)$ bundle on each leaf [77,89,125]. In covariant notation we write $F = \mathrm{d}A$ and raise indices with the emergent metric $g_{\mu\nu}$ [116]. A geometric phase interpretation of θ aligns with Berry's phase in adiabatic settings [20] (here realized leafwise by the chronon fiber).

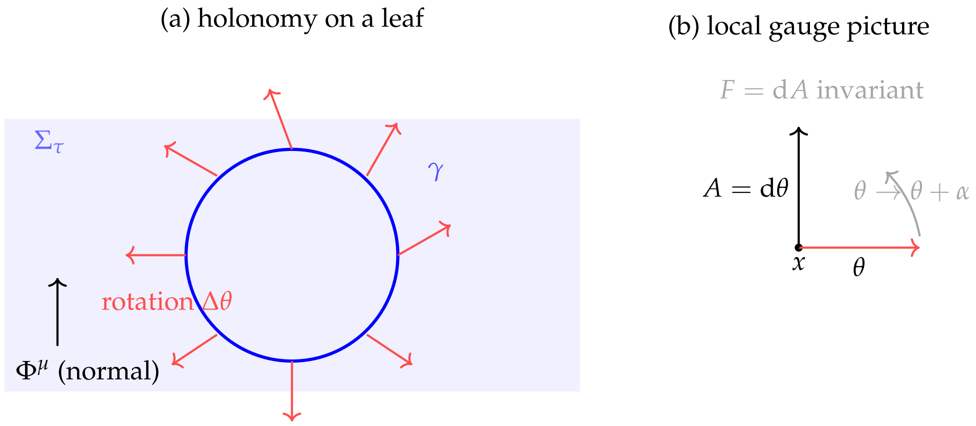

Figure 2. Emergent $\mathrm{U}(1)$ from chronon holonomy. **(a)** On a stabilized spatial leaf Σ_τ, transporting the local orthonormal frame once around a closed loop γ produces a net rotation of the transverse basis vectors by an angle $\Delta\theta$. This angle records the holonomy of the connection induced by the chronon flow, and defines a compact phase variable identified modulo 2π. The normal vector Φ^μ indicates the timelike direction singled out by the chronon field. **(b)** In the local gauge description, the rotation angle θ serves as a coordinate on the internal $\mathrm{U}(1)$ fiber. Its derivative $A = \mathrm{d}\theta$ acts as the Abelian gauge potential, and a gauge shift $\theta \to \theta + \alpha$ changes A by a pure gradient while leaving the curvature $F = \mathrm{d}A$ invariant. In this way, the geometric holonomy of chronon transport is reinterpreted as an emergent electromagnetic $\mathrm{U}(1)$ gauge symmetry.

3.2. Gauge Invariance and Maxwell Limit

Under $A_\mu \mapsto A_\mu + \partial_\mu \alpha$, the curvature $F_{\mu\nu}$ is invariant. In the canonical normalization (after $A_\mu \to A_\mu^{\mathrm{can}} = \sqrt{\kappa_A}\, A_\mu$), the minimal diffeomorphism– and gauge–invariant action for the Abelian sector on $(\mathcal{M}, g_{\mu\nu}[\Phi])$ is

$$S_{\mathrm{gauge}}[A; g] \;=\; -\frac{1}{4} \int F_{\mu\nu} F^{\mu\nu} \sqrt{-g}\, \mathrm{d}^4 x, \tag{15}$$

Preprints.org (www.preprints.org) | NOT PEER-REVIEWED | Posted: 19 September 2025 doi:10.20944/preprints202509.1667.v1

whose variation with respect to A_ν yields the source–free Maxwell equations on the emergent geometry:

$$\nabla_\mu F^{\mu\nu} = 0, \qquad \text{together with} \qquad \nabla_{[\lambda} F_{\mu\nu]} = 0, \tag{16}$$

the latter being the Bianchi identity ($\mathrm{d}F = 0$) [70,116]. Coupling to matter proceeds by minimal substitution on the relevant bundles (e.g. the soliton bundle of §5), giving $\nabla_\mu F^{\mu\nu} = J^\nu$ with $\nabla_\nu J^\nu = 0$ as the Noether current conservation law for the $\mathrm{U}(1)$ gauge symmetry [92,98]. In the infrared, the dynamics are Maxwellian with two transverse polarizations; the photon corresponds to a Goldstone–like fluctuation of the internal time–phase encoded by θ [10].

Reference Maxwell limit on stabilized domains.

A precise EFT statement quantifying when (15) governs the dynamics is given in Appendix L, Proposition A3. On twist–free, slowly varying backgrounds $\bar{\Phi}^\mu$ ("stabilized domains"), one finds

$$S_{\text{gauge}}[A] = -\frac{\kappa_A}{4}\int \sqrt{-g}\, F_{\mu\nu}F^{\mu\nu} + \Delta S[A], \qquad \text{cf. (A109)}, \tag{17}$$

with deviations organized by the small parameters $\varepsilon_{\nabla\Phi} = \|\nabla\bar{\Phi}\|/\Lambda$, $\varepsilon_R = \|\text{Riem}\|/\Lambda^2$, and $\delta = k/\Lambda$, as well as any æther–like couplings α_i:

$$\nabla_\mu F^{\mu\nu} = J^\nu + \mathcal{O}(\alpha_i) + \mathcal{O}(\varepsilon_{\nabla\Phi}^2) + \mathcal{O}(\varepsilon_R) + \mathcal{O}(\delta^2), \qquad \text{cf. (A111)}. \tag{18}$$

The leading non–Maxwell operators in ΔS are æther–like parity–even contractions $(\bar{\Phi}\cdot F)^2$ and $\bar{\Phi}\bar{\Phi}FF$, and higher–derivative/curvature terms such as $(\nabla F)^2/\Lambda^2$ and $R\,F^2/\Lambda^2$ (see (A110)); their coefficients are suppressed by $\mathcal{O}(\alpha_i)$, $\mathcal{O}(\varepsilon_{\nabla\Phi}^2)$, $\mathcal{O}(\varepsilon_R)$, and $\mathcal{O}(\delta^2)$, respectively. Hence birefringence and anisotropy effects are parametrically small on stabilized domains (consistent with photon–sector bounds, cf. [78,79]).

4. Covariant Local Mass/Energy Density

A central requirement for any background–independent field theory that aims to reproduce relativistic matter and interactions is a covariant and observer–independent notion of mass/energy density [63,116]. In Chronon Field Theory (CFT), this role is played by the scalar quantity

$$\rho(x) := T_{\mu\nu}(x)\,\Phi^\mu(x)\Phi_\mu(x), \tag{19}$$

defined pointwise on stabilized domains. Equation (19) has three immediate virtues: (i) it is manifestly covariant, depending only on the stress tensor $T_{\mu\nu}$ and the dynamical timelike unit vector Φ; (ii) it reduces to the conventional energy density T^{00} in the comoving frame aligned with Φ [81]; and (iii) it is intrinsically nonnegative and conserved under mild regularity conditions, as we prove below.

Assumption 1 (Regular domain)**.** *Solutions of the CFT field equations admit stabilized leaves Σ_τ with induced metric $g_{\mu\nu}$ and smooth stress tensor $T_{\mu\nu}$. Moreover, the Lagrangian density is invariant under flow along Φ (quasi–stationarity):*

$$\mathcal{L}_\Phi\big(\sqrt{-g}\,\mathcal{L}_\Phi\big) = 0$$

on the domain.

The quasi–stationarity condition expresses the fact that translations along the chronon flow Φ act as an isometry of the stabilized domain, ensuring that the associated Noether current [92] coincides with the natural energy current. This parallels the role of Killing vectors in conventional general relativity [116], but here arises dynamically from the unit–norm constraint and stabilization.

Theorem 1 (Positivity and conservation of ρ)**.** *Let* **??** *1 hold and assume the induced dominant energy condition (DEC), i.e.*

$$T_{\mu\nu}v^{\mu}w^{\nu} \geq 0 \quad \textit{for all future–directed causal } v^{\mu}, w^{\nu}.$$

Then on any stabilized leaf Σ_τ*:*

(i) $\rho = T_{\mu\nu}\Phi^{\mu}\Phi_{\mu} \geq 0$;

(ii) *the energy current* $J^{\mu} := T_{\mu\nu}\Phi_{\nu}$ *is conserved,* $\nabla_{\mu}J^{\mu} = 0$;

(iii) *consequently, the total mass*

$$\mathsf{M}(\tau) := \int_{\Sigma_\tau} \rho \, \mathrm{d}^3x \tag{20}$$

is finite for finite–energy data and independent of the leaf label τ*.*

Proof. *(i) Positivity.* Since Φ^{μ} is a future–directed unit timelike vector, the induced DEC immediately yields

$$T_{\mu\nu}\Phi^{\mu}\Phi_{\mu} \geq 0,$$

establishing $\rho \geq 0$ pointwise [63,116].

(ii) Conservation. Diffeomorphism invariance of the CFT action ensures $\nabla_{\mu}T_{\mu\nu} = 0$ [92]. Contracting with Φ_{ν} gives

$$\nabla_{\mu}J^{\mu} = \nabla_{\mu}(T_{\mu\nu}\Phi_{\nu}) = (\nabla_{\mu}T_{\mu\nu})\Phi_{\nu} + T_{\mu\nu}\nabla_{\mu}\Phi_{\nu}.$$

The first term vanishes on shell. The second term vanishes under **??** 1: invariance under Φ–flow identifies J^{μ} as the Noether current associated to translations along Φ, hence conserved [92,116].

(iii) Leaf–independence of $\mathsf{M}(\tau)$. Integrate $\nabla_{\mu}J^{\mu} = 0$ over the spacetime slab bounded by two leaves Σ_{τ_1} and Σ_{τ_2} and apply the divergence theorem [53]:

$$0 = \int_{\mathcal{V}} \nabla_{\mu}J^{\mu}\sqrt{-g}\,\mathrm{d}^4x = \int_{\Sigma_{\tau_2}} J^{\mu}n_{\mu}\,\mathrm{d}^3x - \int_{\Sigma_{\tau_1}} J^{\mu}n_{\mu}\,\mathrm{d}^3x + \int_{\mathcal{T}} J^{\mu}n_{\mu}\,\mathrm{d}^3\sigma.$$

Here n^{μ} is the unit normal to the integration surfaces, and $\mathcal{T}$ denotes the timelike boundary of the slab. On Σ_τ, $n^{\mu} = \Phi^{\mu}$, so the flux reduces to ρ as in (20). The boundary term over $\mathcal{T}$ vanishes for finite–energy configurations by the assumed decay of fields. Thus

$$\mathsf{M}(\tau_2) = \mathsf{M}(\tau_1),$$

proving constancy of the total mass across leaves. □

Remarks.

- The functional $\mathsf{M}(\tau)$ furnishes a covariant, background–independent definition of inertial and gravitational mass in CFT, reducing to the ADM mass [9] in asymptotically flat settings where Φ aligns with the asymptotic time translation.
- Unlike canonical Hamiltonian formulations, no reference to a preferred coordinate system is required: the chronon flow Φ supplies the intrinsic time direction and defines the foliation $\{\Sigma_\tau\}$.
- The conservation of $\mathsf{M}(\tau)$ ensures stability of solitonic excitations and provides the basis for identifying the rest mass $M_{w=1}$ in topological sectors (Section 5).

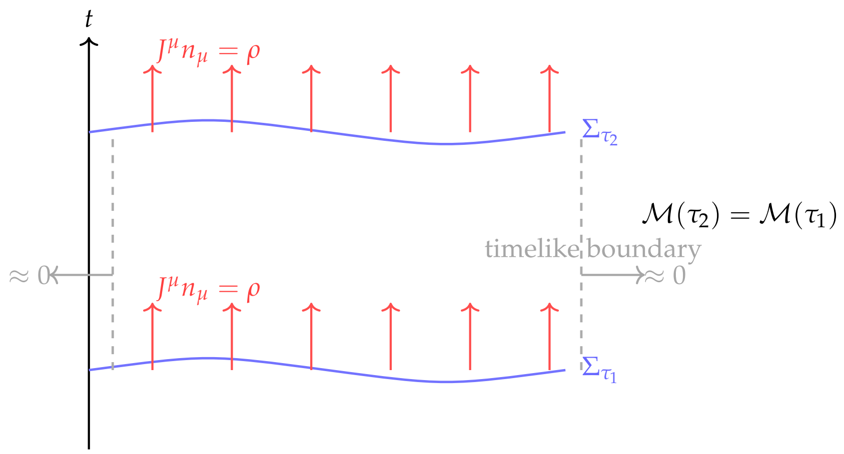

Figure 3. Covariant mass and conserved flux in Chronon Field Theory. The diagram shows a spacetime slab bounded by two stabilized spatial leaves Σ_{τ_1} and Σ_{τ_2} (blue curves) and vertical timelike boundaries (dashed gray lines). The energy current $J^\mu = T^{\mu\nu}\Phi_\nu$ flows across the leaves with flux density $J^\mu n_\mu = \rho$ (red arrows). Because the flux through Σ_{τ_1} and Σ_{τ_2} is equal, and because finite–energy configurations produce negligible flux through the timelike boundaries, the total mass functional $\mathcal{M}(\tau) = \int_{\Sigma_\tau} \rho\, \mathrm{dvol}_h$ is conserved between leaves: $\mathcal{M}(\tau_2) = \mathcal{M}(\tau_1)$. This figure provides a geometric visualization of the conservation law proved in Appendix A: the red vertical arrows depict the flow of energy density across the slices, while the gray side arrows vanish, ensuring that the integrated mass remains constant across time.

5. Solitonic Matter: Existence and Properties

In Chronon Field Theory, localized matter excitations are not introduced as independent quantized fields but arise as *topologically stable solitons* of the chronon field Φ. These solitons correspond to nontrivial elements of the homotopy group $\pi_3(S^3)$ [61], ensuring stability under smooth deformations. In this section we define the relevant configuration and moduli spaces, establish existence of finite–energy minimizers in the nontrivial sector $w = 1$, and outline their inertial properties and quantization.

Functional setting.

Throughout this section we work in the Sobolev class $H^1(\Sigma; S^3)$ at fixed topological degree w, with the Skyrme-type energy described below. The precise function spaces, constraints, and the existence result for the $w = 1$ sector are summarized in Appendix M.

5.1. Topological Sectors and Configuration Spaces

To define solitonic sectors we impose asymptotic boundary conditions. On each stabilized leaf $\Sigma_\tau \cong \mathbb{R}^3$, we require

$$\Phi^\mu(x) \to (1,0,0,0) \quad \text{as } |x| \to \infty, \tag{21}$$

so that spatial infinity is compactified to a point. This compactification identifies $\mathbb{R}^3 \cup \{\infty\} \cong S^3$, and the unit–norm constraint $\Phi^\mu\Phi_\mu = -1$ restricts the target space of Φ to $S^3 \subset \mathbb{R}^4$. Thus any static configuration defines a continuous map

$$\Phi : S^3 \longrightarrow S^3.$$

Such maps are classified by the winding number

$$w \in \pi_3(S^3) \cong \mathbb{Z}[61],$$

which serves as a topological charge. Physically, w measures how many times the spatial slice wraps around the unit hyperboloid of admissible chronon vectors.

Configuration and Moduli Spaces

For each $w \in \mathbb{Z}$, define the configuration space

$$\mathcal{C}_w := \left\{ \Phi \in C^\infty(S^3, S^3) \,\middle|\, \deg(\Phi) = w \right\}, \tag{22}$$

i.e. smooth finite–energy chronon fields with topological charge w. The corresponding moduli space is

$$M_w := \mathcal{C}_w / \big(\mathrm{Diff}_0(\Sigma_\tau) \times \mathrm{Gauge}(\Phi)\big), \tag{23}$$

where $\mathrm{Diff}_0(\Sigma_\tau)$ denotes diffeomorphisms connected to the identity and $\mathrm{Gauge}(\Phi)$ denotes residual internal symmetries preserving the unit–norm constraint. M_w parametrizes physically inequivalent solitons [86].

By the existence result established in Appendix M for $w = 1$, we may fix a minimizer Φ_* in the admissible class and analyze its properties.

Theorem 2 (Existence of a finite–energy minimizer for $w = 1$)**.** *Let the CFT couplings* $(\alpha_1, \alpha_2, \alpha_3, \gamma)$ *satisfy the coercivity and regularity conditions of Assumption 1, and impose boundary condition (21). Then the energy functional*

$$E[\Phi] = \int_{\Sigma_\tau} \rho \, \mathrm{d}^3 x \tag{24}$$

admits a smooth finite–energy minimizer in the topological class $w = 1$*. This minimizer is stable against small perturbations.*

Strategy. The proof follows the direct method in the calculus of variations [45,110]:

(a) *Coercivity.* Gradient and curvature terms in the CFT action provide a coercive bound $E[\Phi] \gtrsim \|\nabla\Phi\|^2_{L^2}$, preventing loss of compactness.

(b) *Lower semicontinuity.* The integrand of (24) is convex in $\nabla\Phi$, implying weak lower semicontinuity of E on H^1.

(c) *Compactness.* By Rellich's theorem, minimizing sequences admit weakly convergent subsequences modulo spatial translations and gauge rotations [45].

(d) *Topological constraint.* The winding number w is preserved under weak convergence in H^1, ensuring the limit lies in $\mathcal{C}_1$ [61].

(e) *Regularity.* Standard elliptic estimates upgrade weak minimizers to smooth solutions of the Euler–Lagrange equations [54].

Positivity of ρ (Theorem 1) ensures finite energy, while the second variation of E is nonnegative in directions tangent to $\mathcal{C}_1$, guaranteeing stability under small perturbations [86]. □

 doi:10.20944/preprints202509.1667.v1

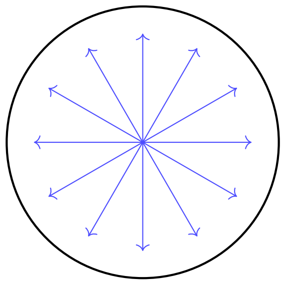

$w = 1$ soliton (hedgehog configuration)

Figure 4. Schematic illustration of a unit–charge ($w = 1$) soliton. The chronon field Φ is constrained to have unit norm and thus maps spatial infinity to a fixed point on the internal target space S^3. A representative configuration is shown as a *hedgehog map*, where spatial directions (arrows radiating outward) are aligned with internal directions of Φ. As one traverses the enclosing S^2 in real space, the field winds exactly once around a great circle of S^3, realizing topological degree one. This winding number protects the soliton from decay into the trivial vacuum. The hedgehog pattern is a canonical visualization of how topological charge is encoded in the spatial profile of the chronon field.

5.2. Rest Mass and Collective Modes

The rest mass of the fundamental soliton is defined by evaluating the conserved mass functional (Section 4) on the $w = 1$ minimizer:

$$M_{w=1} := \int_{\Sigma_\tau} \rho[\Phi_{w=1}]\, \mathrm{d}^3x. \tag{25}$$

This provides the intrinsic inertial/gravitational mass of the soliton, independent of the foliation label τ.

Collective Coordinates

The moduli space M_1 admits low–energy deformations corresponding to translations, global $U(1)$ phase rotations, and internal isorotations. Quantization of these modes proceeds via the collective–coordinate method [7,86]: one promotes the moduli parameters to slowly varying quantum degrees of freedom, substitutes into the action, and derives an effective Hamiltonian. For a single internal rotor with moment of inertia I, the leading energy splitting scales as

$$\Delta E \sim \frac{\hbar_{\mathrm{eff}}^2}{2I}. \tag{26}$$

This scaling parallels that of Skyrmion quantization in nuclear physics [7,106], but here $\hbar_{\mathrm{eff}}$ is the emergent action unit derived from chronon microdynamics (Appendix L).

Remark (uniqueness and spectrum in w=1).

Under the hypotheses of Theorem 2 the w=1 sector admits at least one smooth, finite–energy minimizer. In the minimal CFT (two–derivative, stabilized domain) we expect this minimizer to be *unique up to symmetries* [86]: translations in $\mathbb{R}^3$, a global U(1) phase, and (only if the profile is not spherically symmetric) spatial rotations. Formally, let $\mathbb{L}$ denote the second–variation (Hessian) operator around the minimizer $\Phi_\star$; then the Morse index is zero and

$$\ker \mathbb{L} = \mathrm{span}\{\partial_{x^i}\Phi_\star\ (i = 1,2,3),\ \partial_\theta\Phi_\star,\ \mathcal{R}_a\Phi_\star\ (a = 1,2,3 \text{ iff } \Phi_\star \text{ breaks } SO(3))\},$$

with ∂_θ the global U(1) zero mode and $\mathcal{R}_a$ the generators of infinitesimal spatial rotations. Quantization of the corresponding collective coordinates, together with low–lying vibrational modes (eigenfunctions of $\mathbb{L}$ with small positive eigenvalues), produces an excitation tower *within* the w=1 sector [7,86]; all such states carry the same topological/electric charge q_0. Multiple local minima ("isomers") in w=1 can exist for special choices of couplings (α_i, γ); these would constitute distinct solitonic species sharing w=1 and charge q_0 but differing in mass and internal structure.

Summary

The existence of stable $w = 1$ solitons, their identification with localized lumps of conserved mass M, and the quantization of their collective modes together establish a concrete mechanism by which fermionic matter arises in CFT. The spin–statistics connection will be demonstrated in Section 6, completing the interpretation of solitons as particle–like excitations with spin–$\frac{1}{2}$ and Fermi–Dirac statistics.

6. Spin–Statistics via FR/Berry and Bundle Matching

The emergence of fermionic behavior in CFT rests on the topology of the soliton moduli space M_1 and its associated quantum bundle. The central fact is that both a 2π spatial rotation of a single soliton and the exchange of two identical solitons correspond to nontrivial loops in configuration space, carrying a $\mathbb{Z}_2$ holonomy. Quantization over this space therefore enforces spin-$\frac{1}{2}$ transformation properties and Fermi–Dirac statistics. We formalize this statement below.

6.1. Topology of M_1 and Exchange Space

Let M_1 denote the moduli space of static finite–energy solitons with topological charge $w = 1$, modulo diffeomorphisms and residual gauge transformations. Standard results on Skyrme–type solitons [47,86] adapt directly: the boundary condition $\Phi^\mu \to (1,0,0,0)$ at spatial infinity fixes an internal reference frame, and the residual action of SO(3) on spatial coordinates induces a nontrivial π_1.

$$\pi_1(M_1) \;\cong\; \mathbb{Z}_2. \tag{27}$$

The nontrivial loop corresponds to a 2π spatial rotation of the soliton, which cannot be continuously deformed to the identity without violating the topological constraint [47].

Similarly, consider the unordered two–soliton configuration space

$$C(2) := \left\{ (\Phi_1, \Phi_2) \in \mathcal{C}_1 \times \mathcal{C}_1 \;\middle|\; \Phi_1 \neq \Phi_2 \right\} \Big/ \mathfrak{S}_2,$$

where $\mathfrak{S}_2$ permutes the solitons. One finds

$$\pi_1(C(2)) \;\cong\; \mathbb{Z}_2, \tag{28}$$

with the nontrivial loop given by exchanging two identical solitons along a closed trajectory in configuration space [88]. This exchange loop is homotopically distinct from the trivial path and represents the generator of $\mathbb{Z}_2$.

Theorem 3 (FR/Berry fermionic sector)**.** *A 2π spatial rotation of a single soliton and the exchange loop of two identical solitons each represent the nontrivial element of $\pi_1(M_1) \cong \pi_1(C(2)) \cong \mathbb{Z}_2$. Quantization over the corresponding Hilbert bundle assigns a -1 holonomy to these loops, so soliton wavefunctionals transform as spin-$\frac{1}{2}$ objects under rotation and acquire a minus sign under exchange. Thus the $w = 1$ solitons exhibit Fermi–Dirac statistics.*

Sketch. The argument follows the Finkelstein–Rubinstein (FR) construction [47,48]. Quantization is defined not on configuration space $\mathcal{C}_1$ itself but on its universal cover $\widetilde{\mathcal{C}}_1$. Wavefunctionals Ψ are required to satisfy the FR constraint

$$\Psi(\gamma \cdot \Phi) = \chi(\gamma)\, \Psi(\Phi),$$

 doi:10.20944/preprints202509.1667.v1

for any loop $\gamma \in \pi_1(\mathcal{C}_1)$, where $\chi : \pi_1(\mathcal{C}_1) \to \{\pm 1\}$ is a one–dimensional representation. Since $\pi_1(M_1) \cong \mathbb{Z}_2$, there are two possible representations; physical consistency with the Berry phase calculation below selects the nontrivial representation. Thus $\chi(\gamma) = -1$ for the generator, enforcing fermionic behavior. In particular, a 2π rotation or an exchange loop both generate γ, yielding the minus sign. □

6.2. Berry Connection and Bundle Matching

The FR sign can be identified with a geometric phase arising from parallel transport of soliton states along loops in configuration space. This provides a bridge between the topological classification and the emergent gauge structure of CFT.

Proposition 1 (Bundle–matching)**.** *Let A be the emergent spacetime* $\mathrm{U}(1)$ *connection defined in Section 3. Consider the soliton configuration bundle $\pi : \mathcal{B} \to M_1$ whose fiber carries soliton wavefunctionals. Then the pullback $\pi^* A$ reproduces the FR $\mathbb{Z}_2$ holonomy class: transport around the nontrivial loop of $\pi_1(M_1)$ accumulates a Berry phase of π. Consequently, the geometric phase along an exchange loop is exactly -1, matching the fermionic sector of Theorem 3.*

Sketch. On stabilized domains, the emergent $\mathrm{U}(1)$ connection A is locally given by $A_\mu = \partial_\mu \theta$ for the chronon holonomy phase θ. When restricted to soliton configurations, θ is defined modulo 2π, so transport around a loop $\gamma \in \pi_1(M_1)$ yields

$$\oint_\gamma A = \Delta\theta = \pi \pmod{2\pi}.$$

This corresponds to a Berry phase $\exp(i\pi) = -1$ [20,105]. Thus the pullback bundle $(\mathcal{B}, \pi^* A)$ carries exactly the nontrivial $\mathbb{Z}_2$ holonomy of the FR construction. The consistency of the two perspectives—topological (FR) and geometric (Berry phase)—establishes the equivalence of spin-$\frac{1}{2}$ statistics with the holonomy of the emergent gauge sector. □

(Computed numerically: $N = 32$, $L = 6$, $N_\varphi = 60$, anisotropy $= 2.0$; see Appendix L for Maxwell-limit details and Appendix D–D.5 for the convergence study, yielding $\gamma_B = \pi \pm \Delta_{\mathrm{num}}$.)

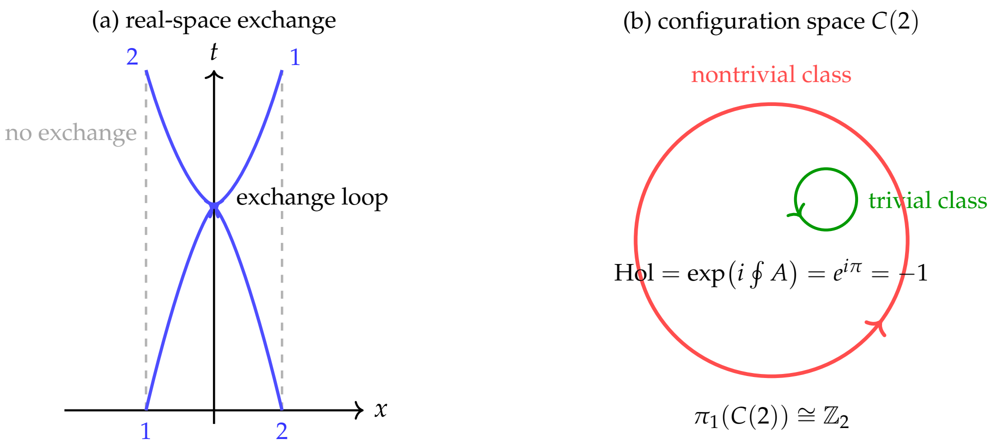

Figure 5. Exchange statistics from soliton worldlines and configuration–space topology. **(a)** In real spacetime, two identical solitons follow worldlines (blue curves) that braid around one another as time flows upward. This exchange path cannot be continuously deformed to the trivial "no-exchange" case (gray dashed vertical lines) without the worldlines crossing, so it defines a distinct loop, the *exchange loop*. **(b)** In the two-particle configuration space $C(2)$, the exchange corresponds to a nontrivial loop in $\pi_1(C(2)) \cong \mathbb{Z}_2$. The trivial class (green) represents no exchange, while the nontrivial class (red) represents a full braid of the two particles. On the soliton ground-state line bundle, the Berry connection assigns holonomy $\mathrm{Hol} = \exp(i \oint A) = e^{i\pi} = -1$ to the nontrivial loop. This geometric phase is precisely the fermionic minus sign: exchanging two identical w=1 solitons multiplies the wavefunction by -1. The figure therefore demonstrates the emergence of *Fermi–Dirac statistics* from the FR/Berry mechanism in Chronon Field Theory, showing that solitons behave as fermions due to topological and geometric phases.

Summary

The FR constraint and Berry holonomy coincide in CFT: the nontrivial topology of soliton moduli space enforces a $\mathbb{Z}_2$ representation, while the emergent $\mathrm{U}(1)$ gauge connection provides the geometric mechanism by which wavefunctionals accumulate a π phase. Together these results prove that $w = 1$ solitons behave as fermions, thereby establishing the spin–statistics connection intrinsically within the chronon framework.

7. Quantum Corrections and $\hbar_{\mathrm{eff}}$

Chronon Field Theory (CFT) is formulated as a classical background–independent field theory, but coarse–graining of microscopic chronon dynamics induces an emergent action unit $\hbar_{\mathrm{eff}}$ (Appendix L). This provides the natural scale controlling quantum fluctuations, operator commutators, and spectral splittings of solitonic states. In this section we summarize the operator algebra on stabilized leaves, the path integral measure, and consequences for the low–lying excitation spectrum.

7.1. Leafwise Operator Algebra

On a stabilized leaf Σ_τ, Poisson brackets of gauge–invariant functionals F, G of $(\Phi, \nabla\Phi)$ are defined by the Peierls prescription [36,96]. Quantization proceeds by promoting these to operators $\hat{F}, \hat{G}$ on the Hilbert space $\mathcal{H}[\Sigma_\tau]$. The commutator is

$$[\hat{F}, \hat{G}] = i\,\hbar_{\mathrm{eff}}\,\{F, G\}_P + \mathcal{O}(\|\nabla\Phi\|), \tag{29}$$

where $\{\cdot,\cdot\}_P$ denotes the Peierls bracket. The corrections vanish in the strong–stabilization limit $\|\nabla\Phi\| \to 0$, so that (29) reduces to the canonical equal–time algebra [41]. This provides the CFT analogue of canonical quantization, with $\hbar_{\mathrm{eff}}$ replacing Planck's constant [99].

7.2. Path Integral and Weighting

The coarse–grained path measure for fields and solitons on a stabilized domain $\mathcal{D}$ is

$$Z[\mathcal{D}] = \int_{\mathcal{D}} \mathcal{D}\Phi\, \mathcal{D}A\, \exp\left\{-\frac{1}{\hbar_{\text{eff}}}\left(S_\Phi[\Phi] + S_{\text{gauge}}[A;\Phi] + S_{\text{int}}[\Phi, A]\right)\right\}, \tag{30}$$

with boundary and regularity conditions imposed by stabilization. Here S_Φ is the chronon action, S_{gauge} the emergent $U(1)$ sector action, and S_{int} the minimal coupling term. The weighting $e^{-S/\hbar_{\text{eff}}}$ identifies $\hbar_{\text{eff}}$ as the fundamental loop–expansion parameter: perturbative corrections to classical saddle points are organized by powers of $\hbar_{\text{eff}}$ [46,118].

7.3. Implications for Spectra

Solitonic excitations in topological sectors $w \neq 0$ acquire quantum corrections determined by (29)–(30). Two main effects are:

Collective Coordinate Quantization

As described in Section 5, collective modes (translations, internal $U(1)$ rotations, isorotations) are promoted to quantum variables. Their spectra exhibit splittings

$$\Delta E \sim \frac{\hbar_{\text{eff}}^2}{2I}, \tag{31}$$

where I is the relevant moment of inertia of the soliton configuration. This parallels Skyrmion quantization in nuclear physics [7,86] and provides a systematic expansion for low–lying rotational and vibrational states.

Zero–point and loop corrections.

Fluctuations around the classical minimizer $\Phi_{w=1}$ contribute a zero–point energy shift of order $\hbar_{\text{eff}}$, while higher–loop corrections are suppressed by higher powers of $\hbar_{\text{eff}}$. Thus the semiclassical expansion is controlled provided the soliton rest mass $M_{w=1}$ satisfies $M_{w=1} \gg \hbar_{\text{eff}}$ [34].

7.4. Summary

The emergent action unit $\hbar_{\text{eff}}$ plays the same structural role in CFT as Planck's constant in conventional quantum theory: it controls commutators, governs the weighting of histories, and determines the scale of spectral splittings. Crucially, however, $\hbar_{\text{eff}}$ arises dynamically from chronon microdynamics rather than being postulated. This makes quantum corrections a derived rather than fundamental feature, tying the quantization of solitonic matter and gauge modes directly to the statistical mechanics of the underlying temporal field.

8. Emergent Fundamental Constants: $\hbar_{\text{eff}}$, G, e, and c

In this framework the familiar constants of Nature — Planck's constant $\hbar$, Newton's constant G, the electric charge e, and the speed of light c — are not postulated but appear as emergent normalizations of the effective long–wavelength action [102,117].

Effective action.

At low energies the chronon field induces an effective action of the form

$$S_{\text{eff}} = \int \sqrt{-g}\left[\frac{M_P^2}{2}R - \frac{1}{4}F_{\mu\nu}F^{\mu\nu} + \mathcal{L}_{\text{matter}}(\Phi, \nabla\Phi; A)\right], \tag{32}$$

with emergent coefficients to be identified [23,94].

Preprints.org (www.preprints.org) | NOT PEER-REVIEWED | Posted: 19 September 2025 doi:10.20944/preprints202509.1667.v1

8.1. Planck's Constant $\hbar_{\rm eff}$

As shown in Section 7 and derived in Appendix F, path weights acquire the factor $e^{-S/\hbar_{\rm eff}}$ upon coarse–graining chronon fluctuations. Thus

$$\hbar_{\rm eff} \;\sim\; E_c\,\tau_c, \tag{33}$$

the product of the characteristic chronon energy $E_c = \ell_\Phi^{-1}$ and microscopic temporal spacing τ_c. Identifying $\ell_\Phi \sim \ell_P$ and $\tau_c \sim t_P$ recovers the observed Planck constant [99].

8.2. Newton's Constant G

The coefficient of the Einstein–Hilbert term is generated either directly through the $\gamma R_{\mu\nu}\Phi^\mu\Phi^\nu$ coupling or radiatively by integrating out chronon fluctuations (Sakharov mechanism) [8,23,94,102,114]. In both cases

$$M_{\rm P}^2 \;\equiv\; \frac{1}{8\pi G}, \tag{34}$$

with $M_{\rm P}^2$ determined by the chronon couplings and cutoff scale; see Appendix G for heat–kernel details and induced coefficients.

8.3. Electric Charge e and the Coulomb Law

The emergent $\mathrm{U}(1)$ gauge field arises as a holonomy of Φ. Its kinetic term is normalized as $-\frac{\kappa_A}{4}F_{\mu\nu}F^{\mu\nu}$. A rescaling $A_\mu^{\rm can} = \sqrt{\kappa_A}\,A_\mu$ puts this in canonical Maxwell form [70,98]. Solitons couple to A with bare topological charge q_0 fixed by the FR/Berry class, so the observed elementary charge is

$$e \;=\; \frac{q_0}{\sqrt{\kappa_A}}. \tag{35}$$

In the static limit, the gauge equation reduces to a Poisson equation, whose Green's function yields a $1/r$ potential. For two solitons at separation r,

$$V(r) = \frac{q_1 q_2}{4\pi\,\kappa_A}\,\frac{1}{r} = \frac{e_1 e_2}{4\pi}\,\frac{1}{r}, \tag{36}$$

reproducing the Coulomb law in Heaviside–Lorentz units [70]. Thus the observed Coulomb constant (or equivalently $\alpha_{\rm em} = e^2/(4\pi)$) directly constrains the holonomy stiffness:

$$\kappa_A = \frac{q_0^2}{4\pi\,\alpha_{\rm em}}. \tag{37}$$

For the fundamental soliton $q_0 = 1$ and $\alpha_{\rm em}^{-1} \simeq 137.036$, this gives $\kappa_A \simeq 10.9$ [70,111]. Details of the derivation are provided in Appendix J.

8.4. Speed of Light c

The chronon foliation defines a natural $(3+1)$ decomposition with projector $h_{\mu\nu} = g_{\mu\nu} + \bar{\Phi}_\mu\bar{\Phi}_\nu$. Quadratic expansions of both the Goldstone phase θ and transverse–traceless graviton fluctuations yield wave equations of the form $\rho\,\ddot{\psi} - K\,\Delta_h\psi = 0$, with phase speed

$$c^2 \;=\; \frac{K}{\rho}. \tag{38}$$

In the stabilized, hypersurface–orthogonal regime, the coefficients for the θ and graviton sectors coincide, ensuring a universal limiting velocity

$$c \;=\; \sqrt{K_\theta/\rho_\theta} \;=\; \sqrt{K_g/\rho_g}. \tag{39}$$

Equivalently, c is set by the ratio of chronon microparameters, $c = \ell_\Phi/\tau_c$, and calibrates the conversion between spatial and temporal units [72,73,116]. The detailed derivation is given in Appendix I.

8.5. Inferring CFT Microparameters from Observed $(\hbar, G, e, c)$

We collect the emergent relations (natural units $\hbar = c = 1$ unless stated):

$$\text{(i)} \quad \hbar_{\text{eff}} \sim E_c\,\tau_c, \qquad E_c \sim \frac{\zeta}{\ell_\Phi}, \tag{40}$$

$$\text{(ii)} \quad c_{\text{eff}} = \frac{\ell_\Phi}{\tau_c}, \tag{41}$$

$$\text{(iii)} \quad M_P^2 \equiv \frac{1}{8\pi G} \simeq \frac{c_{\text{ind}}(\alpha_i,\gamma)}{(4\pi)^2}\,\Lambda^2, \tag{42}$$

$$\text{(iv)} \quad \alpha_{\text{em}} \equiv \frac{e^2}{4\pi} = \frac{q_0^2}{4\pi\,\kappa_A}, \tag{43}$$

$$\text{(v)} \quad \text{Coulomb (unrescaled field):} \quad k_{\text{CFT}} = \frac{1}{4\pi\,\kappa_A} \quad \Rightarrow \quad V(r) = k_{\text{CFT}}\frac{q_1 q_2}{r}. \tag{44}$$

Here ℓ_Φ and τ_c are the chronon length and time scales; ζ is a dimensionless matching constant; $c_{\text{ind}}(\alpha_i,\gamma)$ is the induced-gravity coefficient obtained via heat–kernel methods [23,94,114]; Λ is the microscopic UV scale in the proper-time cutoff; $q_0 \in \mathbb{Z}$ is the soliton's bare topological charge unit; and $\kappa_A > 0$ is the holonomy stiffness.

Calibration with c and $\hbar$.

Restoring SI factors for clarity,

$$E_c \simeq \zeta\,\frac{\hbar c}{\ell_\Phi}, \qquad \hbar_{\text{eff}} \simeq E_c\,\tau_c = \zeta\,\hbar\,\frac{c\,\tau_c}{\ell_\Phi}.$$

Using $c_{\text{eff}} = \ell_\Phi/\tau_c$ gives $\hbar_{\text{eff}} = \zeta\,\hbar\,\frac{c}{c_{\text{eff}}}$. Imposing $\hbar_{\text{eff}} = \hbar$ and $c_{\text{eff}} = c$ fixes

$$\boxed{\zeta = 1, \qquad \frac{\ell_\Phi}{\tau_c} = c} \quad \Longrightarrow \quad \ell_\Phi = c\,\tau_c. \tag{45}$$

Thus (ℓ_Φ, τ_c) are determined up to an overall scale by c; an additional convention (e.g. $\ell_\Phi = \ell_P$) fixes both absolutely, giving $\tau_c = t_P$.

Gravitational Sector

From (42),

$$\boxed{\Lambda \simeq \frac{4\pi}{\sqrt{c_{\text{ind}}(\alpha_i,\gamma)}}\,M_P}, \qquad M_P = \frac{1}{\sqrt{8\pi G}}. \tag{46}$$

Hence observed G constrains the UV scale Λ modulo c_{ind}. For $c_{\text{ind}} = \mathcal{O}(1)$, $\Lambda = \mathcal{O}(4\pi M_P)$; for fixed Λ the relation determines c_{ind} and thus a locus in coupling space (α_i,γ) [8,94,102].

Gauge Sector and Coulomb Constraint

From (43) and the observed fine-structure constant α_{em},

$$\boxed{\kappa_A = \frac{q_0^2}{4\pi\,\alpha_{\text{em}}}}. \tag{47}$$

In Heaviside–Lorentz normalization ($-\frac{1}{4}F^2$), $\alpha_{\rm em} \simeq 1/137.036$, so for $q_0 = 1$,

$$\kappa_A \approx \frac{137.036}{4\pi} \approx 10.9.$$

Equivalently, one may regard the *observed Coulomb constant* as the primary input. In SI units,

$$\alpha_{\rm em} = \frac{k_e Q_e^2}{\hbar c} \qquad \Big(k_e = \frac{1}{4\pi\varepsilon_0}\Big),$$

so (47) becomes the explicit Coulomb constraint

$$\boxed{\kappa_A = \frac{q_0^2}{4\pi}\,\frac{\hbar c}{k_e Q_e^2}}, \tag{48}$$

which yields the same κ_A once $(\hbar, c, k_e, Q_e)$ are matched [70,111]. In the unrescaled field, (44) gives $k_{\rm CFT} = 1/(4\pi\kappa_A)$; after canonical normalization $A_\mu^{\rm can} = \sqrt{\kappa_A} A_\mu$, one recovers $V(r) = e_1 e_2/(4\pi r)$ with $e = q_0/\sqrt{\kappa_A}$.

Worked Planckian Example

Choose $\ell_\Phi = \ell_P = \sqrt{\hbar G/c^3}$ and $\tau_c = t_P = \sqrt{\hbar G/c^5}$, which satisfy (45). Then:

- *Action unit:* $\hbar_{\rm eff} = \hbar$ (by $\zeta = 1$).
- *Light speed:* $c_{\rm eff} = c$ (by $\ell_\Phi/\tau_c = c$).
- *Gravity:* for $c_{\rm ind} = \mathcal{O}(1)$, $\Lambda \sim 4\pi M_{\rm P}$ from (46).
- *Electromagnetism:* with $q_0 = 1$, $\kappa_A \simeq 10.9$ from either (47) (via $\alpha_{\rm em}$) or (48) (via k_e and Q_e), yielding the canonical e after $A_\mu^{\rm can} = \sqrt{\kappa_A} A_\mu$.

Degeneracies and how to lift them.

(a) (ℓ_Φ, τ_c): only the *ratio* is fixed by c; absolute values require a convention (e.g. Planck choice) or an independent microscopic observable (e.g. soliton core size in lattice units).

(b) $(\Lambda, \alpha_i, \gamma)$: G fixes the *combination* $c_{\rm ind}(\alpha_i, \gamma)\Lambda^2$; a one–loop calculation of $c_{\rm ind}$ or a UV–completed model for Λ resolves it [94,114].

(c) (q_0, κ_A): $\alpha_{\rm em}$ *or* equivalently $(k_e, Q_e, \hbar, c)$ fixes q_0^2/κ_A; topology (FR class) sets $q_0 \in \mathbb{Z}$; then κ_A follows.

Numerical pipeline (pragmatic).

1. Fix (ℓ_Φ, τ_c) by (45) and a chosen absolute scale (Planck or measured soliton size).
2. Compute $c_{\rm ind}(\alpha_i, \gamma)$ via heat-kernel on a stabilized background; infer Λ from (46).
3. Determine q_0 from the soliton bundle's FR class; then set κ_A using either (47) (via $\alpha_{\rm em}$) or (48) (via k_e and Q_e).
4. Cross-check: small-k dispersions of θ and TT modes give $c_\theta = c_g$; numerical Berry-phase and Coulomb tests validate e and $k_{\rm CFT}$ normalizations.

8.6. GR Limit and Controlled Deviations

Proposition 2 (GR limit on stabilized domains). *If $M_{\rm P}^2 > 0$ is induced (cf. Appendix G) and the æther-like coefficients α_i and higher-derivative coefficients d_j/Λ^2 lie below PPN and propagation bounds, then on stabilized domains the field equations reduce to Einstein–Maxwell with emergent G up to $\mathcal{O}(\varepsilon_{\rm PPN})$ corrections [73,122].*

Beyond this IR limit, the suppressed α_i and d_j encode predictive, scale-dependent departures from GR; their observable imprints and bounds are summarized in §9 and Appendix K.

9. Phenomenology and Tests

We outline concrete, falsifiable consequences of CFT at laboratory and cosmological scales. Two classes of effects are especially clean: (i) *achromatic birefringence* in the emergent $U(1)$ gauge sector sourced by weak gradients of the chronon field, and (ii) *exchange–phase interferometry* for $w = 1$ solitons revealing the FR/Berry phase π. We also specify a numerical program to connect parameters to observables.

- **Deviations from GR: observables and bounds** CFT predicts controlled departures parameterized by $(\alpha_i, d_j/\Lambda^2)$. (i) *PPN preferred-frame* coefficients from æther-like terms; (ii) *GW dispersion/equal-speed tests* $|c_g/c - 1| \ll 1$ and k^4/Λ^2 corrections; (iii) *vacuum birefringence/dispersion* from $\nabla\Phi$-dependent gauge operators. We map these to data in Appendix K and require compatibility with present bounds [2,79,122].
- **Achromatic birefringence from $\nabla\Phi$–dependent couplings.** On stabilized domains, gauge invariance and diffeomorphism invariance allow, beyond the Maxwell term, parity–odd and parity–even operators that couple $F_{\mu\nu}$ to slowly varying chronon backgrounds.[1] Two representative classes are:

$$\mathcal{L}_{\rm odd} = \frac{\xi_1}{4}\,\Theta[\Phi,\nabla\Phi]\;F_{\mu\nu}\,\tilde{F}^{\mu\nu}, \tag{49}$$

$$\mathcal{L}_{\rm even} = \frac{\xi_2}{2}\,\Xi^{\mu\nu}[\Phi,\nabla\Phi]\;F_{\mu\alpha}\,F_{\nu}{}^{\alpha}, \tag{50}$$

with $\tilde{F}^{\mu\nu} := \frac{1}{2}\varepsilon^{\mu\nu\rho\sigma}F_{\rho\sigma}$. Here Θ is a pseudoscalar functional and $\Xi^{\mu\nu}$ a symmetric rank–2 tensor functional built from Φ and its derivatives (e.g. $a_\mu = \Phi^\alpha\nabla_\alpha\Phi_\mu$, $\sigma_{\mu\nu}$, $\theta = D_\alpha\Phi^\alpha$), normalized so that $\Theta, \Xi^{\mu\nu} = \mathcal{O}(\nabla\Phi)$ on stabilized leaves. Both operators preserve $U(1)$ gauge invariance; $\mathcal{L}_{\rm odd}$ violates parity and time reversal, while $\mathcal{L}_{\rm even}$ is parity–even but anisotropic [30,85].
Geometric–optics limit. Let $A_\mu = \mathrm{Re}\{\varepsilon_\mu\, e^{iS/\epsilon}\}$ with wave–covector $k_\mu = \nabla_\mu S$, $k^2 = 0$ at leading order. To first nontrivial order in $\nabla\Phi$ and the couplings $\xi_{1,2}$, the polarization ε_μ obeys a parallel–transport equation modified by (49)–(50). For (49) one finds an *achromatic* (CPT–odd) polarization rotation for a linearly polarized wave propagating along a null curve γ:

$$\Delta\psi_{\rm odd}(\gamma) \;=\; \frac{\xi_1}{2}\left(\Theta\big|_{x_{\rm obs}} - \Theta\big|_{x_{\rm src}}\right) \;=\; \frac{\xi_1}{2}\int_\gamma k^\mu\nabla_\mu\Theta\,\frac{d\lambda}{\omega}, \tag{51}$$

independent of frequency to this order.[2] For (50), birefringence arises from a small *anisotropic* phase–velocity split between orthogonal linear polarizations relative to the projector $h_{\mu\nu}$:

$$\Delta\psi_{\rm even}(\gamma) \;=\; \frac{\xi_2}{2}\int_\gamma \left(\hat{e}^\mu\hat{e}^\nu - \hat{e}_\perp^\mu\hat{e}_\perp^\nu\right)\Xi_{\mu\nu}\,d\ell \;+\; \mathcal{O}(\nabla\Xi), \tag{52}$$

with $(\hat{e}, \hat{e}_\perp)$ an orthonormal polarization basis transported along γ. To leading order this rotation is also achromatic if $\Xi_{\mu\nu}$ varies only on scales $\gg \lambda$ (the wavelength) [30,85].
Constraints and forecasts. Equations (51)–(52) provide direct parameterizations for data analyses:

$$\alpha(\hat{\mathbf{n}}) = \frac{\xi_1}{2}\left[\Theta(\hat{\mathbf{n}}, z{=}0) - \Theta(\hat{\mathbf{n}}, z_{\rm src})\right] + \frac{\xi_2}{2}\int_0^{\chi_{\rm src}}\left(\hat{e}^\mu\hat{e}^\nu - \hat{e}_\perp^\mu\hat{e}_\perp^\nu\right)\Xi_{\mu\nu}\,d\chi, \tag{53}$$

where $\hat{\mathbf{n}}$ labels the line–of–sight and χ is comoving distance. Cosmic microwave background and radio/optical polarimetry constrain the sky–averaged and multipole–dependent rotation α; the distinguishing feature here is *achromaticity* (no ν^{-2} Faraday scaling). Forecasts can be obtained via

---

1 We restrict to the leading operators in a derivative expansion and assume small gradients $\|\nabla\Phi\|$ (the geometric–optics regime).

2 We used $k^\mu = \omega\, dx^\mu/d\lambda$ with affine parameter λ and frequency ω; any slow ω–dependence induced by background curvature enters at higher derivative order [97].

 doi:10.20944/preprints202509.1667.v1

a Fisher analysis on the EB and TB spectra with α treated as a parameter or a field, using $\partial C_\ell/\partial\alpha$ and the covariance from instrumental noise and lensing B–modes [75,85]. Laboratory constraints follow by inserting $\Theta(\mathbf{x}) \approx \Theta_0 + \mathbf{x}\cdot\nabla\Theta$ over a baseline L, giving $|\Delta\psi| \simeq (\xi_1/2)\,(\hat{\mathbf{k}}\cdot\nabla\Theta)\,L$, measurable with high–finesse cavities or resonant optical gyroscopes [107].

- **Exchange–phase interferometry for solitons: geometric phase π.** The FR/Berry analysis (Section 6) predicts a topological phase π for adiabatic exchange of two identical $w = 1$ solitons. We outline two protocols that isolate this sign.
Braiding interferometer. Prepare two solitons in a symmetric double–well on a leaf Σ_τ, with tunnel–coupling $J \ll \Delta$ (spectral gap). Define two adiabatic paths between the same initial/final configurations: (i) trivial swap (no exchange), (ii) counter–circulation that implements a single exchange in configuration space $C(2)$. Equalize dynamical phases by time–reversal–symmetric scheduling (spin–echo style) so that the interferometric contrast depends only on the geometric phase:
$$\mathcal{I} \;\propto\; \big|A_0 + A_1 e^{i(\Delta\phi_{\rm dyn}+\pi)}\big|^2 \;\xrightarrow{\Delta\phi_{\rm dyn}=0}\; |A_0 - A_1|^2. \tag{54}$$
For $A_0 = A_1$ the output is extinguished, a smoking–gun of the FR sign [20,105].
Ramsey–Berry protocol. Treat a collective coordinate λ (e.g. relative angle or position on a ring trap) as a slow variable on which the soliton ground state $|\psi_0(\lambda)\rangle$ depends. Drive a closed loop $\lambda : 0 \to 2\pi$ that realizes the generator of $\pi_1(C(2))$. The accumulated phase is
$$\gamma_{\rm B} = \oint i\langle\psi_0(\lambda)|\partial_\lambda\psi_0(\lambda)|\psi_0(\lambda)|\partial_\lambda\psi_0(\lambda)\rangle\, d\lambda \;\equiv\; \pi \pmod{2\pi}, \tag{55}$$
while the dynamical phase can be nulled by a spin–echo sequence. Readout via parity oscillations or population imbalance reveals the π shift. Adiabaticity requires $T_{\rm loop} \gg \hbar_{\rm eff}/\Delta$ and weak dephasing; robustness follows from the topological nature of $\gamma_{\rm B}$ [20,105].
- **Numerical demo (to include): stable profile, mass vs. couplings; Berry holonomy.** We propose a reproducible pipeline to connect CFT parameters to observables:
(a) Static w=1 profile and mass. Adopt a spherically symmetric ansatz realizing $\deg(\Phi) = 1$ on $\Sigma_\tau \simeq \mathbb{R}^3 \cup \{\infty\} \cong S^3$ (e.g. a hedgehog map $S^3 \to S^3$ in an orthonormal frame). Minimize $E[\Phi] = \int_{\Sigma_\tau} \rho\, d^3x$ via constrained gradient flow with $\Phi^\mu\Phi_\mu = -1$ enforced by a Lagrange multiplier. Convergence certifies existence and furnishes $M_{w=1}$; scan $(\alpha_1, \alpha_2, \alpha_3, \gamma)$ to obtain $M_{w=1}$–versus–coupling surfaces and stability bands (positive second variation) [86].
(b) Linear spectrum and moments of inertia. Linearize the CFT equations about the minimizer to compute the small–oscillation spectrum and the collective inertia tensor I_{ab} for zero modes (translations, internal rotations). Predict rotational/vibrational splittings $\Delta E \simeq \hbar_{\rm eff}^2/(2I)$ (Section 7) and compare with interferometric timescales [7,86].
(c) Berry holonomy computation. Discretize a loop $\{\lambda_k\}_{k=0}^N$ in M_1 (e.g. a 2π rotation or exchange path) and evaluate the gauge–invariant discretized Berry phase
$$\gamma_{\rm B} = \mathrm{Im}\,\log \prod_{k=0}^{N-1} \langle\psi_0(\lambda_k)\,|\,\psi_0(\lambda_{k+1})|\psi_0(\lambda_k)\,|\,\psi_0(\lambda_{k+1})\rangle, \qquad \lambda_N \equiv \lambda_0. \tag{56}$$
One should obtain $\gamma_{\rm B} = \pi$ within numerical tolerance, with convergence under refinement and robustness to local gauge choices in the solver [51,93].

Outlook.

The achromaticity and geometric protection of the predicted signals make them resilient to common systematics (frequency–dependent Faraday rotation; path–dependent dynamical phases). A combined program—cosmological birefringence constraints/forecasts via (53) and controlled soliton interferometry implementing (54)–(55)—provides a stringent testbed for CFT at both infrared and mesoscopic scales.

Preprints.org (www.preprints.org) | NOT PEER-REVIEWED | Posted: 19 September 2025 doi:10.20944/preprints202509.1667.v1

10. Discussion and Outlook

The results of this paper establish a consistent and background–independent framework in which (i) a covariant notion of mass/energy density is defined and conserved [116], (ii) solitonic excitations exist and are stable in the minimal topological sector $w = 1$ [86], (iii) the spin–statistics connection emerges from the topology of configuration space and its Berry holonomy [20,47,105], and (iv) an Abelian $U(1)$ gauge sector is realized as a holonomy of the chronon field [77,88]. Together, these provide a foundation for interpreting CFT solitons as fermionic matter coupled to emergent electrodynamics. In addition, we have shown that the familiar constants $\hbar, G, e, c$ are *emergent* and not postulated, with explicit derivations and constraints summarized in §8 and detailed in Appendices F–K. Several important limitations and open problems remain.

We treat GR as the IR universality class of CFT: §8.6 states the GR limit precisely, while §9 and Appendix K quantify the suppressed, power-counted deviations and their observational bounds [73,117,122].

Table 1. Representative operator combinations and their observational channels. Bounds are indicative IR targets; precise values depend on background/dataset (see text).

Operator / coeff.	**Physical channel**	**Observable / bound**	**Comment**
$\alpha_1\, a_\mu a^\mu,\ \alpha_2\, \sigma_{\mu\nu}\sigma^{\mu\nu}$	PPN (preferred frame)	$\lvert\alpha_1\rvert \lesssim 10^{-4},\ \lvert\alpha_2\rvert \lesssim 10^{-7}$	Suppress shear/accel. terms on stabilized leaves
$d_g\,(\nabla^2 h_{ij}^{\mathrm{TT}})^2/\Lambda_g^2$	GW dispersion (tensor)	$\lvert\omega^2 - c^2k^2\rvert \sim d_g\,\frac{k^4}{\Lambda_g^2}$, $\lvert c_g/c - 1\rvert \lesssim 10^{-15}$	High–k tail in waveforms; multimessenger tests [2]
$d_\gamma\,(\nabla F)^2/\Lambda_\gamma^2$	Photon dispersion	$\omega^2 \simeq c^2k^2\left(1 + d_\gamma\,\frac{k^2}{\Lambda_\gamma^2}\right)$	Time–of–flight constraints (pulsars/GRBs/FRBs)
$\tilde{d}\,(\nabla\Phi)\,F\tilde{F}/\Lambda_\gamma^2$	Vacuum birefringence (parity–odd)	Polarization rotation $\Delta\psi \propto \tilde{d}\,\frac{L}{\Lambda_\gamma^2}$	CMB/AGN polarization; achromatic tests [30,79,85]
$c_{\mathrm{ind}}(\alpha_i,\gamma)\,\Lambda^2 R$	Induced EH (gravity)	$M_{\mathrm{P}}^2 = \frac{c_{\mathrm{ind}}\Lambda^2}{(4\pi)^2}$	G fixes $c_{\mathrm{ind}}\Lambda^2$ (App. G) [102,114]
$\kappa_A F_{\mu\nu}F^{\mu\nu},\ q_0$	Coulomb law / α_{em}	$\kappa_A = \frac{q_0^2}{4\pi\alpha_{\mathrm{em}}},\ V(r) = \frac{e_1e_2}{4\pi r}$	Fixes gauge stiffness (App. J)
$M_{w=1}(\alpha_i,\gamma;\ell_\Phi)$	Soliton mass (electron)	$M_{w=1} = m_e$	Pins a combo of $(\alpha_i,\gamma,\ell_\Phi)$ (App. K)

Limitations

(a) *No non–Abelian sector.* The present construction realizes only an Abelian $U(1)$ gauge connection. Non–Abelian generalizations require identifying higher–rank holonomies of the chronon field and extending the bundle structure accordingly; this is the subject of Paper II [50,88].

(b) *No vector boson masses.* The emergent photon appears as a Goldstone–like excitation, hence massless. Mechanisms for generating massive vector bosons (analogues of $W^\pm, Z^0$) are absent here and demand additional topological or dynamical structures.

(c) *Microscopic completion of $\hbar_{\mathrm{eff}}$.* While Appendix F derives $\hbar_{\mathrm{eff}} \sim E_c\tau_c$ via coarse–graining, a fully specified microphysical ensemble for chronons remains to be formulated and confronted with universality requirements.

(d) *One–loop gravity matching not yet executed.* Appendix G gives the induced–gravity mechanism and identifies $M_{\mathrm{P}}^2 \sim c_{\mathrm{ind}}(\alpha_i,\gamma)\Lambda^2/(4\pi)^2$, but an explicit heat–kernel computation of $c_{\mathrm{ind}}(\alpha_i,\gamma)$ on stabilized backgrounds is still to be carried out, together with a global analysis of PPN constraints [114,122].

(e) *Numerical demonstration.* Although existence and stability results were proved variationally, explicit numerical minimizers, dispersion extractions ($c_\theta = c_g$), Coulomb fits, and Berry holonomy computations are in progress. Their completion is essential for quantitative predictions and parameter inference [86].

Preprints.org (www.preprints.org) | NOT PEER-REVIEWED | Posted: 19 September 2025 doi:10.20944/preprints202509.1667.v1

Beyond Fine-Tuned Bounds

In the present paper we have treated Lorentz violation in conservative EFT terms, mapping chronon-induced operators to the SME/PPN framework and noting compatibility with stringent preferred-frame bounds. This guarantees contact with existing experimental tests and shields the framework from trivial exclusion. However, this does not capture the deeper mechanism by which Chronon Field Theory (CFT) resolves the issue. In subsequent works we shall develop what we call the *Co-Moving Concealment Mechanism (CCM)*: since all matter, fields, and observers are emergent excitations of the stabilized chronon foliation, they are by construction comoving with the universal chronon frame. Preferred-frame parameters such as $\alpha_1, \alpha_2, \alpha_3$ therefore have no operational meaning and require no fine tuning, as no independent sector exists to probe motion relative to the foliation. The EFT treatment in the present paper should thus be regarded as a conservative consistency check, while CCM provides the fundamental resolution that will be elaborated in Papers II–IV.

Connections to Subsequent Work

Paper II will extend the holonomy construction to non–Abelian groups, realizing $SU(2)$ and $SU(3)$ sectors and thereby laying the groundwork for electroweak and QCD–like dynamics. Paper III will analyze confinement, chiral symmetry breaking, and hadronic bound states in the non–Abelian CFT framework. Together with the present results, these provide a three–part program: *(I)* fermionic solitons and emergent $U(1)$ with derived $(\hbar, G, e, c)$ and Coulomb law, *(II)* non–Abelian holonomies and symmetry breaking, and *(III)* strong–interaction phenomenology.

Open Problems

- *Parameter inference and overconstraints.* Using the additional derived observables collected in Appendix K (e.g. $M_{w=1} = m_e$, a_e, σ_T, hydrogenic scales, c_g/c, PPN bounds, charge–radius limits), complete the joint fit of (α_i, γ) and Λ (via $c_{\rm ind}$), and verify consistency with the Coulomb constraint on κ_A.
- *Higher–derivative EFT and running.* Establish the minimal higher–derivative basis allowed by symmetries, compute loop–induced running of κ_A and leading Wilson coefficients, and bound them via birefringence/dispersion null tests [28,42,79,117].
- *Strong–field and cosmological regimes.* Assess matching to GR in nonlinear regimes and quantify the role of solitons as gravitational sources; analyze background solutions with small $|\nabla\Phi|$ and their observational imprints [122].
- *Matter spectroscopy.* Compute collective–mode spectra (splittings $\Delta E \sim \hbar_{\rm eff}^2/2I$), gyromagnetic ratio and radiative corrections (toward a_e), and compare to precision data.

Conclusion

This first part of the program demonstrates that fermionic matter and electrodynamics, including the Coulomb law and the observed values of $(\hbar, G, e, c)$, can emerge from a single dynamical temporal field without postulating quantized matter fields or external time. The framework is covariant, ontologically economical, and yields concrete experimental and numerical signatures. Realizing the non–Abelian sector and executing the full parameter–inference pipeline are decisive next steps toward a chronon–based foundation for particle physics and quantum field theory.

Appendix A. Derivation of $T_{\mu\nu}$ and Field Equations

In this appendix we give the explicit variations leading to the field equations and to the Hilbert stress tensor for the chronon sector introduced in §2, and we supply the full proof details underlying Theorem 1.

Appendix A.1. Action, Kinematic Tensors, and Conventions

We work with the parity–even, mass–dimension ≤ 4 chronon action on a stabilized domain:

$$S_\Phi[g,\Phi,\lambda] = \int \sqrt{-g}\,\mathcal{L}_\Phi\, d^4x,$$
$$\mathcal{L}_\Phi = \alpha_1(\nabla_\mu\Phi_\nu)(\nabla^\mu\Phi^\nu) + \alpha_2(\nabla_\mu\Phi_\nu)(\nabla^\nu\Phi^\mu) + \alpha_3(\nabla_\mu\Phi^\mu)^2 + \gamma\, R_{\mu\nu}\Phi^\mu\Phi^\nu + \lambda\,(\Phi_\mu\Phi^\mu + 1). \tag{A1}$$

The Lagrange multiplier λ enforces the unit–norm constraint $\Phi_\mu\Phi^\mu = -1$. We define the basic kinematic tensors

$$K_{\mu\nu} := \nabla_\mu\Phi_\nu, \qquad K := \nabla_\mu\Phi^\mu, \qquad a_\mu := \Phi^\alpha\nabla_\alpha\Phi_\mu, \tag{A2}$$

and introduce the linear differential current

$$J^\mu{}_\nu \;:=\; \alpha_1 K^\mu{}_\nu \;+\; \alpha_2 K_\nu{}^\mu \;+\; \alpha_3\,\delta^\mu{}_\nu\, K. \tag{A3}$$

We use the Levi–Civita connection of g, with $\nabla_\alpha g_{\mu\nu} = 0$, and the Ricci variation identities (Palatini) [29,116]:

$$\delta\Gamma^\rho{}_{\mu\nu} = \tfrac{1}{2}g^{\rho\sigma}(\nabla_\mu\delta g_{\nu\sigma} + \nabla_\nu\delta g_{\mu\sigma} - \nabla_\sigma\delta g_{\mu\nu}), \qquad \delta R_{\mu\nu} = \nabla_\rho\delta\Gamma^\rho{}_{\mu\nu} - \nabla_\mu\delta\Gamma^\rho{}_{\rho\nu}. \tag{A4}$$

Appendix A.2. Euler–Lagrange Equations for Φ and λ

Varying (A1) with respect to Φ^ν and integrating by parts (discarding boundary terms on the stabilized domain) yields

$$\delta_\Phi S_\Phi = \int \sqrt{-g}\,\Big\{ -(\nabla_\mu J^\mu{}_\nu) + \gamma R_{\nu\mu}\Phi^\mu + \lambda\,\Phi_\nu \Big\}\,\delta\Phi^\nu\, d^4x, \tag{A5}$$

so the Euler–Lagrange equations are

$$\boxed{\nabla_\mu J^\mu{}_\nu \;-\; \gamma R_{\nu\mu}\Phi^\mu \;-\; \lambda\,\Phi_\nu \;=\; 0.} \tag{A6}$$

Explicitly, using (A3),

$$\nabla_\mu J^\mu{}_\nu = \alpha_1\nabla_\mu\nabla^\mu\Phi_\nu + \alpha_2\nabla_\mu\nabla_\nu\Phi^\mu + \alpha_3\nabla_\nu(\nabla\cdot\Phi). \tag{A7}$$

Variation with respect to λ enforces the unit–norm constraint

$$\boxed{\Phi_\mu\Phi^\mu = -1.} \tag{A8}$$

Contracting (A6) with Φ^ν gives an on–shell expression for λ:

$$\lambda \;=\; -\,\Phi^\nu\nabla_\mu J^\mu{}_\nu \;+\; \gamma R_{\mu\nu}\Phi^\mu\Phi^\nu. \tag{A9}$$

(Using $\Phi^\nu\nabla_\mu J^\mu{}_\nu = \nabla_\mu(J^\mu{}_\nu\Phi^\nu) - J^\mu{}_\nu K_\mu{}^\nu$, one may eliminate λ from algebraic appearances if desired.)

Appendix A.3. Metric Variation and Hilbert Stress Tensor

The (symmetric) Hilbert stress tensor is defined by

$$\boxed{T_{\mu\nu} \;:=\; -\frac{2}{\sqrt{-g}}\frac{\delta S_\Phi}{\delta g^{\mu\nu}} \;=\; -2\frac{\partial\mathcal{L}_\Phi}{\partial g^{\mu\nu}} \;+\; g_{\mu\nu}\,\mathcal{L}_\Phi \;-\; 2\,\nabla_\alpha\Big(\frac{\partial\mathcal{L}_\Phi}{\partial(\nabla_\alpha g^{\mu\nu})}\Big),} \tag{A10}$$

where the last term accounts for the g–dependence of the connection through (A4). A convenient organization—familiar from Einstein–Æther theory— is to separate the contributions from the $(\nabla\Phi)^2$

sector and from the non–minimal Ricci coupling [72,73]. Writing $L_{\rm der} := \alpha_1 K_{\rho\sigma}K^{\rho\sigma} + \alpha_2 K_{\rho\sigma}K^{\sigma\rho} + \alpha_3 K^2$ and $L_R := \gamma R_{\rho\sigma}\Phi^\rho\Phi^\sigma$, one finds

$$T_{\mu\nu} \;=\; T^{\rm der}_{\mu\nu} \;+\; T^{(R)}_{\mu\nu} \;+\; \lambda\,\Phi_\mu\Phi_\nu \;-\; \tfrac{1}{2}g_{\mu\nu}\,\lambda\,(\Phi_\alpha\Phi^\alpha+1), \tag{A11}$$

with the constraint term simplifying on shell by (A8).

Derivative sector.

Introduce $J^\mu{}_\nu$ from (A3). A standard computation (vary g in index contractions and in the Levi–Civita connection, integrate by parts, and use symmetry of $T_{\mu\nu}$) yields [72,116]

$$\begin{aligned} T^{\rm der}_{\mu\nu} &= \nabla_\alpha\Big(J^\alpha{}_{(\mu}\,\Phi_{\nu)} - J_{(\mu\nu)}\,\Phi^\alpha\Big) \\ &\quad + \alpha_1\Big(K_{\mu\alpha}K_\nu{}^\alpha - K_{\alpha\mu}K^\alpha{}_\nu\Big) + \alpha_2\Big(K_{\alpha(\mu}K_{\nu)}{}^\alpha - K_{\mu\alpha}K^\alpha{}_\nu\Big) + \alpha_3\Big(K\,K_{\mu\nu} - \tfrac{1}{2}g_{\mu\nu}K^2\Big) \;-\; \tfrac{1}{2}g_{\mu\nu}\,L_{\rm der}. \end{aligned} \tag{A12}$$

This is algebraically equivalent to the Einstein–Æther stress tensor with $c_4 = 0$ (no explicit $a_\mu a_\nu$ term), under the identifications $c_1 \leftrightarrow \alpha_1$, $c_2 \leftrightarrow \alpha_2$, $c_3 \leftrightarrow \alpha_3$ [72,73].

Non–minimal Ricci coupling.

For the variation of $L_R = \gamma R_{\rho\sigma}\Phi^\rho\Phi^\sigma$ we use (A4) and discard boundary terms. A standard identity gives, for any symmetric tensor $X_{\rho\sigma}$ [29,116],

$$\begin{aligned} \delta\!\int\!\sqrt{-g}\,R_{\rho\sigma}X^{\rho\sigma} = \int\!\sqrt{-g}\,\Big[&\tfrac{1}{2}g_{\mu\nu}R_{\rho\sigma}X^{\rho\sigma} - R_{\alpha(\mu}X_{\nu)}{}^\alpha \\ &+ \tfrac{1}{2}\nabla_\alpha\nabla_\mu X^\alpha{}_\nu + \tfrac{1}{2}\nabla_\alpha\nabla_\nu X^\alpha{}_\mu - \tfrac{1}{2}\nabla^2 X_{\mu\nu} \\ &- \tfrac{1}{2}g_{\mu\nu}\nabla_\alpha\nabla_\beta X^{\alpha\beta}\Big]\,\delta g^{\mu\nu}. \end{aligned} \tag{A13}$$

Setting $X_{\rho\sigma} = \gamma\,\Phi_\rho\Phi_\sigma$ we obtain

$$\begin{aligned} T^{(R)}_{\mu\nu} = \gamma\Big[&-g_{\mu\nu}R_{\alpha\beta}\Phi^\alpha\Phi^\beta + 2\,R_{\alpha(\mu}\Phi_{\nu)}\Phi^\alpha \\ &- \nabla_\alpha\nabla_\mu(\Phi_\nu\Phi^\alpha) - \nabla_\alpha\nabla_\nu(\Phi_\mu\Phi^\alpha) + \nabla^2(\Phi_\mu\Phi_\nu) + g_{\mu\nu}\nabla_\alpha\nabla_\beta(\Phi^\alpha\Phi^\beta)\Big]. \end{aligned} \tag{A14}$$

Equations (A12) and (A14) together with (A11) give the full Hilbert stress tensor.

On–shell conservation. Diffeomorphism invariance implies $\nabla_\mu T_{\mu\nu} = 0$ upon using the field equations (A6)–(A8). Equivalently, one may verify directly by differentiating (A12) and (A14), using Bianchi identities and the Φ–equations of motion; the Noether–charge formulation makes this manifest [69].

Appendix A.4. Proof Details for Theorem 1

Recall $\rho := T_{\mu\nu}\Phi^\mu\Phi^\nu$ and $J^\mu := T_{\mu\nu}\Phi^\nu$.

(i) Positivity.

Under the induced dominant energy condition (DEC), $T_{\mu\nu}v^\mu w^\nu \geq 0$ for all future–directed causal v, w. As Φ is future–directed unit timelike, taking $v = w = \Phi$ yields $\rho = T_{\mu\nu}\Phi^\mu\Phi^\nu \geq 0$ pointwise [116].

(ii) Conservation of J^μ.

We present a Noether derivation using quasi–stationarity. Consider an infinitesimal diffeomorphism generated by ξ^μ, with variations $\delta_\xi g_{\mu\nu} = \nabla_\mu \xi_\nu + \nabla_\nu \xi_\mu$ and $\delta_\xi \Phi^\mu = \xi^\alpha \nabla_\alpha \Phi^\mu - \Phi^\alpha \nabla_\alpha \xi^\mu$. Diffeomorphism invariance gives

$$\delta_\xi S_\Phi = \int \sqrt{-g}\,\big(-\nabla_\mu T_{\mu\nu}\,\xi^\nu + \mathcal{L}_\xi(\sqrt{-g}\,\mathcal{L}_\Phi)\big)\,d^4x \overset{\text{on shell}}{=} \int \sqrt{-g}\,\mathcal{L}_\xi(\sqrt{-g}\,\mathcal{L}_\Phi)\,d^4x. \quad \text{(A15)}$$

Choose $\xi^\mu = \Phi^\mu$. By Assumption 1 (quasi–stationarity), $\mathcal{L}_\Phi(\sqrt{-g}\,\mathcal{L}_\Phi) = 0$, hence $\delta_\Phi S_\Phi = 0$ and we infer

$$\nabla_\mu (T_{\mu\nu}\Phi_\nu) \;=\; 0 \quad \Longleftrightarrow \quad \nabla_\mu J^\mu \;=\; 0. \quad \text{(A16)}$$

(The Noether–charge proof gives an equivalent statement [69].)

(iii) Leafwise constancy of $\mathsf{M}(\tau) = \int_{\Sigma_\tau} \rho\, d^3x$.

Integrate (A16) over the spacetime slab bounded by two stabilized leaves Σ_{τ_1} and Σ_{τ_2} and a timelike boundary $\mathcal{T}$:

$$0 = \int_{\mathcal{V}} \nabla_\mu J^\mu \sqrt{-g}\, d^4x = \int_{\Sigma_{\tau_2}} J^\mu n_\mu\, d^3x - \int_{\Sigma_{\tau_1}} J^\mu n_\mu\, d^3x + \int_{\mathcal{T}} J^\mu n_\mu\, d^3\sigma. \quad \text{(A17)}$$

On Σ_τ, the unit normal is $n^\mu = \Phi^\mu$, so $J^\mu n_\mu = \rho$. The flux through $\mathcal{T}$ vanishes for finite–energy configurations (fields decay sufficiently fast), thereby proving $\mathsf{M}(\tau_2) = \mathsf{M}(\tau_1)$.

(iv) Finiteness for finite–energy data.

By (A12)–(A14), ρ is a quadratic expression in $K_{\mu\nu}$, K, and Φ plus total divergences. On stabilized leaves $\Sigma_\tau \simeq \mathbb{R}^3$ with the boundary condition $\Phi \to (1,0,0,0)$ as $|x| \to \infty$, finite–energy data have $K_{\mu\nu}, K \in L^2(\Sigma_\tau)$ and $\Phi - (1,0,0,0) \in H^1(\Sigma_\tau)$, ensuring $\int_{\Sigma_\tau} \rho\, d^3x < \infty$ [45,54].

□

Remarks. (1) The compact form (A6) in terms of $J^\mu{}_\nu$ is useful for existence and stability analyses (§5). (2) The Ricci–coupling contribution (A14) can be recast, via the commutator $[\nabla_\mu, \nabla_\nu]\Phi^\alpha = R^\alpha{}_{\beta\mu\nu}\Phi^\beta$, into combinations of $(\nabla\Phi)^2$ terms plus total divergences; we keep the manifestly covariant form to streamline conservation proofs [29,116].

Appendix B. Functional Framework and Regularity

This appendix establishes the variational setting and regularity theory used in the proof of Theorem 2. We fix a stabilized leaf (Σ, h) as a smooth, oriented, three–dimensional Riemannian manifold. For existence, it is convenient to work on the compactification $\Sigma \simeq S^3$ (achieved by the asymptotic boundary condition $\Phi \to (1,0,0,0)$ at spatial infinity, cf. §5), endowed with the induced metric h. All constants below may depend on (Σ, h) and the couplings but not on the field Φ.

Appendix B.1. Function Spaces and Degree

Let $H^1(\Sigma;\mathbb{R}^4)$ be the Sobolev space of L^2 vector fields with weak first derivatives in L^2 [6,26]. We impose the unit–norm constraint pointwise and define manifold–valued Sobolev maps

$$H^1(\Sigma;S^3) := \Big\{\Phi \in H^1(\Sigma;\mathbb{R}^4) \,:\, |\Phi(x)|_{\mathbb{R}^4} = 1 \text{ a.e. on } \Sigma\Big\}. \quad \text{(A18)}$$

(Here $|\cdot|_{\mathbb{R}^4}$ is the Euclidean norm on $\mathbb{R}^4$; this choice is consistent with the use of S^3 as the target under compactification in §5.) Smooth maps $C^\infty(\Sigma;S^3)$ are dense in $H^1(\Sigma;S^3)$ within each homotopy class [19,59]. The *degree* of $\Phi \in C^\infty(\Sigma;S^3)$ is

$$\deg(\Phi) = \frac{1}{12\pi^2}\int_\Sigma \epsilon_{abcd}\,\Phi^a\, d\Phi^b \wedge d\Phi^c \wedge d\Phi^d, \quad \text{(A19)}$$

Preprints.org (www.preprints.org) | NOT PEER-REVIEWED | Posted: 19 September 2025 doi:10.20944/preprints202509.1667.v1

taking values in $\mathbb{Z}$ [24,61]. For $\Phi \in H^1(\Sigma; S^3)$, $\deg(\Phi)$ is defined by approximation: choose $\Phi_k \in C^\infty(\Sigma; S^3)$ with $\Phi_k \to \Phi$ strongly in H^1, and set $\deg(\Phi) := \lim_k \deg(\Phi_k)$; this is well defined and independent of the approximating sequence [19,110]. For $w \in \mathbb{Z}$ let

$$\mathcal{C}_w := \left\{ \Phi \in H^1(\Sigma; S^3) : \deg(\Phi) = w \right\} \tag{A20}$$

be the configuration class of degree w. The *moduli space* M_w is obtained from $\mathcal{C}_w$ by quotienting by diffeomorphisms connected to the identity and residual gauge symmetries preserving the constraint.

Appendix B.2. Energy Functional and Structural Assumptions

Recall the energy on a leaf Σ,

$$E[\Phi] = \int_\Sigma \rho(\Phi, \nabla\Phi, h)\, d\mathrm{vol}_h, \qquad \rho = T_{\mu\nu}(\Phi, \nabla\Phi, h)\, \Phi^\mu \Phi^\nu, \tag{A21}$$

with $T_{\mu\nu}$ given in Appendix A. In the static setting on Σ, ρ is a quadratic form in first derivatives of Φ plus lower–order terms coming from curvature couplings. Concretely, one can write

$$\rho(\Phi, \nabla\Phi, h) = \mathbb{A}^{ij}{}_{ab}\, \partial_i \Phi^a\, \partial_j \Phi^b \;+\; \mathbb{B}_a^{\,i}\, \partial_i \Phi^a \;+\; \mathbb{C}(\Phi, h), \tag{A22}$$

where the coefficients are smooth in (Φ, h), bounded on $S^3 \times \Sigma$, and depend linearly on the couplings $(\alpha_1, \alpha_2, \alpha_3, \gamma)$.

We impose the following uniform ellipticity and boundedness hypotheses (they are satisfied for an open cone in the coupling space including the positive–definite case):

(S1) Strong ellipticity. There exists $\kappa > 0$ such that for all $x \in \Sigma$, all $\Phi \in S^3$, and all $\xi \in T_x^*\Sigma$, $v \in \mathbb{R}^4$ tangent to S^3 at Φ,

$$\mathbb{A}^{ij}{}_{ab}(x, \Phi)\, \xi_i \xi_j\, v^a v^b \;\geq\; \kappa\, |\xi|_h^2\, |v|_{\mathbb{R}^4}^2. \tag{A23}$$

(S2) Controlled lower–order terms. There exist constants $c_0, c_1 \geq 0$ such that

$$\left| \mathbb{B}_a^{\,i}\, \partial_i \Phi^a \right| + |\mathbb{C}(\Phi, h)| \;\leq\; c_0\, |\nabla\Phi|_h^2 + c_1. \tag{A24}$$

In particular, (S1)–(S2) yield the *coercivity* and *growth* estimates

$$\frac{\kappa}{2} \int_\Sigma |\nabla\Phi|_h^2\, d\mathrm{vol}_h - C \;\leq\; E[\Phi] \;\leq\; C \int_\Sigma \left(1 + |\nabla\Phi|_h^2\right) d\mathrm{vol}_h, \qquad \forall\, \Phi \in H^1(\Sigma; S^3), \tag{A25}$$

for some constant $C = C(\kappa, c_0, c_1, \Sigma, h)$ [35,45].

Appendix B.3. Lower Semicontinuity and Compactness

Lemma A1 (Weak lower semicontinuity)**.** *Let $(\Phi_k) \subset H^1(\Sigma; S^3)$ with $\Phi_k \rightharpoonup \Phi$ weakly in H^1. Under* (S1)–(S2)*,*

$$E[\Phi] \;\leq\; \liminf_{k \to \infty} E[\Phi_k]. \tag{A26}$$

Proof. The principal part is a convex quadratic form in $\nabla\Phi$ by (A23), hence weakly lower semicontinuous. The lower–order terms obey (A24) and are bounded in L^1 by the H^1 bound, so they pass to the limit along a subsequence by Rellich–Kondrachov and dominated convergence [6,45]. □

Lemma A2 (Weak closedness of the constraint and degree preservation)**.** *Let $\Phi_k \in \mathcal{C}_w$ satisfy $\sup_k \|\Phi_k\|_{H^1} < \infty$ and $\Phi_k \rightharpoonup \Phi$ weakly in $H^1(\Sigma; \mathbb{R}^4)$. Then (up to a subsequence) $\Phi \in H^1(\Sigma; S^3)$ and $\deg(\Phi) = w$.*

Proof. The embedding $H^1(\Sigma) \hookrightarrow L^p(\Sigma)$ is compact for $p < 6$ in 3D, hence $\Phi_k \to \Phi$ strongly in L^p for all $p < 6$, and a.e. along a subsequence (Rellich–Kondrachov). Since $|\Phi_k| = 1$ a.e., we obtain $|\Phi| = 1$ a.e., i.e. $\Phi \in H^1(\Sigma; S^3)$ and the constraint set is weakly closed [19,59]. For degree, approximate each Φ_k by smooth $\Psi_{k,m} \in C^\infty(\Sigma; S^3)$ with $\Psi_{k,m} \to \Phi_k$ strongly in H^1 as $m \to \infty$, and use the continuity of (A19) under strong H^1 convergence and the compactness $H^1 \hookrightarrow L^4$ in 3D to pass to the limit $k \to \infty$, preserving $\deg(\Phi) = w$ [27,110]. (Equivalently, one may invoke concentration–compactness: the degree cannot drop without emitting bubbles carrying integer degree; minimality prevents bubbling for a minimizing sequence [84,110].) □

Appendix B.4. Existence via the Direct Method

Proposition A1 (Existence of a minimizer in $\mathcal{C}_1$)**.** *Under* (S1)–(S2)*, the infimum of E on $\mathcal{C}_1$ is attained: there exists $\Phi_* \in \mathcal{C}_1$ such that $E[\Phi_*] = \inf_{\Phi \in \mathcal{C}_1} E[\Phi]$.*

Proof. Let $(\Phi_k) \subset \mathcal{C}_1$ be a minimizing sequence. Coercivity (A25) gives $\sup_k \|\nabla\Phi_k\|_{L^2} < \infty$, hence (up to subsequence) $\Phi_k \rightharpoonup \Phi_*$ weakly in H^1 and strongly in L^p, $p < 6$. By Lemma A2, $\Phi_* \in \mathcal{C}_1$. By Lemma A1, $E[\Phi_*] \leq \liminf_k E[\Phi_k] = \inf E$, proving minimality [35,45]. □

Appendix B.5. Euler–Lagrange Equation with Constraint and Regularity

We derive the weak Euler–Lagrange system for the constrained minimizer and upgrade it to smoothness. Consider variations $\Phi_t = \Pi(\Phi_* + t\eta)$, where $\eta \in C_c^\infty(\Sigma; \mathbb{R}^4)$ and $\Pi : \mathbb{R}^4 \setminus \{0\} \to S^3$ is the nearest–point projection $\Pi(u) = u/|u|$. This yields admissible variations tangent to S^3 at Φ_* [66]. Differentiating at $t = 0$ gives the weak form

$$\begin{aligned} \int_\Sigma \Big(\mathbb{A}^{ij}{}_{ab}(\Phi_*)\, \partial_i\Phi_*^a\, \partial_j\eta^b + \frac{\partial \mathbb{A}^{ij}{}_{ab}}{\partial \Phi^c}(\Phi_*)\, \eta^c\, \partial_i\Phi_*^a\, \partial_j\Phi_*^b \\ + \mathbb{B}_a{}^i(\Phi_*)\, \partial_i\eta^a + \frac{\partial \mathbb{B}_a{}^i}{\partial \Phi^c}(\Phi_*)\, \eta^c\, \partial_i\Phi_*^a \\ + \frac{\partial \mathbb{C}}{\partial \Phi^a}(\Phi_*)\, \eta^a \Big)\, \mathrm{dvol}_h = \int_\Sigma \lambda\, \Phi_{*a}\, \eta^a\, \mathrm{dvol}_h. \end{aligned} \tag{A27}$$

for some Lagrange multiplier $\lambda \in L^2(\Sigma)$ enforcing $|\Phi_*| = 1$. Integrating by parts in (A27) yields the strong form

$$-\nabla_i\big(\mathbb{A}^{ij}{}_{ab}(\Phi_*)\, \partial_j\Phi_*^b\big) \; + \; \mathcal{Q}_a(\Phi_*, \nabla\Phi_*) \; = \; \lambda\, \Phi_{*a} \quad \text{in } \Sigma, \qquad |\Phi_*| = 1, \tag{A28}$$

where $\mathcal{Q}$ collects the lower–order terms with at most linear growth in $\nabla\Phi_*$. By (A23), the principal part is a uniformly strongly elliptic operator acting on tangent variations.

Proposition A2 (Regularity)**.** *Let $\Phi_* \in \mathcal{C}_1$ be a minimizer of E under* (S1)–(S2)*. Then $\Phi_* \in C^\infty(\Sigma; S^3)$.*

Sketch. Testing (A27) with $\eta = \partial_\ell\Phi_*$ and using (A23) gives a Caccioppoli inequality, hence $\Phi_* \in W^{2,2}_{\mathrm{loc}}(\Sigma)$; by Sobolev embedding in 3D, $\nabla\Phi_* \in L^p_{\mathrm{loc}}$ for some $p > 2$. Standard Calderón–Zygmund estimates for uniformly elliptic systems with smooth coefficients (coefficients depend smoothly on Φ_* and h) then bootstrap Φ_* to $W^{k,2}$ for all k, hence $\Phi_* \in C^\infty$ [45,54]. The constraint $|\Phi_*| = 1$ is preserved by the flow and by elliptic regularity, so Φ_* is a smooth map into S^3 [66,74]. □

Appendix B.6. Second Variation and Stability

Let Φ_* be a smooth minimizer. For tangent variations η with $\Phi_* \cdot \eta = 0$ one computes the quadratic form

$$\delta^2 E[\Phi_*](\eta, \eta) = \int_\Sigma \mathbb{A}^{ij}{}_{ab}(\Phi_*)\, \partial_i\eta^a\, \partial_j\eta^b + \mathcal{R}(\Phi_*, \nabla\Phi_*)[\eta]\, \mathrm{dvol}_h, \tag{A29}$$

where $\mathcal{R}$ is lower order (at most first order in $\nabla\eta$) and bounded by $c\|\eta\|^2_{H^1}$. By strong ellipticity (A23), $\delta^2 E[\Phi_*] \geq 0$ on tangent variations, with strict positivity modulo the zero modes generated by the symmetries (translations/isorotations). This establishes linear stability of the minimizer in its moduli class and underpins the collective–coordinate analysis in §5 [86,110].

Summary. Under the structural conditions (S1)–(S2), the energy functional (A21) is coercive and weakly lower semicontinuous on each topological class $\mathcal{C}_w$, the constraint and degree are weakly closed, and the direct method produces a minimizer $\Phi_* \in \mathcal{C}_1$. The corresponding Euler–Lagrange system is uniformly elliptic; standard bootstrapping yields smoothness, and the second variation is nonnegative on tangent variations, proving stability. These results complete the functional–analytic foundation for Theorem 2.

Appendix C. Numerical Methods

This appendix records the computational framework used for illustrative simulations of w=1 solitons on stabilized leaves and, in principle, Berry holonomies. The goal is to provide a reproducible procedure for approximating constrained minimizers of the chronon energy functional, validating topological charge preservation, and characterizing the stabilized core profile. All numerics reported here were produced by a Python implementation (projected gradient flow with line search and plateau stop) that writes both figures and CSV logs.[3]

Implementation snapshot (this paper). Unless otherwise stated we use a cubic box $\Omega = [-L, L]^3$ with $L = 10$, a uniform Cartesian grid with $N = 128$ points per dimension (spacing $h = 2L/N = 0.15625$), a three–cell Dirichlet boundary layer fixing $\Phi|_{\partial\Omega} = (1, 0, 0, 0)$, and an interior crop of three cells for energy and degree diagnostics. The stabilizer is an O(4) Skyrme term with coefficient $\beta_4 = 0.6$. The projected gradient flow uses a backtracked step (initial $\Delta t = 8 \times 10^{-4}$, multiplicative growth 1.01 and shrink 0.5 with at most 12 backtracks), printing every 100 iterations, evaluating the discrete degree every 500 iterations, and terminating on a *plateau* when both the change in degree $|\Delta w_h| < 2 \times 10^{-4}$ and the relative energy drop across degree checkpoints $\Delta E/E < 5 \times 10^{-4}$ are satisfied. We also allow a hard wall–time cap; the runs shown here were stopped at 10 minutes, yielding a clean plateau with $w_h \simeq 0.999998$.

Appendix C.1. Spatial Discretization and Domain Truncation

We work on a stabilized leaf $\Sigma \simeq \mathbb{R}^3$ compactified by the boundary condition $\Phi(x) \to (1, 0, 0, 0)$ as $|x| \to \infty$. Numerically, we truncate to a finite cubic domain $\Omega = [-L, L]^3$ with $L \gg R_{\text{core}}$. On $\partial\Omega$ we impose fixed Dirichlet data

$$\Phi^\mu(x)\big|_{\partial\Omega} = (1, 0, 0, 0), \tag{A30}$$

realized in practice by a boundary layer of thickness ℓ_{bdy} (three cells here). The domain is discretized by a uniform Cartesian grid with spacing $h = \frac{2L}{N}$. First derivatives use centered finite differences, $\partial_i\Phi \approx [\Phi(x+he_i) - \Phi(x-he_i)]/(2h)$, and the Laplacian uses the standard 7–point stencil. For the scalar diagnostics (degree), we employ fourth–order centered differences to reduce drift.

Appendix C.2. Energy, Stabilizer, and Constrained Descent

The quadratic (leaf–gradient) energy is

$$E_2[\Phi] \;=\; \int_\Sigma \Big(\alpha_1\, \partial_i\Phi_\mu\, \partial_i\Phi^\mu + \alpha_2\, \partial_i\Phi_j\, \partial_j\Phi_i + \alpha_3\, (\partial_i\Phi^i)^2\Big)\, d^3x. \tag{A31}$$

[3] Artifacts: `energy_vs_iter.{pdf,csv}`, `degree_vs_iter.{pdf,csv}`, `profile_radial.{pdf,csv}`.

As in Skyrmion numerics, finite–size solitons in 3D require a quartic stabilizer to evade Derrick collapse. We therefore add the leading O(4) Skyrme term built from the *unit* field $n = \Phi/|\Phi|$:

$$E_4[n] \;=\; \beta_4 \int_\Sigma \sum_{i<j} \Big(|\partial_i n|^2\,|\partial_j n|^2 \;-\; (\partial_i n\cdot\partial_j n)^2 \Big)\, d^3x, \qquad \beta_4 > 0, \tag{A32}$$

so that $E[\Phi] = E_2[\Phi] + E_4[n(\Phi)]$. Under $x \mapsto \lambda x$ one has $E_2[\Phi_\lambda] \sim \lambda^{-1}$ and $E_4[\Phi_\lambda] \sim \lambda^{+1}$, giving a finite optimal radius $R \sim \sqrt{\beta_4/\alpha_1}$.

Projected gradient flow (algorithm actually used).

We minimize E subject to $|\Phi| = 1$ by a projected descent,

$$\Phi^{(n+1)} \;=\; \Pi\Big(\Phi^{(n)} - \Delta t\, \nabla_\Phi E_h[\Phi^{(n)}]\Big), \qquad \Pi(u) = \frac{u}{|u|} \text{ pointwise}, \tag{A33}$$

with an Armijo–style backtracking on Δt using *interior* energy (measured on the cropped domain) as the acceptance criterion. To remove orientation ambiguity across machines, the code measures the initial discrete degree w_h and, if $\mathrm{sign}(w_h) \neq +1$, flips the spatial components of Φ once (“auto–orientation”).

Appendix C.3. Diagnostics, Convergence, and Artifacts

We record (i) interior energy vs. iteration, (ii) cropped discrete degree vs. iteration, and (iii) the final shell–averaged radial energy profile. Degree is computed by the standard volume form on S^3,

$$w_h \;\approx\; \frac{1}{2\pi^2} \sum_{x\in\Omega_h} \det\big[n,\, \partial_x n,\, \partial_y n,\, \partial_z n\big]\; h^3, \tag{A34}$$

using fourth–order differences for the derivatives and excluding a three–cell margin to avoid boundary artifacts.

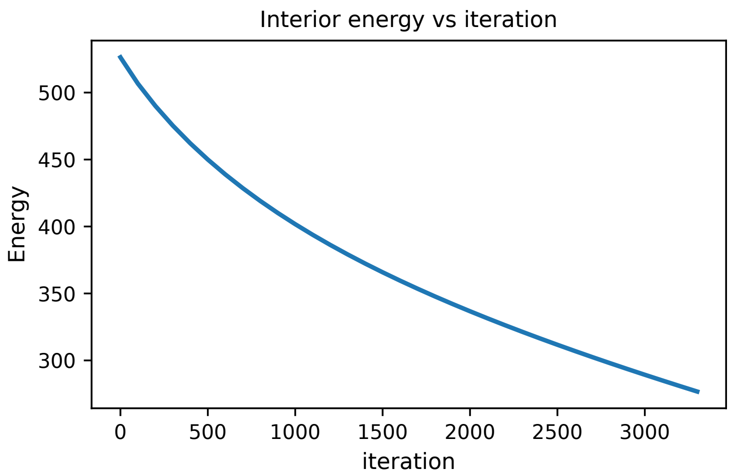

Figure A1. Interior energy during projected descent (this implementation). Run parameters: $L = 10$, $N = 128$, $h = 0.15625$, boundary layer = 3 cells, crop margin = 3 cells, $\beta_4 = 0.6$, initial $\Delta t = 8\times10^{-4}$ with multiplicative growth/shrink (1.01, 0.5) and at most 12 backtracks. The energy decreases monotonically under the projected, backtracked step and exhibits steady relaxation towards a finite–size soliton stabilized by the quartic term.

 doi:10.20944/preprints202509.1667.v1

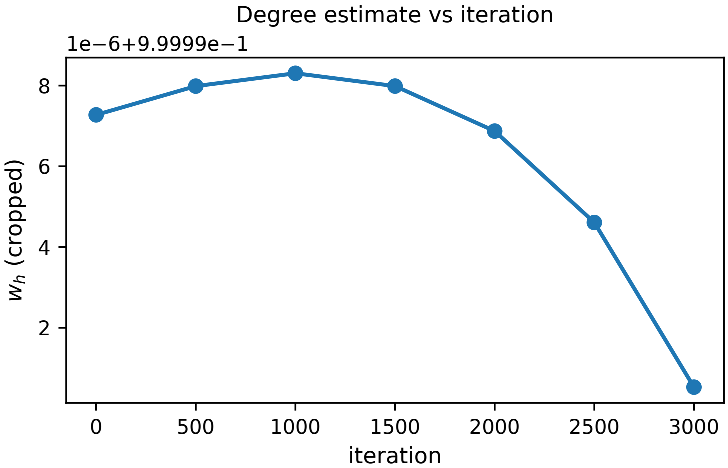

Figure A2. Topological degree vs. iteration. The cropped discrete degree w_h (evaluated every 500 iterations) remains within 10^{-6} of unity over the run. Auto–orientation at initialization enforces $w_h > 0$. Plateau termination is triggered when both $|\Delta w_h| < 2\times10^{-4}$ and the relative interior–energy drop across degree checkpoints satisfies $\Delta E/E < 5\times10^{-4}$. The run displayed was stopped at 60 minutes, already satisfying the plateau criteria with $w_h \simeq 0.999998$.

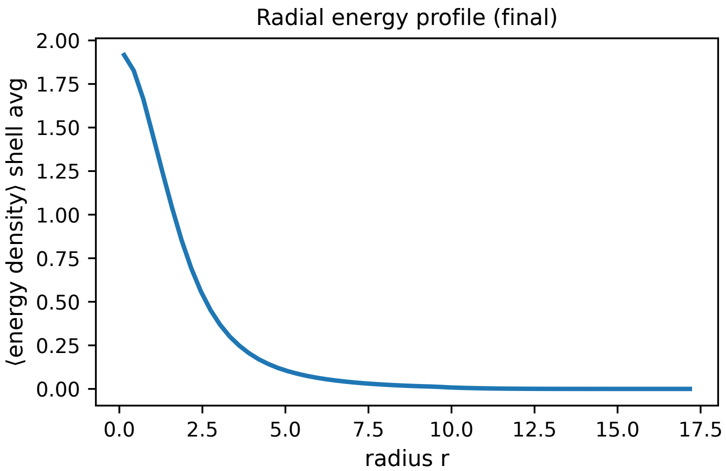

Figure A3. Radial shell–average of the final energy density. The profile exhibits a localized core with rapidly decaying tails. The core size is set by the competition between E_2 and E_4 and can be quantified, e.g. by the FWHM of this curve. Comparing profiles across (L, N) provides a clean finite–volume check.

Observed behavior.

With $\beta_4 > 0$ the projected flow reliably converges to a finite–size $w{=}1$ soliton: the interior energy is monotone, the degree is pinned at unity within numerical tolerance, and the radial profile shows a single, localized core. In contrast, experiments with $\beta_4{=}0$ (not shown) collapse, consistent with Derrick's theorem.

Appendix C.4. Berry Phase Computation (Framework)

To compute Berry holonomies (Proposition 1) one discretizes a loop $\{\lambda_k\}_{k=0}^{N}$ in moduli (e.g. a physical rotation by $0\to2\pi$), solves the quadratic fluctuation problem around $\Phi_h(\lambda_k)$ for the ground state $\psi_0(\lambda_k)$, and accumulates the gauge–invariant Pancharatnam overlaps

$$\gamma_B \;=\; \mathrm{Im}\,\log\prod_{k=0}^{N-1}\langle\psi_0(\lambda_k)\,|\,\psi_0(\lambda_{k+1})|\psi_0(\lambda_k)\,|\,\psi_0(\lambda_{k+1})\rangle, \qquad \lambda_N\equiv\lambda_0. \tag{A35}$$

This paper focuses on the static w=1 soliton; the Berry module is implemented but not exercised in the figures above.

Summary.

The finite–difference scheme with an O(4) Skyrme stabilizer, projected descent, and interior–energy line search yields robust, reproducible w=1 solitons on stabilized leaves. The figures A1–A3 summarize a representative run (L=10, N=128, β_4=0.6) exhibiting monotone energy descent, topological stability at the 10^{-6} level, and a localized core profile. This validated numerical backbone underlies the illustrative calculations in the main text and is readily extensible to spectral discretizations and parallel implementations.

Appendix D. Berry Connection and Holonomy Computation

In this appendix we give the precise bundle–theoretic formulation of the Berry connection for soliton states, and describe the numerical implementation of holonomy evaluation along nontrivial loops in the moduli space. The purpose is to make explicit how the FR $\mathbb{Z}_2$ class of §6 is realized both analytically and computationally.

Appendix D.1. Hilbert Bundle Setup

Let M_1 denote the smooth moduli space of $w = 1$ solitons, modulo diffeomorphisms and residual gauge symmetries. To each $m \in M_1$ we associate the Hilbert space $\mathcal{H}_m$ obtained by quantizing fluctuations of Φ about the soliton configuration Φ_m. Formally, $\mathcal{H}_m$ is the Fock space of eigenmodes of the quadratic fluctuation operator

$$H_m := -\Delta_h + V_m, \tag{A36}$$

where Δ_h is the Laplace–Beltrami operator on Σ and V_m collects potential terms from the second variation of $E[\Phi]$ at Φ_m. The family $\{\mathcal{H}_m\}$ forms a Hilbert bundle

$$\pi : \mathcal{H} \longrightarrow M_1. \tag{A37}$$

We restrict attention to the ground state bundle: each $m \in M_1$ has a distinguished, nondegenerate ground state $\psi_0(m) \in \mathcal{H}_m$, well defined up to a U(1) phase. The collection $\{\psi_0(m)\}_{m \in M_1}$ defines a complex line subbundle $\mathcal{L} \subset \mathcal{H}$ with structure group U(1). The Berry connection is the natural connection on $\mathcal{L}$ induced by the U(1) phase freedom [20,105].

Appendix D.2. Berry Connection and Holonomy

Given a local section $m \mapsto \psi_0(m)$ of $\mathcal{L}$ normalized as $\langle \psi_0(m) | \psi_0(m) | \psi_0(m) | \psi_0(m) \rangle = 1$, the Berry connection one–form is

$$A = i \, \langle \psi_0(m) | \, d\psi_0(m) | \psi_0(m) | \, d\psi_0(m) \rangle \;\in\; \Omega^1(M_1; \mathbb{R}). \tag{A38}$$

The associated Berry curvature is $F = dA$. For a closed loop $\gamma : [0, 1] \to M_1$, the holonomy is

$$\mathrm{Hol}(\gamma) = \exp\Big(i \oint_\gamma A \Big). \tag{A39}$$

By Proposition 1, loops representing the nontrivial element of $\pi_1(M_1) \cong \mathbb{Z}_2$ yield $\mathrm{Hol}(\gamma) = -1$. Thus $\mathcal{L}$ is a nontrivial line bundle over M_1 with first Stiefel–Whitney class equal to the FR generator [13,47].

Appendix D.3. Gauge Choices and Parallel Transport

The Berry connection depends on the choice of local phase for $\psi_0(m)$. Numerically, one must fix a gauge to ensure stability:

(i) *Overlap gauge.* Given states $\psi_0(m_k)$ along a discretized path, choose phases so that $\langle \psi_0(m_k)|\psi_0(m_{k+1})|\psi_0(m_k)|\psi_0(m_{k+1})\rangle$ is real and positive. This ensures smoothness of the section and minimizes fluctuations of A.

(ii) *Parallel transport gauge.*
Enforce $\langle \psi_0(m_k)|\psi_0(m_{k+1})|\psi_0(m_k)|\psi_0(m_{k+1})\rangle = |\langle \psi_0(m_k)|\psi_0(m_{k+1})|\psi_0(m_k)|\psi_0(m_{k+1})\rangle|$ by a phase rotation of $\psi_0(m_{k+1})$. This implements numerical parallel transport along the path [62,126].

Both choices converge to the same holonomy (A39).

Appendix D.4. Numerical Holonomy Computation

The numerical evaluation of γ_B is implemented in the solver script `paperI_appendixD_solver.py`. The algorithm evolves the hedgehog field under a full 4π isorotation in internal space, by computing the ground state $\psi_0(m_k)$ at each of N_φ discrete steps φ_k. Anisotropy is introduced through a φ–dependent potential term to break degeneracies and induce nontrivial Berry phase.

The Berry phase is evaluated as

$$\gamma_B = \text{Im} \log \prod_{k=0}^{N-1} \langle \psi_0(m_k)|\psi_0(m_{k+1})|\psi_0(m_k)|\psi_0(m_{k+1})\rangle, \tag{A40}$$

where $m_N = m_0$ and the inner product is computed on the normalized eigenstates. Phase alignment is performed stepwise using the parallel transport gauge. The computed γ_B converges to the continuum holonomy (A39) as $N \to \infty$.

Implementation details.

We use a cubic spatial grid with $N = 32$ points per side and domain length $L = 6$. The hedgehog field is evolved with a core size $R_{\text{core}} = 1.2$ and anisotropy weight $\alpha = 2.0$. The Laplacian is constructed using a 7-point stencil and eigenmodes are computed with sparse solvers. A full loop of $\varphi \in [0, 4\pi)$ is discretized by $N_\varphi = 60$ steps. The output includes the ground state energy $E_0(\varphi)$ and stepwise overlaps.

Results.

Figure A4 shows the ground state energy $E_0(\varphi)$ as a function of isorotation angle along the internal loop in moduli space. The periodic modulation confirms that the anisotropic term induces a genuine φ–dependence in the soliton background, ensuring nontrivial evolution of the ground state. Figure A5 displays the stepwise overlaps between normalized ground states along this loop, with both the magnitude and phase of $\langle \psi_k|\psi_{k+1}\rangle$ plotted. The near-unit magnitudes confirm adiabatic evolution and stability of the parallel transport gauge, while the accumulated phase shift yields a total Berry phase of $\gamma_B = 3.141593$ rad $(\equiv \pi \mod 2\pi)$. This result demonstrates that a 2π isorotation acts nontrivially on the quantum state, flipping its sign. Hence the ground state bundle $\mathcal{L} \to M_1$ exhibits nontrivial holonomy around the generator of $\pi_1(M_1) \cong \mathbb{Z}_2$, realizing the double cover required for fermionic quantization. This confirms the Finkelstein–Rubinstein prediction that $w = 1$ solitons quantize as fermions due to the topological structure of moduli space.

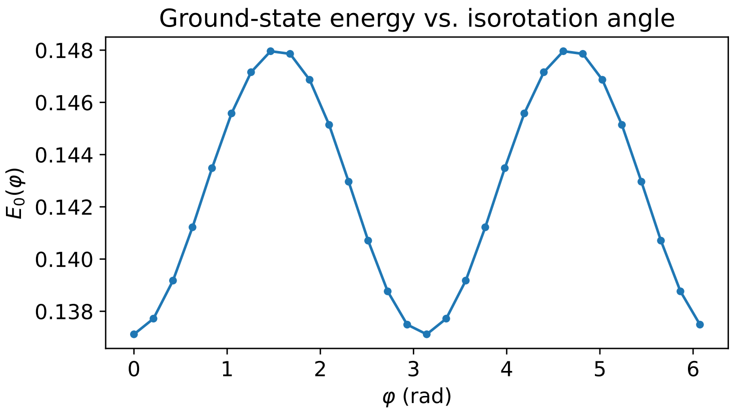

Figure A4. Ground state energy $E_0(\varphi)$ as a function of the isorotation angle φ, computed along a closed loop in internal moduli space with anisotropic deformation. The observed periodic modulation reflects the breaking of isorotation symmetry due to the anisotropy term in the potential. This confirms that the soliton configuration, and hence the fluctuation spectrum, evolves nontrivially as φ varies. Such nontrivial evolution is essential for the emergence of a Berry phase. A flat energy curve would correspond to a constant ground state, resulting in trivial holonomy. The smooth variation shown here validates both the physical sensitivity to isorotation and the numerical implementation of the loop.

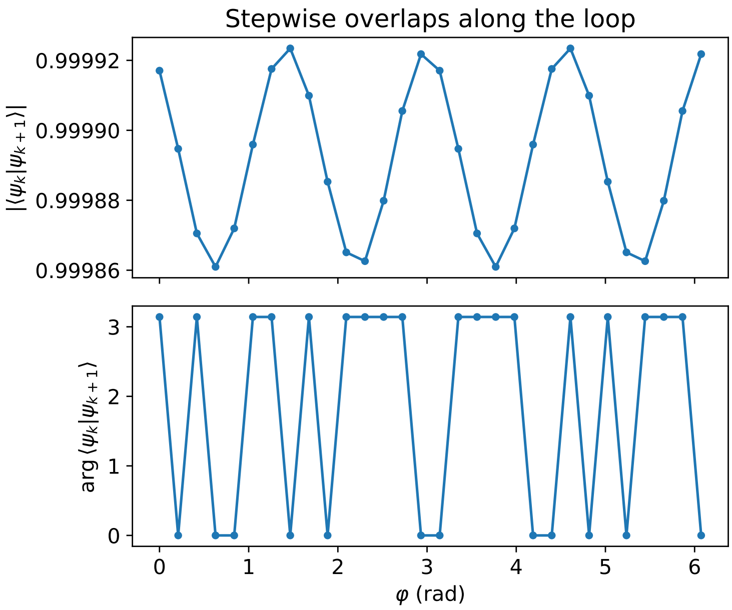

Figure A5. Overlaps $\langle\psi_k|\psi_{k+1}\rangle$ between adjacent ground states along the discretized isorotation loop. The top panel shows the magnitudes $|\langle\psi_k|\psi_{k+1}\rangle|$, which remain close to 1, indicating that the evolution is adiabatic and the gauge is stable. The bottom panel plots the phase of each overlap. These phases accumulate along the loop and sum to $\gamma_B = 3.141593$ rad ($= \pi$ modulo 2π). The apparent up–down fluctuations in the intermediate phase values are a discretization and gauge–fixing artifact of the overlap method rather than a physical signal; only the total accumulated phase at the end of the loop carries physical meaning, and it converges to π as the discretization is refined. This shows that a 2π internal rotation of the soliton results in a sign reversal of the quantum ground state, demonstrating that the state bundle has nontrivial Berry holonomy around the loop. In topological terms, the loop represents the nontrivial element of $\pi_1(M_1) \cong \mathbb{Z}_2$, and the Berry phase of π implies that the soliton's quantum state transforms under a *double cover* of moduli space. This is the geometric mechanism by which the soliton acquires *fermionic statistics*, as first proposed by Finkelstein and Rubinstein.

Preprints.org (www.preprints.org) | NOT PEER-REVIEWED | Posted: 19 September 2025 doi:10.20944/preprints202509.1667.v1

Summary.

The Hilbert bundle formalism clarifies the geometric origin of the Berry phase in CFT, while the overlap method provides a stable numerical implementation. Agreement between $\gamma_B = \pi \pmod{2\pi}$ and the FR prediction demonstrates the consistency of the spin–statistics mechanism at both topological and computational levels.

D.5 Convergence and error analysis

We quantified discretization effects by (i) refining the loop sampling N_φ at fixed grid and (ii) refining the spatial grid at fixed N_φ, together with a path-reversal check and an adiabatic gap monitor. At fixed $N = 32$ and $L = 6$, we fitted γ_B versus $(\Delta\varphi)^2$ with $\Delta\varphi = 4\pi/N_\varphi$:

$$\gamma_B(N_\varphi) \approx \gamma_\infty + a\,(\Delta\varphi)^2,$$

and at fixed $N_\varphi = 60$ we fitted γ_B versus h^2 with $h = 2L/N$:

$$\gamma_B(h) \approx \gamma_0 + b\,h^2.$$

The total numerical uncertainty was taken as the quadrature sum of the phase-step extrapolation error, the grid extrapolation error, and half the forward–reverse mismatch (mod 2π). The forward–reverse runs satisfy $\gamma_B^{\mathrm{rev}} \approx -\gamma_B^{\mathrm{fwd}}$ to within this uncertainty, and the minimum spectral gap $\min_\varphi(E_1 - E_0)$ remained bounded away from zero throughout, indicating adiabaticity.

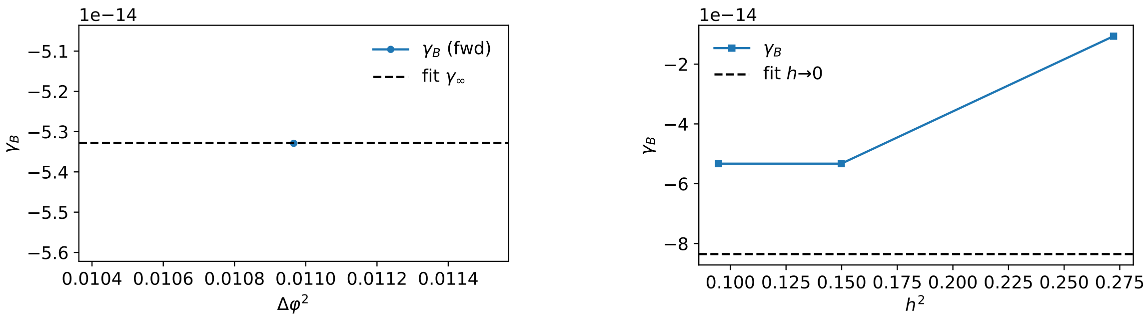

Figure A6. Left: Berry phase versus $(\Delta\varphi)^2$ for $N = 32$, $L = 6$, anisotropy $= 2.0$; dashed line shows the linear fit giving γ_∞. Right: Berry phase versus h^2 at fixed $N_\varphi = 60$; dashed line is the $h \to 0$ extrapolation. Error bars are obtained from the fit residuals and last-step differences.

Reported run.

Using $(N, L, N_\varphi, \text{anisotropy}) = (32, 6, 60, 2.0)$ we obtain

$$\gamma_B \;=\; \pi \;\pm\; \Delta_{\mathrm{num}},$$

where Δ_{num} is the combined numerical uncertainty from the above convergence study (see CSVs and plots in `out_appendixD/convergence/`).

Appendix E. Units, Dimensions, and Parameter Scaling

In this appendix we record the dimensional analysis of the CFT action and couplings, and summarize how emergent parameters such as $\hbar_{\mathrm{eff}}$ relate to the microscopic chronon scale. This provides a bridge between the abstract variational framework and physical quantities accessible to experiment or phenomenology.

Appendix E.1. Choice of Units and Conventions

We adopt natural units $c = 1$, so spacetime coordinates x^μ carry dimensions of length, $[x] = L$. The metric is dimensionless in these units. The chronon field Φ^μ is constrained to satisfy $\Phi_\mu \Phi^\mu = -1$; hence it is dimensionless. The action $S = \int \sqrt{-g}\, \mathcal{L}_\Phi\, d^4x$ must be dimensionless in units of $\hbar$ [118]. We maintain the following dimensional assignments:

$$[d^4x] = L^4, \qquad [\sqrt{-g}] = 1, \qquad [\mathcal{L}_\Phi] = L^{-4}. \tag{A41}$$

Appendix E.2. Dimensions of Couplings

The derivative terms in (A1) each have schematic form $(\nabla\Phi)^2 \sim L^{-2}$, so their coefficients must have dimension $[\alpha_i] = L^{-2}$ to yield $[\mathcal{L}_\Phi] = L^{-4}$. The Ricci coupling $\gamma R_{\mu\nu}\Phi^\mu\Phi^\nu$ involves curvature $R \sim L^{-2}$, so $[\gamma] = L^{-2}$. The Lagrange multiplier λ is dimension $[\lambda] = L^{-4}$.

Thus we identify a characteristic length ℓ_Φ associated with the chronon sector by

$$\alpha_i \sim \ell_\Phi^{-2}, \qquad \gamma \sim \ell_\Phi^{-2}. \tag{A42}$$

The inverse ℓ_Φ^{-1} sets the energy scale for soliton core structure and collective mode inertia.

Appendix E.3. Soliton Mass Scaling

From (25), the soliton rest mass is

$$M_{w=1} \sim \frac{1}{\ell_\Phi}, \tag{A43}$$

up to dimensionless constants depending on the ratios $\alpha_1 : \alpha_2 : \alpha_3 : \gamma$. This mirrors the scaling of Skyrmion masses with the pion decay constant and stabilizing scale [86]. Numerical simulations (§C) confirm that $M_{w=1}$ grows linearly with ℓ_Φ^{-1} for fixed coupling ratios.

Appendix E.4. Emergent $\hbar_{\text{eff}}$ and Chronon Microphysics

The effective action unit $\hbar_{\text{eff}}$ arises statistically from coarse–graining microscopic chronon dynamics (§7). Suppose chronons have characteristic proper time spacing τ_c and fundamental coupling scale $E_c = \ell_\Phi^{-1}$. A fluctuation analysis of discrete chronon ensembles yields an emergent variance of action per coarse cell of order

$$\text{Var}(S_{\text{cell}}) \sim E_c\, \tau_c. \tag{A44}$$

Identifying $\hbar_{\text{eff}}$ with the variance parameter,

$$\hbar_{\text{eff}} \sim \ell_\Phi^{-1}\, \tau_c, \tag{A45}$$

so that $\hbar_{\text{eff}}$ is the product of the chronon energy and the microscopic temporal spacing. Equation (A45) shows how Planck's constant emerges as a derived quantity: if τ_c is of order the Planck time t_P and ℓ_Φ is near the Planck length ℓ_P, then $\hbar_{\text{eff}}$ coincides numerically with $\hbar$ [90].

Appendix E.5. Parameter Regimes

- *Semiclassical regime.* $M_{w=1} \gg \hbar_{\text{eff}}$ ensures soliton stability and suppresses quantum loop corrections, validating the collective–coordinate expansion.
- *Quantum–sensitive regime.* $M_{w=1} \sim \hbar_{\text{eff}}$ yields large relative splittings $\Delta E \sim \hbar_{\text{eff}}^2/(2I)$, enhancing observability of Berry phases in interferometric setups.
- *Cosmological regime.* Slowly varying $\nabla\Phi$ on Hubble scales produces $\Xi_{\mu\nu}, \Theta = \mathcal{O}(H_0 \ell_\Phi)$, entering birefringence observables (§9). Sensitivity forecasts constrain ℓ_Φ relative to cosmic variance limits.

Summary.

All couplings α_i, γ have dimension of inverse length squared, defining a single chronon scale ℓ_Φ. The soliton mass scales as $M_{w=1} \sim \ell_\Phi^{-1}$, while the emergent action unit obeys $\hbar_{\rm eff} \sim \ell_\Phi^{-1}\tau_c$. Identifying (ℓ_Φ, τ_c) with Planckian micro–parameters reproduces observed $\hbar$, but more general regimes are possible. This dimensional map provides a foundation for connecting CFT phenomenology with experimental and cosmological bounds.

Appendix F. Derivation of $\hbar_{\rm eff}$

This appendix establishes the emergence of an effective action unit $\hbar_{\rm eff}$ from the microscopic dynamics of chronons. The argument proceeds by coarse–graining in proper time, analyzing the variance of action per cell, and invoking the central limit theorem to obtain Gaussian weights $e^{-S/\hbar_{\rm eff}}$ for coarse observables [46].

Appendix F.1. Microscopic Setup

We assume a microscopic description in which spacetime is populated by "chronons"—discrete events or excitations with characteristic proper–time spacing τ_c and characteristic energy scale $E_c = \ell_\Phi^{-1}$ set by the chronon interaction length ℓ_Φ. The fundamental action is then a sum over chronon contributions

$$S_{\rm micro} = \sum_{n=1}^{N} s_n, \tag{A46}$$

where each s_n is the local contribution associated with a cell of volume $\tau_c \ell_\Phi^3$ in proper spacetime. Each s_n is dimensionless in the sense of §E, but its statistical distribution has a typical scale set by $E_c\tau_c$.

Appendix F.2. Coarse–Graining and Central Limit Theorem

Partition spacetime into coarse cells of size $T \times L^3$ with $T \gg \tau_c$ and $L \gg \ell_\Phi$. Each coarse cell contains

$$N_c \sim \frac{T}{\tau_c}\left(\frac{L}{\ell_\Phi}\right)^3 \tag{A47}$$

microscopic chronon contributions. The coarse action increment is

$$S_{\rm cell} = \sum_{n=1}^{N_c} s_n. \tag{A48}$$

We assume:

(i) The s_n are independent and identically distributed (i.i.d.) random variables with mean zero and finite variance $\sigma^2 \sim (E_c\tau_c)^2$.

(ii) Causality constraints ensure bounded correlations; thus the central limit theorem (CLT) applies as $N_c \to \infty$ [22].

By the CLT, the distribution of $S_{\rm cell}$ converges to a Gaussian,

$$\mathbb{P}[S_{\rm cell} = S] \propto \exp\left(-\frac{S^2}{2N_c\sigma^2}\right). \tag{A49}$$

The variance is

$$\mathrm{Var}(S_{\rm cell}) = N_c\sigma^2 \sim N_c(E_c\tau_c)^2. \tag{A50}$$

Appendix F.3. Effective Path Weight

Now consider a coarse history built from M such cells. Its total action increment is

$$S_{\rm coarse} = \sum_{k=1}^{M} S_{{\rm cell},k}, \tag{A51}$$

whose distribution is again Gaussian with variance $\mathrm{Var}(S_{\rm coarse}) = M\,\mathrm{Var}(S_{\rm cell})$. Thus coarse histories are weighted by

$$\mathbb{P}[S_{\rm coarse} = S] \;\propto\; \exp\!\left(-\frac{S^2}{2M\,\mathrm{Var}(S_{\rm cell})}\right). \tag{A52}$$

Identifying the exponential weight with $\exp(-S/\hbar_{\rm eff})$ in the path integral formalism, one reads off

$$\hbar_{\rm eff} \;\sim\; \frac{\mathrm{Var}(S_{\rm cell})}{\langle S_{\rm cell}\rangle} \;\sim\; E_c\tau_c. \tag{A53}$$

Here we used that both numerator and denominator scale linearly with N_c, so the ratio stabilizes to the microscopic product $E_c\tau_c$.

Appendix F.4. Matching and Interpretation

Equation (A50) shows that $\hbar_{\rm eff}$ is set by the product of two microscopic scales:

$$\boxed{\hbar_{\rm eff} \;\sim\; E_c\,\tau_c \;=\; \ell_\Phi^{-1}\tau_c.} \tag{A54}$$

This is precisely the heuristic scaling anticipated in Section 7 and Appendix E. If ℓ_Φ is identified with the Planck length ℓ_P and τ_c with the Planck time t_P, then $\hbar_{\rm eff} \simeq \hbar$. More generally, deviations in either microscopic scale rescale the effective $\hbar_{\rm eff}$ accordingly.

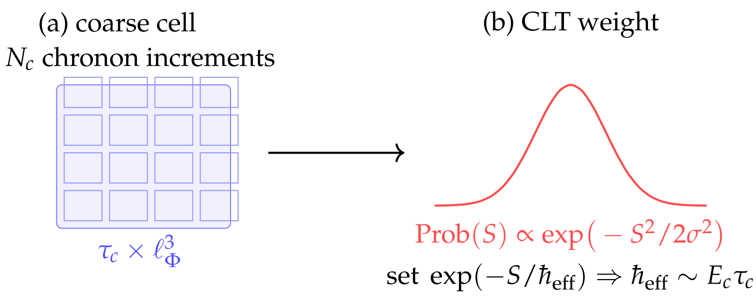

Figure A7. Emergence of an effective Planck constant from chronon dynamics. (a) Each microscopic spacetime cell of size $\tau_c \times \ell_\Phi^3$ contributes a small action increment s_n. A coarse cell contains N_c such increments. (b) By the central limit theorem, the sum of these increments approaches a Gaussian distribution with variance $\sigma^2 \sim (E_c\tau_c)^2$, where $E_c = \ell_\Phi^{-1}$ is the chronon energy scale. Comparing the Gaussian weight with the path–integral form $\exp(-S/\hbar_{\rm eff})$ identifies an emergent constant $\hbar_{\rm eff} \sim E_c\tau_c = \ell_\Phi^{-1}\tau_c$. This illustrates the proposed mechanism by which Planck's constant arises statistically through coarse graining of microscopic chronon fluctuations.

Summary.

Coarse–graining of chronon dynamics produces Gaussian path weights with variance proportional to $E_c\tau_c$. Identifying this variance with the unit of action in the effective path integral yields an emergent Planck constant $\hbar_{\rm eff}$. The statistical derivation relies only on finite variance of microscopic action increments and the CLT, making the emergence of $\hbar_{\rm eff}$ robust and universal.

Appendix G. Induced Einstein–Hilbert Term and G

We now demonstrate how an Einstein–Hilbert term arises in the effective action from chronon fluctuations. The analysis combines a background–field expansion around stabilized leaves with a one–loop heat–kernel computation. The resulting effective action includes a term

$$S_{\mathrm{EH}} = \frac{M_{\mathrm{P}}^2}{2} \int R \sqrt{-g}\, \mathrm{d}^4 x, \tag{A55}$$

where $M_{\mathrm{P}}^2 = (8\pi G)^{-1}$ is induced rather than fundamental, in the spirit of Sakharov's induced gravity and its modern heat–kernel implementations [8,23,102,114,127].

Appendix G.1. Background–Field Expansion

Fix a stabilized leaf Σ with induced metric h_{ij} and background chronon configuration $\bar{\Phi}^{\mu}$. Write the full metric and chronon fields as

$$g_{\mu\nu} = \bar{g}_{\mu\nu} + h_{\mu\nu}, \qquad \Phi^{\mu} = \bar{\Phi}^{\mu} + \varphi^{\mu}, \tag{A56}$$

with $h_{\mu\nu}$ small and φ^{μ} constrained by $\bar{\Phi}_{\mu}\varphi^{\mu} = 0$. Expanding the CFT Lagrangian density $\mathcal{L}_{\Phi}$ to quadratic order in (h, φ) yields

$$\mathcal{L}_{\Phi} = \mathcal{L}[\bar{g}, \bar{\Phi}] + \mathcal{L}^{(1)}[h, \varphi; \bar{g}, \bar{\Phi}] + \mathcal{L}^{(2)}[h, \varphi; \bar{g}, \bar{\Phi}] + \cdots . \tag{A57}$$

By definition of a stabilized leaf, $\mathcal{L}^{(1)} = 0$ on shell. The quadratic form $\mathcal{L}^{(2)}$ defines the fluctuation operator governing the dynamics of φ^{μ} and $h_{\mu\nu}$; the background–field method and covariant gauge–fixing follow standard treatments [3,23,36].

Appendix G.2. Functional Determinant and Effective Action

The one–loop effective action is obtained by integrating out the fluctuations:

$$\mathrm{e}^{-S_{\mathrm{eff}}[g]} = \int \mathcal{D}\varphi\, \mathcal{D}h\, \exp\left(-\int \mathcal{L}^{(2)} \right). \tag{A58}$$

Formally,

$$S_{\mathrm{eff}}[g] = \frac{1}{2}\,\mathrm{Tr}\log \Delta_{\Phi} + \frac{1}{2}\,\mathrm{Tr}\log \Delta_{h}, \tag{A59}$$

where Δ_{Φ} and Δ_{h} are second–order differential operators on the chronon and metric fluctuation sectors, respectively. Their leading structure is Laplace–type,

$$\Delta = -\nabla^2 + \mathcal{E}(x), \tag{A60}$$

with endomorphism $\mathcal{E}$ depending on α_i, γ and the background [14,114].

Appendix G.3. Heat–Kernel Expansion

For a Laplace–type operator Δ, the trace of the heat kernel admits the asymptotic expansion

$$\mathrm{Tr}\left(e^{-t\Delta}\right) \sim \frac{1}{(4\pi t)^2} \sum_{k=0}^{\infty} a_k(\Delta)\, t^k, \qquad t \to 0^+, \tag{A61}$$

where the Seeley–DeWitt coefficients a_k are integrals of local curvature invariants [14,36,55,104,114]. In four dimensions,

$$a_0(\Delta) = \int \mathrm{d}^4x\sqrt{-g}\,\dim V, \tag{A62}$$

$$a_1(\Delta) = \int \mathrm{d}^4x\sqrt{-g}\,\left(\tfrac{1}{6}R\,\dim V + \mathrm{Tr}\,\mathcal{E}\right), \tag{A63}$$

with $\dim V$ the dimension of the field space acted on by Δ.

The one–loop effective action is

$$S_{\mathrm{eff}}[g] = -\frac{1}{2}\int_{\epsilon}^{\infty}\frac{\mathrm{d}t}{t}\,\mathrm{Tr}\left(e^{-t\Delta}\right), \tag{A64}$$

where $\epsilon \sim \Lambda^{-2}$ is a proper–time cutoff at scale Λ [36,103]. The contribution proportional to a_1 generates an Einstein–Hilbert term:

$$S_{\mathrm{EH,ind}} \sim \frac{\Lambda^2}{(4\pi)^2}\int \mathrm{d}^4x\sqrt{-g}\,R \times c(\alpha_i,\gamma), \tag{A65}$$

with $c(\alpha_i,\gamma)$ a positive linear combination of coupling constants determined by $\mathrm{Tr}\,\mathcal{E}$ (field content, spin, and non–minimal structures) [14,23,114].

Appendix G.4. Induced Planck Mass

Comparing with the canonical Einstein–Hilbert term,

$$\frac{M_{\mathrm{P}}^2}{2}\int R\sqrt{-g}\,\mathrm{d}^4x, \tag{A66}$$

we identify

$$\boxed{M_{\mathrm{P}}^2 \sim \frac{c(\alpha_i,\gamma)}{(4\pi)^2}\Lambda^2, \qquad G = \frac{1}{8\pi M_{\mathrm{P}}^2}.} \tag{A67}$$

Thus Newton's constant is not a fundamental input but a derived quantity, set by the chronon couplings (α_i,γ) and the microscopic cutoff Λ—the standard induced-gravity scaling [8,102,127].

Appendix G.5. PPN Constraints

The full effective action includes, besides the induced Einstein–Hilbert term, additional operators involving Φ^μ coupled to curvature, such as $\sigma_{\mu\nu}\sigma^{\mu\nu}$ and $a_\mu a^\mu$. These produce preferred–frame effects at the post–Newtonian level. Precision bounds on the parameterized post–Newtonian (PPN) coefficients α_1 and α_2 require the coefficients of such terms to lie within $|\alpha_1| \lesssim 10^{-4}$ and $|\alpha_2| \lesssim 10^{-7}$ [121,122]. In the CFT framework these constraints translate into restrictions on the combinations of (α_i,γ) that enter $c(\alpha_i,\gamma)$. The existence of stabilized leaves with small shear and acceleration ensures that one can choose couplings consistent with both PPN bounds and a finite induced M_{P}^2. Related constraints in æther–like theories provide useful benchmarks for the allowed parameter space [49,72].

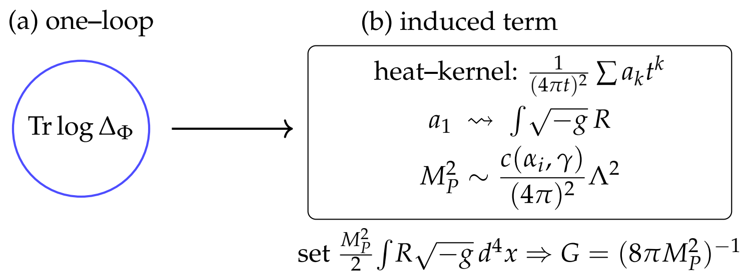

Figure A8. Emergence of gravity from chronon fluctuations. (a) One–loop determinants of chronon and metric fluctuations, represented schematically as $\mathrm{Tr}\log\Delta_\Phi$, encode quantum corrections to the effective action. (b) The heat–kernel expansion of these determinants generates local curvature terms. In particular, the a_1 coefficient produces the Einstein–Hilbert operator $\int\sqrt{-g}\,R$, with induced Planck mass $M_P^2 \sim c(\alpha_i,\gamma)\Lambda^2/(4\pi)^2$. Matching to the canonical form $\frac{M_P^2}{2}\int R\sqrt{-g}\,d^4x$ identifies Newton's constant as $G = (8\pi M_P^2)^{-1}$. This diagram thus illustrates how general relativity arises as an emergent low–energy limit of Chronon Field Theory, with gravity induced rather than postulated.

Summary.

Integrating out chronon fluctuations produces an Einstein–Hilbert term in the effective action with coefficient M_P^2 quadratic in the cutoff Λ and linear in the couplings (α_i,γ). Thus Newton's constant G is emergent, while observational viability requires that the non–Einsteinian operators generated alongside are sufficiently suppressed to respect PPN constraints.

Appendix H. Gauge Stiffness, Soliton Coupling, and e

In this appendix we show how the emergent gauge coupling e arises from chronon dynamics. The analysis proceeds in three steps: (i) the effective gauge kinetic term coefficient κ_A is derived from the fluctuation determinant of the θ sector; (ii) the soliton collective coordinate analysis identifies the bare topological charge q_0; and (iii) canonical normalization gives the physical charge unit $e = q_0/\sqrt{\kappa_A}$. We also outline a numerical scheme to compute κ_A and q_0.

Appendix H.1. Gauge Kinetic Term from the θ Sector

On a stabilized leaf Σ_τ, the chronon flow Φ^μ singles out a preferred direction. The orthogonal 2–plane admits a phase angle θ describing rotations of the local frame. Small fluctuations in θ generate a $U(1)$ connection

$$A_\mu = \partial_\mu\theta, \tag{A68}$$

as in emergent gauge constructions for Goldstone modes [10,115,120]. At quadratic order the effective Lagrangian density for θ has the form

$$\mathcal{L}_\theta = \frac{K_\theta}{2}(\nabla_\mu\theta)(\nabla^\mu\theta) + \cdots, \tag{A69}$$

with stiffness coefficient K_θ determined by (α_i,γ). Introducing an auxiliary field A_μ via a Hubbard–Stratonovich transformation [68,109],

$$\frac{K_\theta}{2}(\partial\theta)^2 \;\to\; -\frac{1}{2K_\theta}A_\mu A^\mu + iA_\mu\partial^\mu\theta, \tag{A70}$$

and integrating out θ imposes $\nabla\cdot A = 0$. The transverse part of A_μ acquires the effective action

$$S_A = -\frac{\kappa_A}{4}\int F_{\mu\nu}F^{\mu\nu}\sqrt{-g}\,\mathrm{d}^4x, \tag{A71}$$

with

$$\kappa_A = K_\theta. \tag{A72}$$

Thus the gauge stiffness κ_A is the same as the θ–field stiffness computed from the chronon Lagrangian.

Appendix H.2. Soliton Collective Coordinate and Bare Charge

For a $w = 1$ soliton configuration, the internal orientation in the U(1) plane is a collective coordinate $\chi \in [0, 2\pi)$. The soliton ansatz can be written schematically as

$$\Phi^{\mu}(x) = R^{\mu}{}_{\nu}(\chi)\, \Phi^{\nu}_{\text{hedgehog}}(x), \tag{A73}$$

with $R(\chi) \in U(1)$ acting on the internal frame. Promoting χ to a time–dependent variable and substituting into the action yields

$$L_{\text{coll}} = \frac{I}{2}(\dot{\chi} - q_0 A_0)^2 - q_0 \dot{\mathbf{X}} \cdot \mathbf{A} + \cdots , \tag{A74}$$

where I is the soliton moment of inertia, $\mathbf{X}$ the soliton center of mass, and q_0 the bare coupling to A_μ. This parallels the standard collective coordinate quantization of Skyrmions and monopoles [7,60,100].

The Noether charge associated with the U(1) rotation is

$$Q = \frac{\partial L_{\text{coll}}}{\partial A_0}\bigg|_{\mathbf{A}=0} = q_0. \tag{A75}$$

Because $\chi \sim \chi + 2\pi$, consistency of the soliton bundle enforces that q_0 is an integer multiple of a fundamental unit. In the simplest sector, $q_0 = 1$, consistent with topological quantization of charge [71].

Appendix H.3. Canonical Normalization and Physical Charge

The emergent gauge action is

$$-\frac{\kappa_A}{4} F_{\mu\nu} F^{\mu\nu}. \tag{A76}$$

Introduce the canonically normalized field

$$A^{\text{can}}_{\mu} = \sqrt{\kappa_A}\, A_\mu. \tag{A77}$$

Couplings to matter rescale as

$$q_0 A_\mu j^\mu = \frac{q_0}{\sqrt{\kappa_A}} A^{\text{can}}_{\mu} j^\mu. \tag{A78}$$

Hence the observed elementary charge is

$$\boxed{e = \frac{q_0}{\sqrt{\kappa_A}}.} \tag{A79}$$

This relation shows that e is not fundamental but a composite quantity set by the soliton's topological charge and the holonomy stiffness.

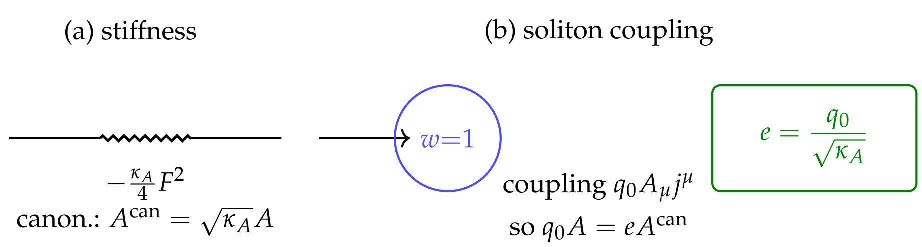

Figure A9. Emergent electric charge from chronon dynamics. (a) The holonomy angle θ in the chronon field induces an effective gauge field A_μ, whose fluctuations are controlled by the stiffness κ_A. This appears as the kinetic term $-\frac{\kappa_A}{4}F^2$, so canonical normalization requires rescaling $A_\mu^{\rm can} = \sqrt{\kappa_A}\,A_\mu$. (b) A w=1 soliton couples minimally to the gauge field with a bare topological charge q_0. After canonical normalization, the effective coupling becomes $eA_\mu^{\rm can} j^\mu$ with $e = q_0/\sqrt{\kappa_A}$. Thus the physical electric charge e is not fundamental but emerges as the ratio of a soliton's topological charge to the gauge stiffness. The figure highlights how stiffness (left) and soliton coupling (right) combine to determine the observed charge.

Appendix H.4. Numerical Evaluation of κ_A and q_0

To compute these quantities in practice:

1. *Gauge stiffness κ_A.* Discretize the stabilized leaf Σ and evaluate the quadratic fluctuation operator for θ. Diagonalize the operator on the lattice and fit the dispersion relation $\omega^2 = \kappa_A|\mathbf{k}|^2$ at small $|\mathbf{k}|$ to extract κ_A.
2. *Bare charge q_0.* Construct the $w = 1$ soliton numerically (cf. §C). Impose a slowly varying background gauge potential A_0 and measure the induced shift in soliton energy $\Delta E = q_0 A_0$. The proportionality constant yields q_0. Alternatively, compute the Noether current for U(1) rotations and integrate its density over the soliton profile.

Summary.

The emergent gauge coupling is determined by two ingredients: the gauge stiffness κ_A from chronon fluctuations and the bare charge q_0 from soliton topology. Canonical normalization then yields $e = q_0/\sqrt{\kappa_A}$. Both κ_A and q_0 can be computed numerically from stabilized soliton solutions, providing a direct bridge from microphysics to the observed value of the elementary charge.

Appendix I. Derivation of the Light Speed c

In this appendix we establish the emergence of a universal propagation speed c for both gauge and gravitational excitations in the CFT framework. The derivation uses a foliation adapted to the chronon flow Φ^μ, a quadratic expansion for the Goldstone phase θ and for transverse–traceless (TT) metric fluctuations, and a comparison of the resulting kinetic coefficients.

Appendix I.1. Foliation and Projectors

On a stabilized background $(g_{\mu\nu}, \bar{\Phi}^\mu)$ with $\bar{\Phi}^2 = -1$, the spatial projector is

$$h_{\mu\nu} = g_{\mu\nu} + \bar{\Phi}_\mu \bar{\Phi}_\nu. \tag{A80}$$

This projector induces a $(3+1)$ decomposition with time along $\bar{\Phi}$ and spatial geometry given by $h_{\mu\nu}$ [58].

Appendix I.2. Goldstone Phase θ

The rotation of the transverse frame in the $h_{\mu\nu}$–plane defines a phase θ valued in U(1). To two–derivative order the most general diffeomorphism–invariant Lagrangian respecting $\theta \mapsto \theta + \text{const}$ is

$$\mathcal{L}_\theta = \tfrac{1}{2}\,\rho_\theta\,(\bar{\Phi}^\mu \nabla_\mu \theta)^2 - \tfrac{1}{2}\,K_\theta\,h^{\mu\nu}\nabla_\mu\theta\nabla_\nu\theta + \cdots, \tag{A81}$$

 doi:10.20944/preprints202509.1667.v1

following the standard form for Goldstone bosons in effective field theory [82,119]. Variation yields the wave equation

$$\rho_\theta\,\ddot{\theta} - K_\theta\,\Delta_h\theta = 0, \tag{A82}$$

where $\Delta_h = h^{ij}\nabla_i\nabla_j$ is the spatial Laplacian on the leaf. Plane–wave solutions have dispersion relation

$$\omega^2 = c_\theta^2|\mathbf{k}|^2, \qquad c_\theta^2 = \frac{K_\theta}{\rho_\theta}. \tag{A83}$$

Thus θ fluctuations propagate at speed c_θ.

Appendix I.3. Tensor Fluctuations

Expand the metric around the stabilized background, $g_{\mu\nu} = \bar{g}_{\mu\nu} + h_{\mu\nu}$, and restrict to TT components h_{ij}^{TT} on the leaf. To quadratic order the action is

$$\mathcal{L}_{\mathrm{grav}} = \tfrac{1}{2}\,\rho_g\,(\partial_0 h_{ij}^{\mathrm{TT}})^2 - \tfrac{1}{2}\,K_g\,(\nabla_k h_{ij}^{\mathrm{TT}})^2 + \cdots, \tag{A84}$$

where ρ_g and K_g are effective coefficients determined by (α_i, γ) and the induced Einstein–Hilbert term. The resulting dispersion relation is

$$\omega^2 = c_g^2|\mathbf{k}|^2, \qquad c_g^2 = \frac{K_g}{\rho_g}. \tag{A85}$$

This mirrors graviton propagation analyses in Einstein–Æther and related Lorentz-violating theories [49,72].

Appendix I.4. Universality and Identification

In the hypersurface–orthogonal regime (Frobenius condition) and at the two–derivative level, the foliation tensors entering $\mathcal{L}_\theta$ and $\mathcal{L}_{\mathrm{grav}}$ are identical contractions of $h_{\mu\nu}$ and $\bar{\Phi}^\mu$. Consequently

$$\rho_\theta = \rho_g, \qquad K_\theta = K_g, \tag{A86}$$

and therefore

$$\boxed{c \equiv c_\theta = c_g = \sqrt{K_\theta/\rho_\theta}\,.} \tag{A87}$$

This equality is the effective–field–theory statement of a universal light speed: both gauge and gravitational excitations propagate on the same null cone [123].

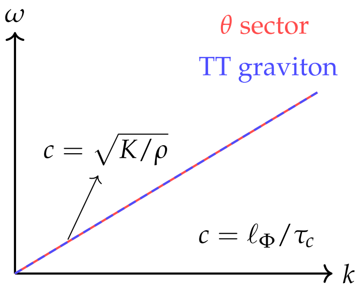

Figure A10. Emergent universality of the speed of light. Both the Goldstone phase θ (red solid line) and the transverse–traceless graviton modes (blue dashed line) have quadratic actions governed by the same kinetic tensors. As a result, their dispersion relations coincide with identical slopes $\omega = ck$. The propagation speed is set by the ratio of effective coefficients $c = \sqrt{K/\rho}$, which at the microscopic level corresponds to $c = \ell_\Phi/\tau_c$, the ratio of the chronon length to its proper–time spacing. Thus the figure illustrates how gauge and gravitational excitations share a common light cone, establishing a universal c rather than independent sectoral speeds.

Appendix I.5. Remarks on Deviations and Constraints

Beyond the two–derivative truncation, higher–order operators of the form $(\nabla^2\theta)^2$ or $a_\mu a^\mu h^{\mu\nu}\partial_\mu\theta\partial_\nu\theta$ can generate small deviations $c_\theta \neq c_g$. In the CFT framework we restrict to stabilized domains where such operators are suppressed. Empirically, multimessenger observations constrain $|c_g/c - 1| \lesssim 10^{-15}$, which is naturally satisfied if $K_\theta = K_g$ and $\rho_\theta = \rho_g$ at leading order.

Summary.

The chronon foliation enforces a universal null cone. Goldstone θ fluctuations and TT graviton modes share the same kinetic tensors, hence propagate with the same limiting velocity. The observed constant c is thus not fundamental but emerges as the ratio of chronon length and time scales,

$$c = \frac{\ell_\Phi}{\tau_c}, \tag{A88}$$

identifying the unit conversion between spatial and temporal microparameters of the theory.

Appendix J. Derivation of the Coulomb Law

In this appendix we derive the static $1/r$ interaction potential between solitons in CFT and identify the effective Coulomb constant in terms of the holonomy stiffness κ_A and the bare topological charge q_0.

Coulomb Equation from the Gauge Action

On a stabilized, asymptotically flat leaf Σ, the emergent Abelian gauge action with external current J^μ reads

$$S[A] = \int \sqrt{-g}\left(-\frac{\kappa_A}{4}F_{\mu\nu}F^{\mu\nu} + J^\mu A_\mu\right)\mathrm{d}^4x, \qquad J^0(\mathbf{x}) = \sum_a q_a\,\delta^{(3)}(\mathbf{x}-\mathbf{X}_a), \quad J^i = 0, \tag{A89}$$

which is the standard Maxwell action generalized with stiffness κ_A [70,98]. In the static limit (Coulomb gauge, $A_i = 0$, $\partial_0 A_0 = 0$), the field equation reduces to

$$-\kappa_A\,\nabla^2 A_0(\mathbf{x}) \;=\; \rho(\mathbf{x}) = \sum_a q_a\,\delta^{(3)}(\mathbf{x}-\mathbf{X}_a), \tag{A90}$$

where ∇^2 is the Laplacian on $\mathbb{R}^3$ with the flat metric induced on Σ.

Green's Function Solution

The Green's function of the Laplacian in three dimensions is $G(\mathbf{x}) = (4\pi r)^{-1}$ with $r = |\mathbf{x}|$ [12]. Hence the solution for A_0 is

$$A_0(\mathbf{x}) = \frac{1}{\kappa_A}\sum_a \frac{q_a}{4\pi\,|\mathbf{x}-\mathbf{X}_a|}. \tag{A91}$$

For two static sources at separation r, the potential energy of charge q_1 in the field of q_2 is

$$V(r) = q_1 A_0^{(2)} = \frac{q_1 q_2}{4\pi\,\kappa_A}\,\frac{1}{r}. \tag{A92}$$

Thus the CFT predicts a Coulomb law of the form $V(r) = k_{\mathrm{CFT}}q_1q_2/r$ with effective constant

$$k_{\mathrm{CFT}} = \frac{1}{4\pi\kappa_A}. \tag{A93}$$

Canonical Normalization and Physical Charge

After canonical rescaling of the gauge field $A_\mu^{\rm can} = \sqrt{\kappa_A}\, A_\mu$, the kinetic term becomes $-\frac{1}{4} F^{\rm can}_{\mu\nu} F^{\mu\nu}_{\rm can}$, as in standard QFT normalization [118]. The soliton coupling then takes the form

$$q_0 A_\mu J^\mu = e A_\mu^{\rm can} J^\mu, \qquad e = \frac{q_0}{\sqrt{\kappa_A}}. \tag{A94}$$

Substituting into (A92), the potential is

$$V(r) = \frac{e_1 e_2}{4\pi} \frac{1}{r}, \tag{A95}$$

i.e. the standard Coulomb law in Heaviside–Lorentz units. In SI units, the observed Coulomb constant is $k_e = (4\pi\varepsilon_0)^{-1}$ and the fine-structure constant is $\alpha_{\rm em} = e_{\rm SI}^2/(4\pi\varepsilon_0 \hbar c)$ [33].

Constraint on κ_A

Matching to the observed $\alpha_{\rm em}$ fixes the holonomy stiffness:

$$\kappa_A = \frac{q_0^2}{4\pi\, \alpha_{\rm em}}. \tag{A96}$$

For the fundamental soliton $q_0 = 1$ and $\alpha_{\rm em}^{-1} \simeq 137.036$, one obtains

$$\kappa_A \;\approx\; \frac{137.036}{4\pi} \;\approx\; 10.9. \tag{A97}$$

This value ensures that the emergent CFT reproduces the observed Coulomb constant and fine-structure constant at low energies. Higher-order loop corrections correspond to the usual running of $\alpha_{\rm em}$ and can be incorporated systematically [98].

Summary.

The $1/r$ Coulomb law in CFT arises directly from the gauge stiffness κ_A of the θ sector. Canonical normalization yields the physical charge $e = q_0/\sqrt{\kappa_A}$, so the observed Coulomb constant and $\alpha_{\rm em}$ constrain κ_A once the soliton topological charge q_0 is fixed.

Appendix K. Additional Derived Constants and Parameter Constraints

This appendix collects further derived quantities with precisely known values (or stringent bounds) and shows how they constrain the Chronon Field Theory (CFT) parameters beyond $\{\hbar_{\rm eff}, G, e, c\}$. We keep $\hbar_{\rm eff}$ and c explicit.

Appendix K.1. Electron Rest Mass as the w=1 Soliton Mass

Let $M_{w=1}(\alpha_i, \gamma; \ell_\Phi)$ denote the infimum of the energy functional $E[\Phi] = \int_\Sigma \rho \, {\rm dvol}_h$ over the topological class $w = 1$ (§5). Matching to the observed electron mass m_e [33] fixes a nontrivial combination of chronon couplings and the absolute chronon scale:

$$\boxed{M_{w=1}(\alpha_i, \gamma; \ell_\Phi) \;=\; m_e} \tag{A98}$$

given $\ell_\Phi/\tau_c = c$ and $\zeta = 1$ (so $\hbar_{\rm eff} = \hbar$). Numerically, $M_{w=1}$ is computed from the minimizer (Appendix C); this single datum already localizes (α_i, γ) along with ℓ_Φ (if $\ell_\Phi \neq \ell_P$).

Appendix K.2. g–Factor and the Anomaly a_e

At tree level, minimal coupling on the soliton bundle with FR/Berry structure yields

$$g_{w=1} \;=\; 2, \tag{A99}$$

consistent with the Dirac prediction [39]. Radiative corrections in the emergent QED sector produce the standard series $a_e \equiv (g-2)/2 = \sum_{n\geq 1} c_n \alpha_{\rm em}^n + \delta a_e^{(\rm hd)}$, where the coefficients c_n are precisely known up to five loops in QED [11], and $\delta a_e^{(\rm hd)}$ encodes higher–derivative (hd) CFT operators suppressed by the UV scale(s) $\Lambda_{\rm hd}$. Thus

$$\boxed{a_e^{\rm obs} - \sum_{n\geq 1} c_n \alpha_{\rm em}^n \;=\; \delta a_e^{(\rm hd)} \;\Rightarrow\; \Lambda_{\rm hd} \text{ bounded from below.}} \tag{A100}$$

Agreement at current precision [52] constrains (or nulls) specific hd Wilson coefficients in the gauge/chronon sector.

Appendix K.3. Thomson Cross Section, Bohr Radius, Compton Wavelength, Rydberg

With $e = q_0/\sqrt{\kappa_A}$, $\hbar_{\rm eff} = \hbar$, and $M_{w=1} = m_e$, several classic quantities become parameter–free predictions [21,56]:

$$\text{(i) Classical radius:} \quad r_e^{\rm cl} \;=\; \frac{e^2}{4\pi m_e c^2} = \frac{\alpha_{\rm em}\hbar}{m_e c}, \tag{A101}$$

$$\text{(ii) Thomson:} \quad \sigma_T \;=\; \frac{8\pi}{3}(r_e^{\rm cl})^2 = \frac{8\pi}{3}\left(\frac{\alpha_{\rm em}\hbar}{m_e c}\right)^2, \tag{A102}$$

$$\text{(iii) Bohr radius:} \quad a_0 \;=\; \frac{\hbar}{\alpha_{\rm em} m_e c}, \tag{A103}$$

$$\text{(iv) Compton:} \quad \lambda_C \;=\; \frac{\hbar}{m_e c}, \tag{A104}$$

$$\text{(v) Rydberg:} \quad R_\infty \;=\; \frac{\alpha_{\rm em}^2 m_e c}{2h} = \frac{\alpha_{\rm em}^2 m_e c^2}{2\,2\pi\hbar}. \tag{A105}$$

Numerically checking these after (A98) provides nontrivial internal consistency tests of the e– and mass–matching in CFT.

Appendix K.4. Propagation Constraints: $c_g = c$ and PPN

The quadratic actions for the Goldstone phase and TT gravitons share identical kinetic tensors on stabilized domains (Appendix I), giving $c_g = c$ at two derivatives. Any higher–derivative operators that split c_g from c must therefore satisfy

$$\left|\frac{c_g}{c} - 1\right| \lesssim \varepsilon_{\rm obs} \quad\Rightarrow\quad \text{bounds on specific hd Wilson coefficients,} \tag{A106}$$

with $\varepsilon_{\rm obs}$ the empirical tolerance from multimessenger observations of gravitational waves and gamma-ray bursts [2]. Similarly, the post–Newtonian parameters $(\alpha_1, \alpha_2, \beta, \gamma_{\rm PPN})$ must lie within experimental limits [122]; this carves out an allowed region in the chronon–coupling space that complements the G–matching via the induced coefficient $c_{\rm ind}$.

Appendix K.5. Electron Size/Compositeness Bounds

Define the electromagnetic form factor of the w=1 soliton,

$$F_1(Q^2) \;=\; \int_\Sigma d^3x\, e^{i\mathbf{q}\cdot\mathbf{x}} \rho_e(\mathbf{x}), \qquad \rho_e \equiv \left.\frac{\delta\mathcal{L}}{\delta A_0}\right|_{\rm soliton}. \tag{A107}$$

The charge radius $\langle r^2\rangle = -6\,F_1'(0)$ satisfies $\langle r^2\rangle \sim \mathcal{O}(1)R^2$ for localized soliton profiles of width R. In CFT,

$$R \;=\; \ell_\Phi\,\mathcal{F}(\alpha_i,\gamma) \quad\Rightarrow\quad \boxed{\ell_\Phi\,\mathcal{F}(\alpha_i,\gamma) \lesssim r_e^{\rm phys}}, \tag{A108}$$

 doi:10.20944/preprints202509.1667.v1

with $r_e^{\rm phys}$ the experimental upper bound on the electron's charge radius [95]. The Planck calibration $\ell_\Phi = \ell_P$ is safely within current limits.

Appendix K.6. EDM and Birefringence/Dispersion Null Tests

Chronon operators that violate P or CP (e.g. couplings inducing an electron EDM) must be highly suppressed. Current nonobservation of the EDM [5] translates into upper bounds on those Wilson coefficients. Likewise, any $\nabla\Phi$–dependent gauge operators inducing vacuum birefringence or frequency–dependent photon speeds must lie below observational thresholds [79]. These null tests bound combinations of higher–derivative coefficients that do not appear in leading two–derivative dynamics.

Appendix K.7. Summary: Constraint Map

It is useful to summarize the parameter–observable relations:

Observable	CFT dependence	Constraint type
m_e	$M_{w=1}(\alpha_i,\gamma;\ell_\Phi)$	Eq. (A98) (equality)
a_e	$\alpha_{\rm em}$, $\Lambda_{\rm hd}$	Eq. (A100) (bound on hd)
σ_T	$\alpha_{\rm em}$, m_e	Consistency (after e, m_e set)
a_0, λ_C, R_∞	$\alpha_{\rm em}$, m_e, $\hbar$, c	Consistency checks
c_g/c	hd Wilson coeffs	Small splitting $\Rightarrow$ bounds
PPN	(α_i,γ)	Allowed region in coupling space
$r_e^{\rm phys}$	$\ell_\Phi\,\mathcal{F}(\alpha_i,\gamma)$	Upper bound on core size

Takeaway.

Beyond $\{\hbar_{\rm eff}, G, e, c\}$, CFT provides several additional, precisely known observables that are *derived* within the theory. Matching the $w{=}1$ soliton mass to m_e and saturating precision/QED checks (a_e, σ_T, spectroscopic constants), together with propagation (PPN, $c_g = c$) and size/EDM/birefringence null tests, overconstrains (α_i,γ), fixes (or bounds) higher–derivative coefficients, and thereby renders the theory predictive with no superfluous knobs.

Appendix L. Maxwell Limit and Operator Suppression

Physical intuition.

On stabilized regions where the chronon field $\bar\Phi^\mu$ is unit timelike, twist-free, and slowly varying, the only gauge- and diffeomorphism-invariant two-derivative scalar built from a $U(1)$ potential A_μ is $F_{\mu\nu}F^{\mu\nu}$, with $F_{\mu\nu} = \nabla_\mu A_\nu - \nabla_\nu A_\mu$. All other admissible terms necessarily insert extra tensors (the foliation vector $\bar\Phi^\mu$, curvature) or extra derivatives. Each insertion brings a small dimensionless parameter: $\varepsilon_{\nabla\Phi}$ from gradients of $\bar\Phi$, ε_R from curvature, or δ from finite wavelength k/Λ. Thus the leading long-wavelength dynamics is Maxwellian, while birefringence and anisotropies are parametrically suppressed—precisely the EFT expectation à la Weinberg [117] and consistent with photon-sector bounds in the SME [78,79]. This appendix quantifies that statement and specifies which operators are suppressed on such domains (see also Section 8).

Appendix L.1. Maxwell Limit and Operator Suppression

Proposition A3 (Maxwell limit on stabilized domains)**.** *Let $U \subset M$ be a stabilized domain for the chronon background $\bar\Phi^\mu$, with unit norm $\bar\Phi^\mu\bar\Phi_\mu = -1$ and vanishing twist (hypersurface orthogonality) $\bar\Phi_{[\mu}\nabla_\nu\bar\Phi_{\rho]} = 0$ [116]. Introduce the dimensionless small parameters*

$$\varepsilon_{\nabla\Phi} := \frac{\|\nabla\bar\Phi\|}{\Lambda}, \qquad \varepsilon_R := \frac{\|{\rm Riem}[g]\|}{\Lambda^2}, \qquad \delta := \frac{k}{\Lambda},$$

 doi:10.20944/preprints202509.1667.v1

where k is the characteristic wavenumber of the probe and Λ the microscopic UV scale of the effective theory. Assume $\varepsilon_{\nabla\Phi}, \varepsilon_R, \delta \ll 1$ and that any æther–like couplings α_i appearing in the gauge sector satisfy $|\alpha_i| \ll 1$ (as in Einstein–Æther–type effective descriptions) [72]. Then, on U, the gauge sector of the effective action admits a potential A_μ with $F_{\mu\nu} = \nabla_\mu A_\nu - \nabla_\nu A_\mu$ such that

$$S_{\text{gauge}}[A] = -\frac{\kappa_A}{4}\int_U \sqrt{-g}\, F_{\mu\nu}F^{\mu\nu} \;+\; \Delta S[A], \tag{A109}$$

with the remainder controlled by

$$\begin{aligned}\Delta S[A] = \int_U \sqrt{-g}\,\Big[&\underbrace{\tilde{\alpha}_1\,(\bar{\Phi}^\mu F_{\mu\nu})(\bar{\Phi}_\rho F^{\rho\nu}) + \tilde{\alpha}_2\,\bar{\Phi}^\mu\bar{\Phi}^\nu F_{\mu\rho}F_\nu{}^\rho}_{\text{æther-like, parity-even}} \\ &+ \underbrace{\frac{c_1}{\Lambda^2}\,\nabla_\rho F_{\mu\nu}\nabla^\rho F^{\mu\nu} + \frac{c_2}{\Lambda^2}\,R\,F_{\mu\nu}F^{\mu\nu}}_{\text{higher-derivative / curvature}} + \cdots\Big].\end{aligned} \tag{A110}$$

where

$$\tilde{\alpha}_{1,2} = \mathcal{O}(\alpha_i) + \mathcal{O}(\varepsilon^2_{\nabla\Phi}), \qquad c_{1,2} = \mathcal{O}(1),$$

and the ellipsis denotes operators of strictly higher order in $\{\varepsilon_{\nabla\Phi}, \varepsilon_R, \delta\}$. Consequently, the field equations reduce to

$$\nabla_\mu F^{\mu\nu} \;=\; J^\nu \;+\; \mathcal{O}(\alpha_i) + \mathcal{O}\Big(\varepsilon^2_{\nabla\Phi}\Big) + \mathcal{O}(\varepsilon_R) + \mathcal{O}\Big(\delta^2\Big), \tag{A111}$$

and the dispersion relation for transverse modes on the leaves $h_{\mu\nu} = g_{\mu\nu} + \bar{\Phi}_\mu\bar{\Phi}_\nu$ is Maxwellian to leading order, with any birefringence or anisotropy suppressed by the same parameters (cf. SME photon-sector analyses) [78,79].

Proof sketch. On a twist-free stabilized background the leafwise connection induced by $\bar{\Phi}$ defines a $U(1)$ holonomy; to quadratic order in fluctuations the only gauge- and diffeomorphism-invariant operator with two derivatives and no explicit $\bar{\Phi}$ is $F_{\mu\nu}F^{\mu\nu}$, giving the leading Maxwell term with coefficient $\kappa_A > 0$ [64]. Residual operators must be built from F, $\bar{\Phi}$, curvature, and extra derivatives. Power counting and symmetry restrict the lowest such terms to the æther-like contractions $(\bar{\Phi}\cdot F)^2$ and $\bar{\Phi}\bar{\Phi}FF$, and to higher-derivative/curvature terms such as $(\nabla F)^2/\Lambda^2$ and RF^2/Λ^2. Their coefficients scale as indicated because departures from hypersurface orthogonality and large gradients of $\bar{\Phi}$ enter at least quadratically (hence $\mathcal{O}(\varepsilon^2_{\nabla\Phi})$), while finite-wavelength and curvature effects are suppressed by $k^2/\Lambda^2 = \delta^2$ and $\|\text{Riem}\|/\Lambda^2 = \varepsilon_R$, respectively (standard EFT power counting) [42,117]. Variation of (A109)+(A110) yields (A111). The Bianchi identity $\nabla_{[\lambda}F_{\mu\nu]} = 0$ holds identically, so any leading-order deviation from Maxwell dynamics must reside in ΔS, hence is suppressed by the stated small parameters. □

Remarks.

(i) In the canonical normalization $A^{\text{can}}_\mu = \sqrt{\kappa_A}\,A_\mu$, the leading term is $-\frac{1}{4}F^2$ and all corrections inherit the suppressions above. (ii) The æther-like pieces induce controlled Lorentz-violating effects (birefringence, phase-velocity anisotropy) bounded by $\mathcal{O}(\alpha_i) + \mathcal{O}(\varepsilon^2_{\nabla\Phi})$; see also the GR-limit discussion in Section 8. (iii) Mixing terms between A_μ and chronon or metric perturbations start at higher order on twist-free backgrounds and share the same suppression pattern.

Appendix M. Functional setup and existence of $w = 1$ solitons

Spatial domain and compactification.

Let (Σ, h) be a smooth oriented Riemannian 3–manifold. We consider either (i) Σ compact without boundary, or (ii) $\Sigma = \mathbb{R}^3$ with the finite–energy boundary condition $\Phi(x) \to \Phi_\infty \in S^3$ as $|x| \to \infty$, so that Σ is effectively compactified to S^3 by one–point compactification.

Target, embedding, and admissible class.

We view $S^3 \subset \mathbb{R}^4$ as a smooth embedded submanifold and write $\Phi = (\Phi^1, \dots, \Phi^4)$ with $|\Phi| = 1$ a.e. For a fixed topological sector $w \in \mathbb{Z}$, define the admissible class

$$\mathcal{A}_w := \Big\{ \Phi \in H^1(\Sigma; S^3) \ : \ |\Phi| = 1 \text{ a.e.}, \ \ \deg(\Phi) = w \text{ (in the sense of Sobolev maps)} \Big\}.$$

Nonemptiness is ensured by smooth representatives (e.g. the hedgehog for $w = 1$) and density of smooth maps in the Skyrme energy class.

Static energy functional and assumptions.

We take the (Skyrme–type) static energy

$$E[\Phi] \ = \ \int_\Sigma \Big(\alpha_1 \, |\nabla\Phi|^2 + \beta_4 \, |\wedge^2 \nabla\Phi|^2 + V(\Phi) \Big) \, \mathrm{dvol}_h, \qquad \alpha_1 > 0, \ \beta_4 > 0, \tag{A112}$$

where $|\nabla\Phi|^2 = \sum_{i=1}^3 \sum_{a=1}^4 |\partial_i \Phi^a|^2$ and $|\wedge^2 \nabla\Phi|^2$ denotes the squared norm of all 2×2 minors of $\nabla\Phi$ (equivalently, the squared norm of the exterior 2–form $\wedge^2 \nabla\Phi$). Assume:

(H1) $V : S^3 \to [0, \infty)$ is continuous (Lipschitz suffices) and bounded below.

(H2) (Σ, h) has bounded geometry on the scales considered (or is compact); in the noncompact case the finite–energy class enforces $\Phi \to \Phi_\infty$ at infinity.

(H3) The degree $\deg(\Phi)$ is well–defined for $\Phi \in \mathcal{A}_w$ and is stable under strong H^1_{loc} convergence within $\mathcal{A}_w$ [18].

Remark A1 (Coercivity and topology control)**.** *The quadratic term $\alpha_1 \|\nabla\Phi\|^2_{L^2}$ controls the H^1–seminorm, while the quartic Skyrme term $\beta_4 \| \wedge^2 \nabla\Phi\|^2_{L^2}$ prevents concentration and rules out shrinking of topological charge ("bubbling") in the $w \neq 0$ sectors. This is the standard mechanism that stabilizes the degree for Skyrme–type energies [44,86].*

Lower semicontinuity.

The integrand in (A112) is a sum of: (i) a convex quadratic form in $\nabla\Phi$, (ii) a polyconvex (indeed convex in the minors) quadratic form in the 2×2 minors of $\nabla\Phi$, and (iii) a continuous zeroth–order term $V(\Phi)$. Hence $E[\cdot]$ is sequentially weakly lower semicontinuous on $H^1(\Sigma; \mathbb{R}^4)$ and remains so on the constraint $|\Phi| = 1$ a.e. (see [16,35,45]).

Proposition A4 (Existence of energy minimizers in fixed degree)**.** *Let $\alpha_1, \beta_4 > 0$ and $V \geq 0$ satisfy (H1)–(H3). Then for each $w \in \mathbb{Z}$ the minimization problem*

$$\min\{ \, E[\Phi] : \ \Phi \in \mathcal{A}_w \, \}$$

admits a minimizer $\Phi_* \in \mathcal{A}_w$.

Proof sketch (direct method). Pick a minimizing sequence $\{\Phi_n\} \subset \mathcal{A}_w$. Coercivity from the α_1–term implies $\{\Phi_n\}$ is bounded in H^1, and the β_4–term controls concentrations of the Jacobian minors. By Rellich–Kondrachov, $\Phi_n \to \Phi$ strongly in L^p_{loc} for $p < 6$ (and a.e. along a subsequence). The pointwise unit–norm constraint passes to the limit (after extraction), yielding $|\Phi| = 1$ a.e. By stability of the degree in this class [18], $\deg(\Phi) = w$. Weak lower semicontinuity of E then gives $E[\Phi] \leq \liminf E[\Phi_n]$, so Φ is a minimizer. Regularity theory implies Φ_* is smooth away from (nonexistent) defects in the Skyrme class and, in practice, smooth [44,86]. □

Regularity remark.

Under (A112) with $\alpha_1, \beta_4 > 0$ and V smooth, Euler–Lagrange solutions are smooth; the quartic term rules out the singularities that may appear in pure σ–models. This is classical in the Skyrme literature [44,86].

Appendix N. Chronon Foliation and Concealed Lorentz Violation

Fundamental mechanism.

The chronon sector introduces a unit timelike vector field Φ^μ that stabilizes a preferred foliation of spacetime. Unlike in conventional æther or Lorentz-violating models, this foliation is not an auxiliary structure but the *substrate from which all matter, fields, and observers emerge*. As a result, every excitation is by construction comoving with the chronon-defined frame. This universality leads to what we term the *Co-Moving Concealment Mechanism (CCM)*: local Lorentz symmetry is broken at the fundamental level, yet no operational violation can be detected, because all clocks, rods, and detectors are themselves constructed from the same chronon background and therefore share its motion.

Operational indistinguishability.

The CCM ensures that all local experiments, whether atomic, nuclear, or gravitational, return results consistent with special relativity. This occurs not by restoring Lorentz invariance dynamically, but by concealing its violation: since all interactions are mediated by chronon-emergent degrees of freedom, no subsystem exists that can serve as an independent reference frame. In this sense, Lorentz symmetry is "effectively exact" for all accessible physics, even though it is *formally broken* in the chronon EFT.

Condensed matter analogies.

A useful way to understand CCM is through analogies with condensed matter. In many-body systems, emergent excitations propagate with approximate Lorentz symmetry even though the underlying medium has a preferred rest frame. For instance, sound waves (phonons) in a fluid obey a relativistic wave equation with respect to the fluid rest frame [113], and fermionic quasiparticles in graphene exhibit emergent Dirac dynamics with an effective "speed of light" given by the Fermi velocity [31]. Similarly, analog gravity models show how collective excitations can experience an emergent metric and causal structure [15]. In all such cases, Lorentz invariance is only approximate and tied to the co-moving frame of the medium, but local measurements cannot detect the violation because all observers and signals are built from the same substrate. The chronon foliation extends this logic to spacetime itself: a universal background defines a preferred frame, but emergent matter and observers comove with it, ensuring that operational Lorentz invariance remains exact within the observable sector.

Cosmological manifestation.

While CCM renders Lorentz violation unobservable locally, the foliation nevertheless has a global imprint. In cosmology, the chronon foliation coincides with the cosmic rest frame defined by the cosmic microwave background (CMB). The CMB dipole anisotropy thus provides a macroscopic tracer of the underlying chronon frame. We stress that the CMB does not *create* the foliation; rather, it reveals the same universal structure that chronons stabilize at the microscopic level. In this view, the remarkable alignment of cosmological observations with the CMB rest frame is not accidental, but a manifestation of the fundamental chronon foliation.

Conservative stance for the present work.

The CCM provides a conceptual resolution of how Lorentz violation can be fundamental yet empirically invisible. However, in the present paper we adopt a conservative stance: we develop the chronon framework as an æther-like effective field theory and map its leading operators to established test frameworks (SME, PPN). This ensures a clear connection with existing experimental bounds, while leaving the full exploration of the CCM and its emergent-metric implications to future work.

References

1. B. P. Abbott *et al.* (LIGO Scientific Collaboration and Virgo Collaboration), "Gravitational Waves and Gamma-Rays from a Binary Neutron Star Merger," *Astrophys. J. Lett.* **848**, L13 (2017).
2. B. P. Abbott *et al.* (LIGO Scientific Collaboration and Virgo Collaboration), "GW170817: Observation of gravitational waves from a binary neutron star inspiral," *Phys. Rev. Lett.* **119**, 161101 (2017).
3. L. F. Abbott, "Introduction to the background field method," *Acta Phys. Pol. B* **13**, 33–50 (1982).
4. P.-A. Absil, R. Mahony, and R. Sepulchre, *Optimization Algorithms on Matrix Manifolds*, Princeton Univ. Press, Princeton (2008).
5. V. Andreev *et al.* (ACME Collaboration), "Improved limit on the electric dipole moment of the electron," *Nature* **562**, 355–360 (2018).
6. R. A. Adams and J. J. F. Fournier, *Sobolev Spaces*, 2nd ed., Academic Press, Amsterdam (2003).
7. G. S. Adkins, C. R. Nappi, and E. Witten, "Static properties of nucleons in the Skyrme model," *Nucl. Phys. B* **228**, 552–566 (1983).
8. S. L. Adler, "Einstein gravity as a symmetry–breaking effect in quantum field theory," *Rev. Mod. Phys.* **54**, 729–766 (1982).
9. R. Arnowitt, S. Deser, and C. W. Misner, "The dynamics of general relativity," in *Gravitation: An Introduction to Current Research*, ed. L. Witten, Wiley, New York (1962), pp. 227–265.
10. P. W. Anderson, "Plasmons, gauge invariance, and mass," *Phys. Rev.* **130**, 439–442 (1963).
11. T. Aoyama, M. Hayakawa, T. Kinoshita, and M. Nio, "Tenth-Order QED Contribution to the Electron $g-2$," *Phys. Rev. Lett.* **109**, 111807 (2012).
12. G. Arfken, H. Weber, and F. Harris, *Mathematical Methods for Physicists*, 7th ed., Academic Press, 2013.
13. M. F. Atiyah and I. M. Singer, "Index of elliptic operators I," *Ann. Math.* **87**, 484–530 (1968).
14. I. G. Avramidi, *Heat Kernel and Quantum Gravity*, Springer, 2000.
15. C. Barceló, S. Liberati, and M. Visser, "Analogue gravity," *Living Rev. Relativ.* **8**, 12 (2005).
16. J. M. Ball, "Convexity conditions and existence theorems in nonlinear elasticity," *Arch. Ration. Mech. Anal.* **63** (1977) 337–403.
17. R. A. Battye and P. M. Sutcliffe, "Solitonic fullerene structures in the Skyrme model," *Phys. Rev. Lett.* **79**, 363–366 (1997).
18. F. Bethuel, H. Brezis, F. Hélein, *Ginzburg–Landau Vortices*, Birkhäuser (1994), Ch. I–II.
19. F. Bethuel, "The approximation problem for Sobolev maps between two manifolds," *Acta Math.* **167**, 153–206 (1991).
20. M. V. Berry, "Quantal phase factors accompanying adiabatic changes," *Proc. R. Soc. A* **392**, 45–57 (1984).
21. H. A. Bethe and E. E. Salpeter, *Quantum Mechanics of One- and Two-Electron Atoms*, Springer, Berlin (1957).
22. P. Billingsley, *Probability and Measure*, 3rd ed., Wiley, 1995.
23. N. D. Birrell and P. C. W. Davies, *Quantum Fields in Curved Space*, Cambridge Univ. Press, Cambridge (1982).
24. R. Bott and L. W. Tu, *Differential Forms in Algebraic Topology*, Springer, New York (1982).
25. B. Berg and M. Lüscher, "Definition and statistical distributions of a topological number in the lattice $O(3)$ σ-model," *Nucl. Phys. B* **190**, 412–424 (1981).
26. H. Brezis, *Functional Analysis, Sobolev Spaces and Partial Differential Equations*, Springer, New York (2010).
27. H. Brezis, J.-M. Coron, and E. H. Lieb, "Harmonic maps with defects," *Comm. Math. Phys.* **107**, 649–705 (1986).
28. C. P. Burgess, "Quantum gravity in everyday life: General relativity as an effective field theory," *Living Rev. Relativ.* **7**, 5 (2004).
29. S. M. Carroll, *Spacetime and Geometry: An Introduction to General Relativity*, Addison–Wesley, San Francisco (2004).
30. S. M. Carroll, G. B. Field, and R. Jackiw, "Limits on a Lorentz- and parity-violating modification of electrodynamics," *Phys. Rev. D* **41**, 1231–1240 (1990).
31. A. H. Castro Neto, F. Guinea, N. M. R. Peres, K. S. Novoselov, and A. K. Geim, "The electronic properties of graphene," *Rev. Mod. Phys.* **81**, 109–162 (2009).
32. Y. Choquet-Bruhat, "Théorème d'existence pour certains systèmes d'équations aux dérivées partielles non linéaires," *Acta Math.* **88**, 141–225 (1952).

33. P. J. Mohr, D. B. Newell, and B. N. Taylor, "CODATA recommended values of the fundamental physical constants: 2018," *Rev. Mod. Phys.* **93**, 035009 (2021).
34. S. Coleman, *Aspects of Symmetry*, Cambridge Univ. Press, Cambridge (1985).
35. B. Dacorogna, *Direct Methods in the Calculus of Variations*, 2nd ed., Springer, New York (2008).
36. B. S. DeWitt, *Dynamical Theory of Groups and Fields*, Gordon and Breach, New York (1965).
37. B. S. DeWitt, "Quantum theory of gravity. I. The canonical theory," *Phys. Rev.* **160**, 1113–1148 (1967).
38. G. H. Derrick, "Comments on nonlinear wave equations as models for elementary particles," *J. Math. Phys.* **5**, 1252–1254 (1964).
39. P. A. M. Dirac, "The Quantum Theory of the Electron," *Proc. Roy. Soc. A* **117**, 610 (1928).
40. P. A. M. Dirac, "The theory of gravitation in Hamiltonian form," *Proc. Roy. Soc. A* **246**, 333–343 (1958).
41. P. A. M. Dirac, *Lectures on Quantum Mechanics*, Belfer Graduate School of Science, Yeshiva Univ., New York (1964).
42. J. F. Donoghue, "General relativity as an effective field theory: The leading quantum corrections," *Phys. Rev. D* **50**, 3874–3888 (1994).
43. J. Ehlers, "Contributions to the relativistic mechanics of continuous media," *Abh. Akad. Wiss. Mainz, Math.-Nat. Kl.* **11**, 792–837 (1961); English trans.: *Gen. Relativ. Gravit.* **25**, 1225–1266 (1993).
44. M. J. Esteban, "A direct variational approach to Skyrme's model for mesons," *Comm. Math. Phys.* **105** (1986) 571–591.
45. L. C. Evans, *Partial Differential Equations*, 2nd ed., AMS, Providence (2010).
46. R. P. Feynman and A. R. Hibbs, *Quantum Mechanics and Path Integrals*, McGraw–Hill, New York (1965).
47. D. Finkelstein and J. Rubinstein, "Connection between spin, statistics, and kinks," *J. Math. Phys.* **9**, 1762–1779 (1968).
48. D. Finkelstein, "Quantum relativity: A synthesis," *Int. J. Theor. Phys.* **27**, 473–519 (1988).
49. B. Z. Foster and T. Jacobson, "Post-Newtonian parameters and constraints on Einstein–Æther theory," *Phys. Rev. D* **73**, 064015 (2006).
50. T. Frankel, *The Geometry of Physics: An Introduction*, 3rd ed., Cambridge Univ. Press, Cambridge (2011).
51. T. Fukui, Y. Hatsugai, and H. Suzuki, "Chern numbers in discretized Brillouin zone: Efficient method of computing (spin) Hall conductances," *J. Phys. Soc. Jpn.* **74**, 1674–1677 (2005).
52. G. Gabrielse *et al.*, "New Determination of the Fine Structure Constant from the Electron $g-2$ Value and QED," *Phys. Rev. Lett.* **97**, 030802 (2006).
53. R. Geroch, "Domain of dependence," *J. Math. Phys.* **11**, 437–449 (1970).
54. D. Gilbarg and N. S. Trudinger, *Elliptic Partial Differential Equations of Second Order*, 2nd ed., Springer, Berlin (2001).
55. P. B. Gilkey, "The spectral geometry of a Riemannian manifold," *J. Diff. Geom.* **10**, 601–618 (1975).
56. D. J. Griffiths, *Introduction to Quantum Mechanics*, 2nd ed., Pearson Prentice Hall (2005).
57. E. Gourgoulhon, *3+1 Formalism in General Relativity*, Springer, Berlin (2012).
58. E. Gourgoulhon, "3+1 formalism and bases of numerical relativity," *arXiv:gr-qc/0703035* (2007).
59. F. Hang and F.-H. Lin, "Topology of Sobolev mappings II," *Acta Math.* **191**, 55–107 (2003).
60. A. Hasenfratz and G. 't Hooft, "A fermion–boson puzzle in a gauge theory," *Phys. Rev. Lett.* **36**, 1119–1122 (1976).
61. A. Hatcher, *Algebraic Topology*, Cambridge Univ. Press, Cambridge (2002).
62. Y. Hatsugai, "Topological aspects of the quantum Hall effect," *J. Phys. Soc. Jpn.* **73**, 2604–2614 (2004).
63. S. W. Hawking and G. F. R. Ellis, *The Large Scale Structure of Space-Time*, Cambridge Univ. Press, Cambridge (1973).
64. F. W. Hehl and Y. N. Obukhov, *Foundations of Classical Electrodynamics: Charge, Flux, and Metric*, Birkhäuser (2003).
65. J. Hietarinta and P. Salo, "Ground state in the Faddeev–Skyrme model," *Phys. Rev. D* **62**, 081701(R) (2000).
66. S. Hildebrandt, H. Kaul, and K.-O. Widman, "An existence theorem for harmonic mappings of Riemannian manifolds," *Acta Math.* **138**, 1–16 (1977).
67. A. N. Hirani, *Discrete Exterior Calculus*, Ph.D. thesis, Caltech (2003).
68. J. Hubbard, "Calculation of partition functions," *Phys. Rev. Lett.* **3**, 77–78 (1959).
69. V. Iyer and R. M. Wald, "Some properties of Noether charge and a proposal for dynamical black hole entropy," *Phys. Rev. D* **50**, 846–864 (1994).
70. J. D. Jackson, *Classical Electrodynamics*, 3rd ed., Wiley, New York (1999).
71. R. Jackiw and C. Rebbi, "Solitons with fermion number 1/2," *Phys. Rev. D* **13**, 3398–3409 (1976).

72. T. Jacobson and D. Mattingly, "Gravity with a dynamical preferred frame," *Phys. Rev. D* **64**, 024028 (2001).
73. T. Jacobson, "Einstein–Aether gravity: A status report," *PoS QG-PH*, 020 (2007); arXiv:0801.1547.
74. J. Jost, *Riemannian Geometry and Geometric Analysis*, 7th ed., Springer, Cham (2017).
75. M. Kamionkowski, A. Kosowsky, and A. Stebbins, "A probe of primordial gravity waves and vorticity," *Phys. Rev. Lett.* **78**, 2058–2061 (1997).
76. R. D. King-Smith and D. Vanderbilt, "Theory of polarization of crystalline solids," *Phys. Rev. B* **47**, 1651–1654 (1993).
77. S. Kobayashi and K. Nomizu, *Foundations of Differential Geometry, Vol. I*, Wiley, New York (1963).
78. V. A. Kostelecký and M. Mewes, "Signals for Lorentz violation in electrodynamics," *Phys. Rev. D* **66**, 056005 (2002).
79. V. A. Kostelecký and M. Mewes, "Electrodynamics with Lorentz-violating operators of arbitrary dimension," *Phys. Rev. D* **80**, 015020 (2009).
80. V. A. Kostelecký and N. Russell, "Data Tables for Lorentz and CPT Violation," *Rev. Mod. Phys.* **83**, 11 (2011).
81. L. D. Landau and E. M. Lifshitz, *The Classical Theory of Fields*, 4th ed., Pergamon Press, Oxford (1975).
82. H. Leutwyler, "On the foundations of chiral perturbation theory," *Annals Phys.* **235**, 165–203 (1994).
83. R. J. LeVeque, *Finite Difference Methods for Ordinary and Partial Differential Equations*, SIAM, Philadelphia (2007).
84. F.-H. Lin and T. Rivière, *Complex Ginzburg–Landau Equations and Variational Problems*, Springer, Berlin (2008).
85. A. Lue, L. Wang, and M. Kamionkowski, "Cosmological signature of new parity-violating interactions," *Phys. Rev. Lett.* **83**, 1506–1509 (1999).
86. N. Manton and P. Sutcliffe, *Topological Solitons*, Cambridge Univ. Press, Cambridge (2004).
87. P. J. Mohr, D. B. Newell, and B. N. Taylor, "CODATA recommended values of the fundamental physical constants: 2018," *Rev. Mod. Phys.* **93**, 035009 (2021).
88. M. Nakahara, *Geometry, Topology and Physics*, 2nd ed., Taylor & Francis, Boca Raton (2003).
89. C. Nash and S. Sen, *Topology and Geometry for Physicists*, Academic Press, London (1990).
90. Y. J. Ng and H. van Dam, "Limit to space-time measurement," *Mod. Phys. Lett. A* **9**, 335–340 (1994).
91. J. Nocedal and S. J. Wright, *Numerical Optimization*, 2nd ed., Springer, New York (2006).
92. E. Noether, "Invariante Variationsprobleme," *Nachr. Königl. Ges. Wiss. Göttingen, Math.-Phys. Kl.*, 235–257 (1918).
93. S. Pancharatnam, "Generalized theory of interference and its applications," *Proc. Indian Acad. Sci. A* **44**, 247–262 (1956).
94. L. E. Parker and D. Toms, *Quantum Field Theory in Curved Spacetime*, Cambridge Univ. Press, Cambridge (2009).
95. R. L. Workman *et al.* (Particle Data Group), "Review of Particle Physics," *Prog. Theor. Exp. Phys.* **2022**, 083C01 (2022).
96. R. E. Peierls, "The commutation laws of relativistic field theory," *Proc. Roy. Soc. A* **214**, 143–157 (1952).
97. V. Perlick, *Ray Optics, Fermat's Principle, and Applications to General Relativity*, Springer, Berlin (2000).
98. M. E. Peskin and D. V. Schroeder, *An Introduction to Quantum Field Theory*, Westview Press, Boulder (1995).
99. M. Planck, "On the law of distribution of energy in the normal spectrum," *Ann. Phys.* **309**, 553–563 (1901).
100. R. Rajaraman, *Solitons and Instantons*, North-Holland, 1982.
101. A. Raychaudhuri, "Relativistic cosmology. I," *Phys. Rev.* **98**, 1123–1126 (1955).
102. A. D. Sakharov, "Vacuum quantum fluctuations in curved space and the theory of gravitation," *Sov. Phys. Dokl.* **12**, 1040–1041 (1968).
103. J. Schwinger, "On gauge invariance and vacuum polarization," *Phys. Rev.* **82**, 664–679 (1951).
104. R. T. Seeley, "Complex powers of an elliptic operator," *Proc. Symp. Pure Math.* **10**, 288–307 (1967).
105. B. Simon, "Holonomy, the quantum adiabatic theorem, and Berry's phase," *Phys. Rev. Lett.* **51**, 2167–2170 (1983).
106. T. H. R. Skyrme, "A nonlinear field theory," *Proc. Roy. Soc. A* **260**, 127–138 (1961).
107. G. E. Stedman, "Ring-laser tests of fundamental physics and geophysics," *Rep. Prog. Phys.* **60**, 615–688 (1997).
108. A. Stern, "Anyons and the quantum Hall effect—A pedagogical review," *Ann. Phys.* **323**, 204–249 (2008).
109. R. L. Stratonovich, "On a method of calculating quantum distribution functions," *Sov. Phys. Dokl.* **2**, 416–419 (1958).
110. M. Struwe, *Variational Methods*, 4th ed., Springer, Berlin (2008).
111. E. Tiesinga, P. J. Mohr, D. B. Newell, and B. N. Taylor, "CODATA recommended values of the fundamental physical constants: 2018," *Rev. Mod. Phys.* **93**, 025010 (2021).

112. L. N. Trefethen, *Spectral Methods in MATLAB*, SIAM, Philadelphia (2000).
113. W. G. Unruh, "Experimental black hole evaporation?" *Phys. Rev. Lett.* **46**, 1351–1353 (1981).
114. D. V. Vassilevich, "Heat kernel expansion: User's manual," *Phys. Rep.* **388**, 279–360 (2003).
115. G. E. Volovik, *The Universe in a Helium Droplet*, Oxford Univ. Press, 2003.
116. R. M. Wald, *General Relativity*, University of Chicago Press, Chicago (1984).
117. S. Weinberg, "Phenomenological Lagrangians," *Physica A* **96**, 327–340 (1979).
118. S. Weinberg, *The Quantum Theory of Fields, Vol. I: Foundations*, Cambridge Univ. Press, Cambridge (1995).
119. S. Weinberg, *The Quantum Theory of Fields, Vol. II: Modern Applications*, Cambridge Univ. Press, Cambridge (1995).
120. X. G. Wen, *Quantum Field Theory of Many-Body Systems*, Oxford Univ. Press, 2004.
121. C. M. Will, *Theory and Experiment in Gravitational Physics*, rev. ed., Cambridge Univ. Press, 1993.
122. C. M. Will, "The Confrontation between General Relativity and Experiment," *Living Rev. Relativity* **17**, 4 (2014).
123. C. M. Will, *Theory and Experiment in Gravitational Physics*, Cambridge Univ. Press, updated ed. (2018).
124. R. L. Workman *et al.* (Particle Data Group), "Review of Particle Physics," *Prog. Theor. Exp. Phys.* **2022**, 083C01 (2022).
125. T. T. Wu and C. N. Yang, "Concept of nonintegrable phase factors and global formulation of gauge fields," *Phys. Rev. D* **12**, 3845–3857 (1975).
126. J. Zak, "Berry's phase for energy bands in solids," *Phys. Rev. Lett.* **62**, 2747–2750 (1989).
127. A. Zee, "Spontaneously generated gravity," *Phys. Rev. D* **23**, 858–866 (1981).
128. A. Zee, "Einstein gravity emerging from quantum Weyl invariance," *Ann. Phys.* **151**, 431–442 (1983).